Neuroplastin and Plasma Membrane Ca^{2+} ATPases in murine macrophages: A phenotypical analysis

Dissertation

zur Erlangung des akademischen Grades

Doctor rerum naturalium

(Dr. rer. nat.)

genehmigt durch die Fakultät für Naturwissenschaften der Otto-von-Guericke- Universität Magdeburg

von M.Sc. Nikhil Tiwari

geb. am 29 März 1995 in Indien

Gutachter: Prof. Dr. Eckart Gundelfinger

Prof. Dr. Christian Grimm

eingereicht am: 24th Mai 2024

verteidigt am: 29th Januar 2025

Abbreviation

AkT – Ak strain Transforming

APC – Antigen Presenting Cells

BMDM - Bone Marrow-Derived Macrophages

CBA – Cytometric Bead Analysis

CD – Cluster of Differentiation

CREB – cAMP-Response Element Binding protein

CRCM – Calcium Release-Activated Calcium Modulator (Orai)

DC – Dendritic Cell

DMEM – Dulbecco's Modified Eagle's Medium

ECAR – Extracellular Acidification Rate

ELISA – Enzyme-Linked Immunosorbent Assay

FACS – Fluorescence Activated Cell Sorting

FAM – Carboxyfluorescein

FCCP - Carbonyl cyanide-p-trifluoromethoxy phenylhydrazone

FLICA – Fluorescence Labelled Inhibitor of Caspase

GLUT – Glucose Transporter

HB8M – HoxB8 Progenitors Derived Macrophages

HIF – Hypoxia-Induced Factor

IFN – Interferon

IFNGR – Interferon γ Receptor

Ig – Immunoglobulin

IL – Interleukin

iNOS – Nitric Oxide Synthase, inducible

IP3R – Inositol Triphosphate Receptor

IRF – Interferon Regulatory Factor

LPS – Lipopolysaccharide

MAPK – Mitogen Associated Protein Kinase

MCP – Macrophage Chemoattractant Protein

MCU – Mitochondrial Calcium Uniporter

MCT – Monocarboxylate Transporters

MHC – Major Histocompatibility Complex

MICU – Calcium Uptake Protein, Mitochondrial

NCX – Sodium Calcium Exchanger

NFAT – Nuclear Factor of Activated T cells

NF-κB - Nuclear Factor Kappa-light-chain-enhancer of Activated B cells

Np55 – Neuroplastin 55

Np65 – Neuroplastin 65

Nptn$^{-/-}$ /*Nptn* KO – Neuroplastin Knockout

OCR – Oxygen Consumption Rate

PBS – Phosphate-Buffered Saline

PMCA - Plasma Membrane Calcium ATPase

PMCA1-cKO / PMCA1$^{-/-}$ - Plasma Membrane Calcium ATPase isoform 1 conditional knockout

PRR – Pattern Recognition Receptors

RBC – Red Blood Cells

Rcan – Regulator of Calcineurin

ROS – Reactive Oxygen Species

Rot/AA – Rotenone and Antimycin A

RPMI medium – Roswell Park Memorial Institute Medium

SERCA – Sarcoendoplasmic Reticulum Calcium ATPase

SLC – Solute Carrier

SOCE – Store Operated Calcium Entry

SOCS – Suppressor of Cytokine Signaling

STAT – Signal Transducers and Activators of Transcription

STIM – Stromal Interaction Molecule

TBS – Tris-Buffered Saline

Th – T helper cell

TLR – Toll-like Receptors

TMD – Transmembrane Domain

TRAF – Tumor Necrosis Factor Receptor Associated Factor

TRIF – TIR domain-containing adaptor inducing interferon-β

TRPC – Transient Receptor Potential Canonical

TRPM – Transient Receptor Potential Melastatin

TRPV – Transient Receptor Potential Vanilloids

WT – Wild Type

Summary

Neuroplastin, an immunoglobulin superfamily transmembrane protein, has been implicated in synaptic plasticity and learning and memory. Moreover, Neuroplastin has been established as a close interacting partner of Plasma Membrane Calcium ATPases (PMCAs). This interaction stabilizes PMCAs, and thus, plays a critical role in maintaining Ca^{2+} homeostasis within cells. Recent studies have addressed the roles of Neuroplastin-PMCA in immune cells, for which Ca^{2+} plays a crucial role. While the role of Ca^{2+} is well-defined in T and B lymphocyte activation, its precise function and the mechanisms of its entry and exit in macrophages remain an active area of research. In this study, I first addressed the relevance of Neuroplastin and PMCA (isoform 1) for Ca^{2+} homeostasis in macrophages based on knockout mutants. PMCA1 rather than Neuroplastin emerged as vital for regulating intracellular Ca^{2+} levels. Next, I performed a comparative analysis of signaling, cytokine production, and metabolism in Neuroplastin and PMCA1 knockout macrophages after M1 polarization with IFNγ/LPS. Interestingly, despite loss of >70% of PMCAs, Neuroplastin knockout macrophages showed normal canonical signaling (STAT1, NF-κB, ERK1/2) and no or little differences in cytokine production along with moderate elevation of Ca^{2+} in the ER as well as subdued glycolysis. In contrast, PMCA1 knockout macrophages demonstrated elevated basal and stored Ca^{2+} levels, upregulated ERK1/2 signaling upon stimulation, and significantly upregulated cytokine production after M1 polarization. Also, these macrophages showed elevated OXPHOS and glycolysis (after M1 polarization). These findings provide an understanding of the role of Neuroplastin and PMCA in macrophage function, shedding light on the underlying fundamental difference between a Neuroplastin and a PMCA knockout macrophage. This study also involved a high-throughput RNAseq analysis of PMCA1 knockout macrophages versus controls before and after stimulation. About 2 to 3% of all genes displayed differential expression in the absence of PMCA1 upon stimulation. Within this fraction, genes related to NF-kB- and Ca^{2+}-signaling, as well as to autoimmune diseases, were found enriched. Together, these findings provide valuable insights into the underlying mechanisms enabling macrophages to survive disturbed Ca^{2+} homeostasis and maintain polarization within limits. This knowledge could be harnessed to develop strategies for managing conditions associated with disrupted Ca^{2+} homeostasis, such as degenerative processes and inflammatory diseases.

Zusammenfassung

Neuroplastin, ein Transmembranprotein der Immunglobulin-Superfamilie, ist an der synaptischen Plastizität sowie an Lernen und Gedächtnis beteiligt. Darüber hinaus hat sich Neuroplastin als enger Interaktionspartner von Plasmamembran-Calcium-ATPasen (PMCAs) erwiesen. Diese Interaktion stabilisiert die PMCAs und spielt somit eine wichtige Rolle bei der Aufrechterhaltung der intrazellulären Ca^{2+}-Homöostase. Neuere Studien haben sich mit der Rolle von Neuroplastin-PMCA in Immunzellen befasst, für die Ca^{2+} eine entscheidende Rolle spielt. Während die Rolle von Ca^{2+} bei der Aktivierung von T- und B-Lymphozyten gut definiert ist, werden seine genaue Funktion und die Mechanismen seines Eintritts und Austritts in Makrophagen nach wie vor aktiv beforscht. In dieser Studie habe ich zunächst die Bedeutung von Neuroplastin und PMCA (Isoform 1) für die Ca^{2+}-Homöostase in Makrophagen anhand von Knockout-Mutanten untersucht. Es stellte sich heraus, dass PMCA1, jedoch nicht Neuroplastin, für die Regulierung des intrazellulären Ca^{2+}-Spiegels entscheidend ist. Als nächstes führte ich eine vergleichende Analyse der Signalübertragung, der Zytokinproduktion und des Stoffwechsels in Neuroplastin- und PMCA1-Knockout-Makrophagen nach M1-Polarisierung mit IFNγ/LPS durch. Interessanterweise zeigten Neuroplastin-Knockout-Makrophagen trotz des Verlusts von mehr als 70 % der PMCAs eine normale kanonische Signalübertragung (STAT1, NF-κB, ERK1/2) und keine oder nur geringe Unterschiede in der Zytokinproduktion sowie eine moderate Erhöhung von Ca^{2+} im ER und eine gedämpfte Glykolyse. Im Gegensatz dazu zeigten PMCA1-Knockout-Makrophagen sowohl erhöhtes basales Ca^{2+} als auch deutlich erhöhtes Ca^{2+} im ER-Speicher und zudem eine hochregulierte ERK1/2-Signalgebung nach Stimulation und eine signifikant erhöhte Zytokinproduktion nach M1-Polarisierung. Darüber hinaus zeigten diese Makrophagen erhöhte OXPHOS als auch Glykolyse (nach M1-Polarisierung). Diese Ergebnisse ermöglichen ein Verständnis der Rolle von Neuroplastin und PMCA bei der Makrophagenfunktion und belegen den grundlegenden Unterschied zwischen Neuroplastin- und PMCA-Knockout-Makrophagen. Die vorliegende Studie enthält auch eine Hochdurchsatz-RNAseq-Analyse von PMCA1-Knockout-Makrophagen im Vergleich zu Kontrollen, vor und nach Stimulation. Etwa 2 bis 3 % aller Gene zeigten eine unterschiedliche Expression in Abwesenheit von PMCA1 nach Stimulation. Innerhalb dieser Fraktion sind Gene angereichert, die mit NF-κB - und Ca^{2+}-Signalen sowie mit Autoimmunkrankheiten in Verbindung stehen. Zusammengenommen bieten diese

Ergebnisse wertvolle Einblicke in die zugrundeliegenden Mechanismen, die es Makrophagen ermöglichen, eine gestörte Ca^{2+}-Homöostase zu überleben und ihre Polarisierung in Grenzen zu halten. Dieses Wissen könnte genutzt werden, um Strategien zur Behandlung von Zuständen zu entwickeln, die mit einer gestörten Ca^{2+}-Homöostase einhergehen, wie z.B. degenerative Prozesse und Entzündungskrankheiten.

Table of Contents

1. Introduction

1.1 Macrophages- The vanguard of the immune system:

Macrophages are innate immune cells. They are the most plastic cells of the hematopoietic system and are known for their ubiquitous presence in tissues (Schulz et al., 2012). They are strategically placed to clean up cell debris (Elliott et al., 2010), tumor cells (Feng et al., 2015), and foreign material such as bacteria (Hirayama et al., 2017), contribute to wound healing, and orchestrate the inflammatory process by releasing cytokines and through inflammasome activation (Sefik et al., 2022).

There are two distinct developmental origins of macrophages. Embryonic yolk sac progenitors differentiate into pre-Macrophages or monocytes. They differentiate into long-lived tissue macrophages. Contrary to this, hematopoietic stem cells such as those in the bone marrow give rise to both short-lived and long-lived macrophages, contributions coming during post-natal and adult phases (Dick et al., 2022; Mass et al., 2023).

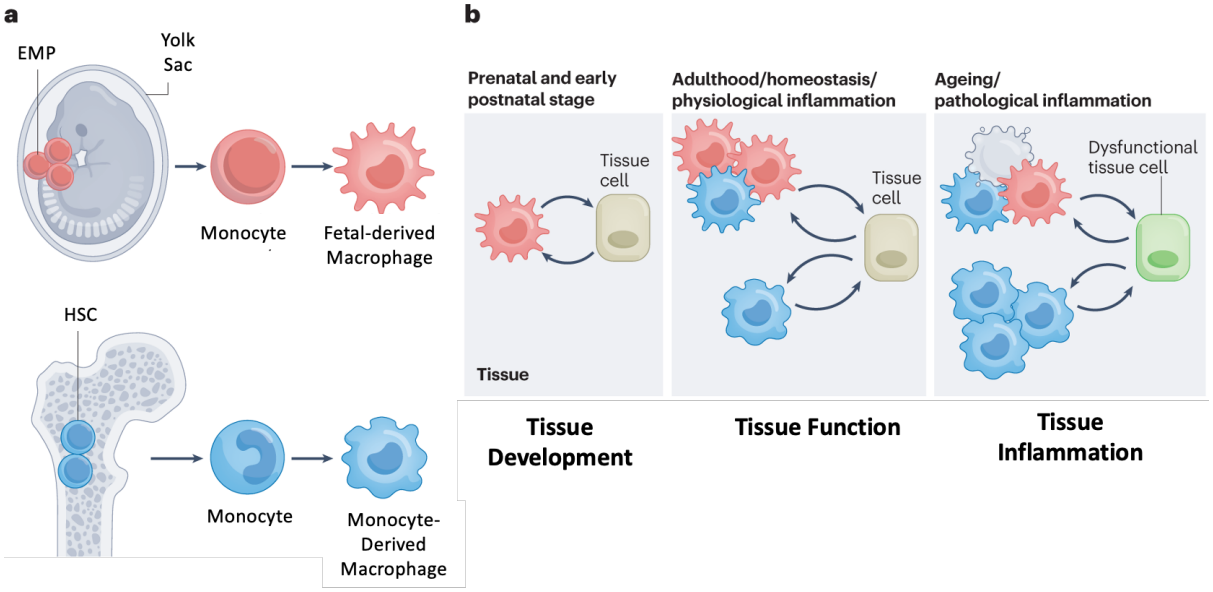

Figure.1 a. Distinct pathways guide the development of tissue macrophages. Originating from yolk sac erythro-myeloid progenitors (EMPs), where monocytes emerge, eventually differentiating into long-lived tissue-resident macrophages. Conversely, hematopoietic stem cells (HSCs) contribute to the production of both short-lived and long-lived macrophages in early postnatal stages and adulthood. These macrophages, derived from EMPs and HSCs, actively participate in cell–cell communication with specialized tissue cells, playing vital roles in sustaining tissue function. EMP-derived macrophages are particularly crucial for tissue development. **b.** In the context of homeostasis, various macrophage

subpopulations collaborate with tissue cells to uphold normal tissue function. However, disruptions in the precisely balanced distribution of macrophages within tissues may occur with aging or in pathological inflammation. Such disruptions can lead to consequences such as the apoptosis of long-lived macrophages or an increased influx of short-lived HSC-derived macrophages, ultimately resulting in impaired tissue function (Mass et al., 2023).

Extravasation of monocytes with various immune functions, most importantly their differentiation into tissue macrophages (Ginhoux et al., 2021), can help maintain tissue homeostasis. Macrophages, as mentioned are key parts of internal organs and tissues and have distinct signatures and phenotypes based on their location. Although single-cell genomics and high throughput phenotyping approaches have helped our understanding of different macrophage subsets (Chen et al., 2021; Yang et al., 2021), it is not fully understood how these macrophages behave in a steady state and upon challenges like environmental triggers, infection, and aberrations like autoimmune disorders.

1.2 Macrophage signaling and polarization:

Macrophages adopt distinct phenotypes manifesting in various functions upon specific stimuli and signals. This process is called macrophage polarization. Polarized macrophages can be classified as classically activated (M1) and alternatively activated (M2) (Yunna et al., 2020), and both can be further divided into subcategories. M1 macrophages mediate pro-inflammatory responses by secreting cytokines, activate endothelial cells, and are responsible for recruiting other immune cells at the site of inflammation (Orecchioni et al., 2019). Typical features of M2 macrophages include phagocytosis of apoptotic cells and the secretion of anti-inflammatory cytokines (Yunna et al., 2020). Apart from this basic categorization, various signaling processes can be involved to specify macrophage function further. It has been discovered that the polarization process is complex and intertwined with the involvement of numerous signaling events.

A predominance of signals leading to the activation of transcription factors like nuclear factor 'kappa-light-chain-enhancer' of activated B-cells (NFκB) and Signal Transducers and Activators of Transcription 1 (STAT1) promotes M1 polarization of macrophages. Microbial products or pro-inflammatory cytokines (e.g., TNF-α) (Wu et al., 2015) induce this

polarization, and the critical mediator of this process is Interferon-gamma (IFNγ), primarily derived from Th1 helper T cells (Simpson et al., 2022). The binding of IFNγ to its receptor (IFNGR) activates receptor-bound Janus Kinases 1 and 2 (JAK1, 2) (Pestka et al., 1997), which in turn phosphorylate STAT1, leading to its translocation to the nucleus (Pestka et al., 1997; Platanias, 2005), where it triggers specific gene expression profiles. This includes the upregulation of major histocompatibility complex (MHC) class II, IL-12, nitric oxide synthase 2 (iNOS or NOS2), and suppressor of cytokine signaling (SOCS) (Adler et al., 2021). Additionally, co-stimulatory molecules like CD-86 (Morales-Lange et al., 2021) and the Toll-like receptors TLR2 and TLR4 also become upregulated.

TLRs are Pattern Recognition Receptors (PRRs) that recognize foreign bodies like bacterial moieties. Bacterial Lipopolysaccharides (LPS) bind to TLR4, activating the TIR-domain-containing adapter-inducing interferon-β (TRIF) and the myeloid differentiation response 88 (MyD88) (Hoogerwerf et al., 2010; Juarez et al., 2010). MyD88 is an essential adaptor molecule for TLR4 that activates a pathway that leads to the nuclear translocation of NF-kB as another crucial step in the polarization of M1 macrophages (Das et al., 2018; Sharif et al., 2007). MyD88 further promotes M1 polarization through activation of the transcription factor activator protein 1 (AP-1) and/or the cAMP response element binding protein (CREB) via Mitogen-activated protein kinase (MAPK) (Xia et al., 2021). These transcriptional pathways promote the expression of various inflammatory genes like proinflammatory cytokines (including tumor necrosis factors (TNF), IL-6, IL-1β, and IL-12), chemokines CXCL10, CXCL11, co-stimulating proteins, and proteins that process antigens (Lacy et al., 2011).

The alternative pathway (M2) of macrophage activation is induced by IL-4 and IL-13, cytokines mainly produced by Th2 cells (Czimmerer et al., 2022; Lundahl et al., 2022). Both cytokines can utilize the IL-4 receptor alpha (IL-4Rα) and, in combination with IL-2 receptors (IL-4Rα, IL-2R) (Keegan et al., 1994; Russell et al., 1993), which trigger the JAK2 or JAK3 pathway, thereby leading to homodimerization of STAT6 or STAT3 and consequently to their nuclear localization (Arpa et al., 2023; Dang et al., 2023; Lundahl et al., 2022). This leads to the expression of M2-specific factors like arginase 1 (Arg1), CD206 (or macrophage mannose receptor 1, Mrc1), resistin-like-α (Retnla or Fizz1) and Ym1 (or chitinase 3-like 3, Chi3l3) (Rath et al., 2014). M2

signaling may as well involve IL-13 utilizing IL-13 receptor alpha 1 (IL-13Rα1), which is linked to Tyk2/Stat1/Stat6 signaling.

a. b.

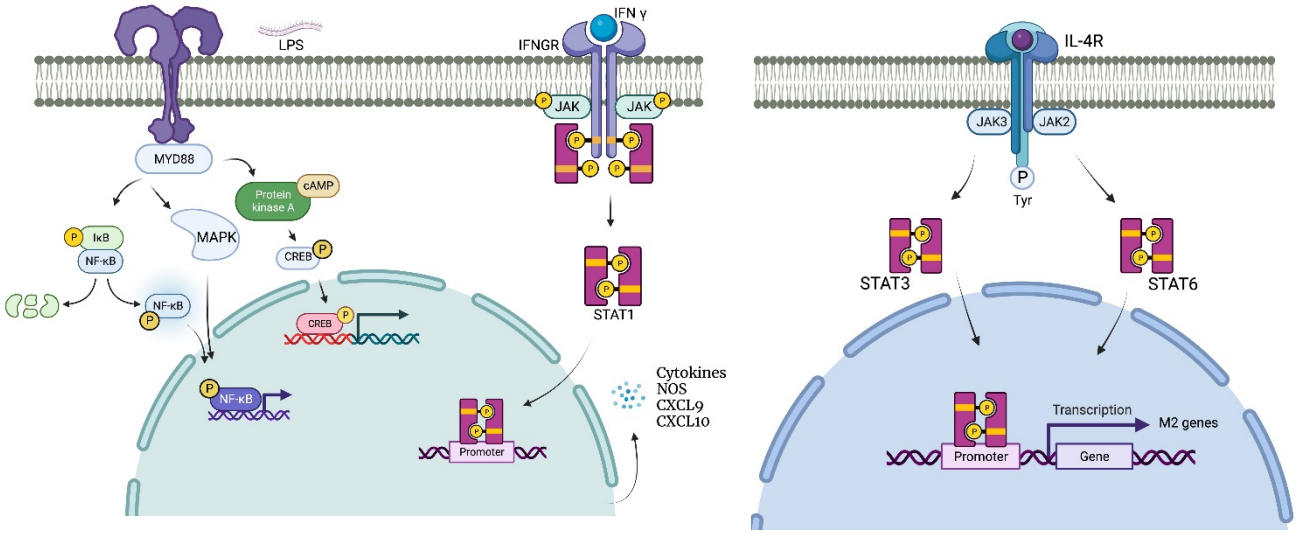

Figure 2 Simplified schematic depicting pro-inflammatory pathways downstream of TLR4 and IFNGR **(a)** and a scenario leading to an M2-specific transcriptional profile downstream of the IL4R **(b)**. The signaling pathway downstream of TLR4 has multiple arms involving MAPK, NF-κB, and CREB. The signaling pathway downstream of IFNGR involves STAT1 phosphorylation, dimerization, and transcriptional activity. Signal transduction downstream of IL-4/IL4R involving STAT3 and STAT6 transcription factors leads to M2 polarization of macrophages.

1.3 The metabolic switch: a hallmark of macrophage activation:

While macrophage signaling pathways lead to context-specific transcriptional profiles, it is now well established that macrophage polarization is closely linked to distinct metabolic phenotypes, which may feed back onto gene expression. The first studies about immune cell metabolism came in the 1950s on Neutrophils and revealed aerobic glycolysis, a phenomenon discovered by Warburg during his research on tumor cells, which manifests in increased levels of glucose uptake, high rate of glycolysis, and lactic acid fermentation in combination with reduced OXPHOS (Awasthi et al., 2019; Nonnenmacher et al., 2018). Of note, apart from the distinctions of M1 and M2 macrophages mentioned earlier, macrophage polarization also involves metabolic reprogramming. Depending on external stimuli, macrophages can switch between an OXPHOS-based aerobic profile and glycolysis (Nonnenmacher et al., 2018).

Macrophages, upon TLR ligation or upon stimulation with IFNγ, increase glucose uptake and glycolysis (Freemerman et al., 2014). Elevated amounts of glycolytic intermediates lead to the generation of NADPH, which aids in producing reactive oxygen species (ROS) as part of the inflammatory response (Garaude et al., 2016). Increased glycolysis also leads to enhanced lactate production. Subsequently, there is a Tricarboxylic acid (TCA) cycle as the cycle could not progress beyond citrate/isocitrate because the enzyme involved in the process (Isocitrate dehydrogenase, Idh1) is downregulated. Further, itaconate is generated, a metabolite with putative anti-microbial potential (Coelho, 2022). The profound reduction of the TCA results in an accumulation of acetyl-CoA and succinate, which in turn may aid in inflammatory gene transcription (Baardman et al., 2018; Bailey et al., 2019; Freemerman et al., 2014; Garaude et al., 2016; Meiser et al., 2016; Wellen et al., 2009). Specifically, succinate leads to stabilization of Hypoxia-Induced Factor 1 (HIF1-α), a key transcription factor involved in the second wave of metabolic reprogramming through gene expression (Tannahill et al., 2013). This second phase is characterized by a decrease in mitochondrial respiration and a dependence on glycolysis, thus like the "Warburg effect". Interestingly, the antimicrobial agent Nitric Oxide (NO), which is produced upon iNOS induction during M1 polarization (see above), is also responsible for reducing the Electron Transport Chain (ETC) activity and inhibiting OXPHOS (Garaude et al., 2016), a distinct phenomenon seen in bone marrow-derived macrophage, but not so evident in human macrophages (Vijayan et al., 2019).

M2 macrophages are characterized by arginase-1 expression, which increases ornithine and polyamine biosynthesis pathways (Puleston et al., 2019). Polyamines are known to facilitate the expression of mitochondrial genes necessary for OXPHOS (Puleston et al., 2019). The energetic profile of these cells is determined by increased expression of genes related to fatty acid uptake, transport, and oxidation and increased uptake of both glucose and fatty acids in culture. Thus, M1 polarized macrophages quickly increase glycolysis to assist the pro-inflammatory process, whereas M2 macrophages do so gradually (Wang et al., 2018) and therefore do not rely heavily on glycolysis but rather on glutamine (Gln) and fatty acid synthesis (Wang et al., 2018).

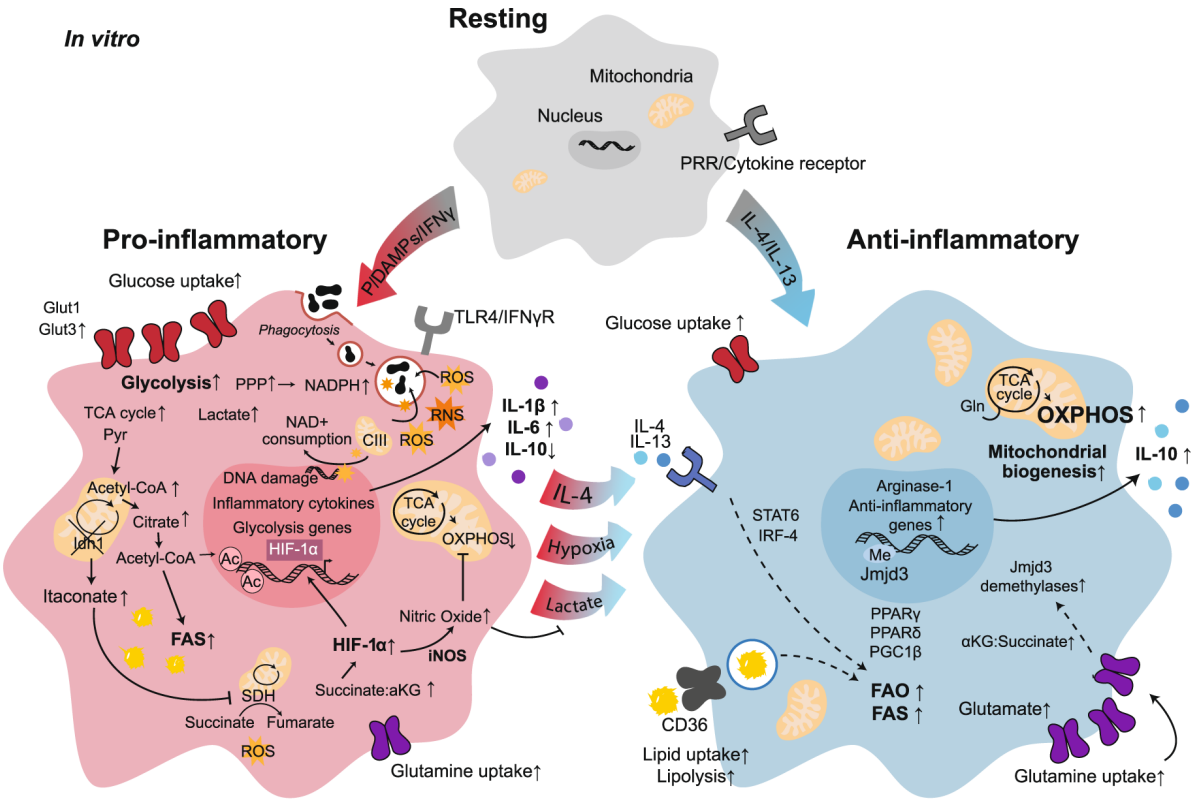

Figure 3: **Macrophage metabolic switching**. Resting macrophages can be classically activated by external stimuli like LPS, which leads to enhanced glycolysis, whereas alternatively activated macrophages with IL-4/IL-13 show enhanced OXPHOS and Fatty acid oxidation (Wculek et al., 2022).

1.4 The Intricate Interplay: Calcium Signaling and Immune Cell:

Calcium (Ca^{2+}) is a pervasive second messenger (Endo, 2006) involved in the control of a plethora of cellular processes, including cell division, migration, and transmitter release (Berridge et al., 2003; Deng et al., 2023; Ridley et al., 2003) and it exerts its roles through binding to effector molecules. While Ca^{2+} signaling is best studied in excitable cells such as neurons and muscles, it has also been implicated in regulating immune cell functions. Typically, the source of Ca^{2+} is external, from where it can enter cells along a steep gradient through plasma membrane-resident channels, e.g., Transient receptor potential (TRP) channels or Ca^{2+} release-activated Ca^{2+} channels (CRAC) (Clapham, 2007). Internal Ca^{2+} stores like the endoplasmic reticulum (ER), the Golgi apparatus, lysosomes, and mitochondria also play important roles in the control of intracellular Ca^{2+}, mediating Ca^{2+} flux by channels like inositol 1,4,5-triphosphate receptors (IP_3R), ryanodine receptors (RyR), some TRP channels (Rosato et al., 2021)or the mitochondrial calcium uniporter (MCU) (Clapham, 2007; Dong,

Shen, et al., 2010; Dong, Wang, et al., 2010). The concentration of free cytosolic Ca^{2+} is usually in the range of only 100 nM, i.e., extremely low as compared to the extracellular milieu (1 to 5 mM) or the ER lumen (typically 0.1 to 0.5 mM (Raffaello et al., 2016)). The concentration of Ca^{2+} in the intracellular stores is also regulated. In particular, the ER sequesters Ca^{2+} in high amounts with the help of Sarcoplasmic/endoplasmic reticulum Ca^{2+} ATPases (SERCA) (Courjaret et al., 2014), which constantly pump Ca^{2+} into the ER, driven by ATP hydrolysis. Ca^{2+} released from ER may directly affect cell functions through effector molecules but may also act indirectly, as exemplified below.

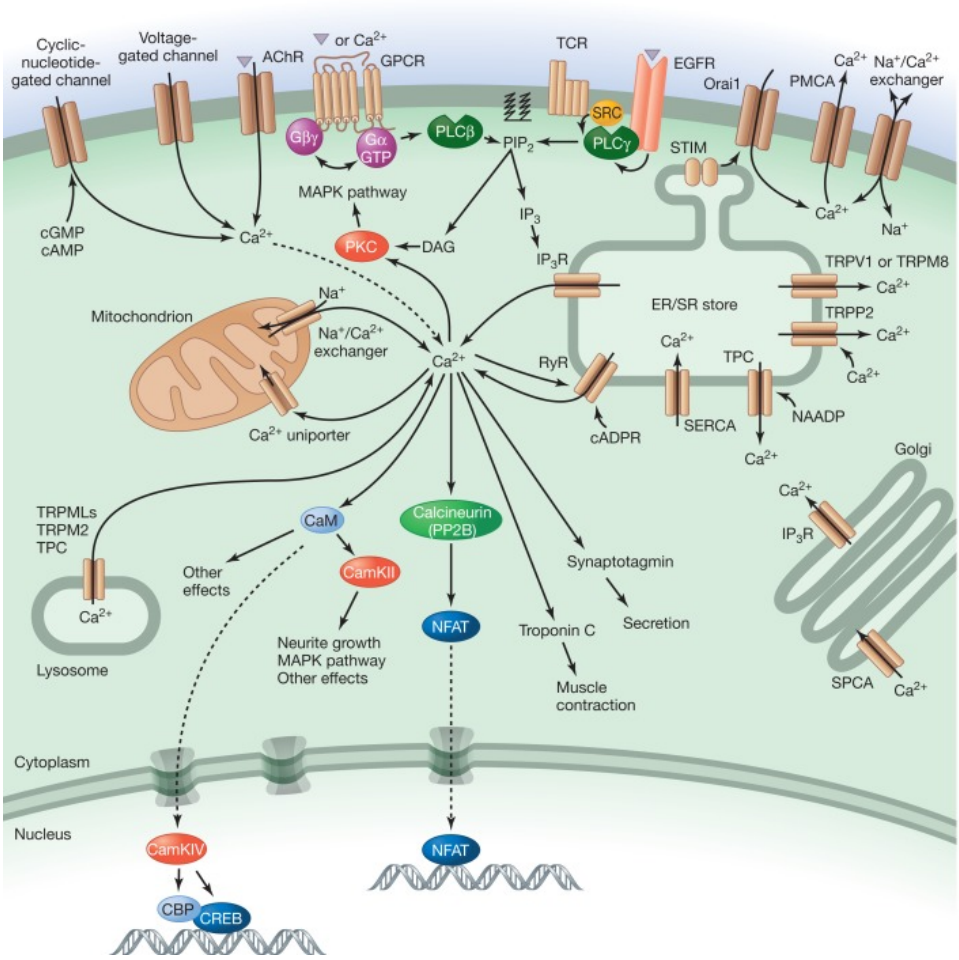

Figure 4: **Modes of entry, exit, and effectors of Ca^{2+} - Calcium finds its way in through various channels (e.g., Voltage-gated channels, TRP ion channels, etc.), receptors like acetylcholine receptors (AChR), GPCRs, and Orai.** For organelles, SERCA plays an important role in pumping Ca^{2+} in ER, whereas MCUs are chief actors for mitochondria transporting the Ca^{2+} inside. Various effectors like CaM, CamKII, Calcineurin, and further downstream transcription factors like CREB and NFAT are also shown (Bootman et al., 2012).

There have been multiple attempts to elucidate the role of calcium in immune cells, with a particular focus on T cells. It has been demonstrated that Ca^{2+} influx mediates T cell function and immunity to infection (Picard et al., 2009; Prakriya et al., 2006). Mechanism also known as Store-operated Calcium Entry (SOCE) (Hogan et al., 2015), has emerged as the major route for Ca^{2+} into T cells upon antigen binding to T-cell receptors (TCRs). The mechanism of canonical SOCE is ensured by the coordinated activity of two families of proteins, Stromal Interaction Molecule (STIM) and ORAI (Prakriya, 2013). STIM1 and STIM2 are single-pass transmembrane ER proteins with their N-terminal domains in ER lumen (Liou et al., 2005; Manji et al., 2000). The ORAI family comprises cell membrane proteins that form the conductive pore of CRAC channels and includes ORAI1–3, which contain four transmembrane domains (TMDs) (Prakriya, 2013), while their N- and C-terminal domains face the cytosol. ER Ca^{2+} depletion, most prominently through activation of IP_3Rs, is sensed by STIM through its ER-luminal Ca^{2+}-binding EF-hand domains (Liou et al., 2005). Specifically, dissociation of Ca^{2+} from the EF hands leads to a conformational change and oligomerization of STIM molecules (Figure 5). The oligomerization, in turn, promotes the coupling of STIM with ORAI at ER-plasma membrane junctions, forming highly selective pores (Hirve et al., 2018; Stathopulos et al., 2006), through which Ca^{2+} enters the cytosol.

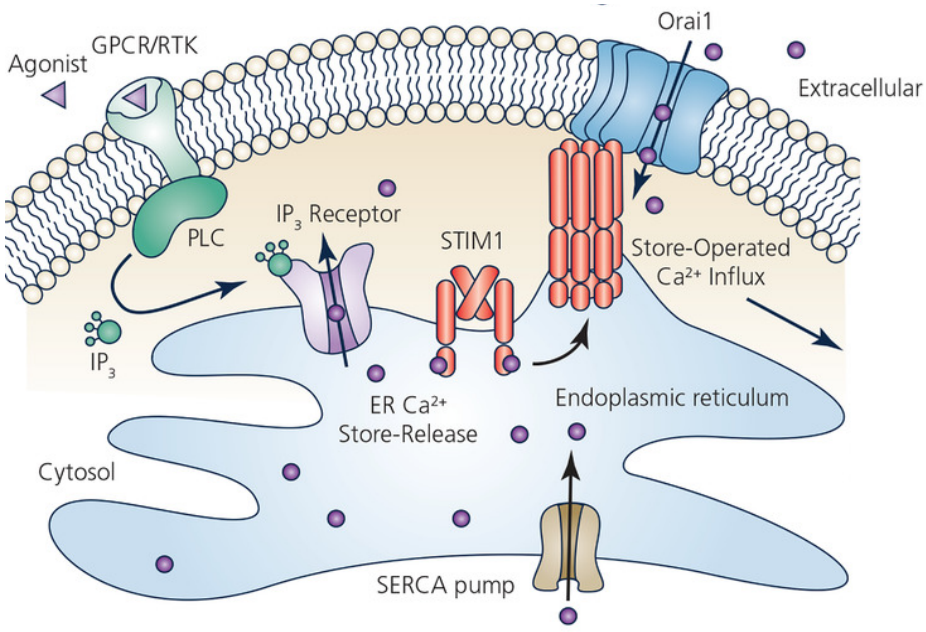

Figure 5: **SOCE Mechanism**- Depletion in Store Calcium leads to oligomerization of STIM and coupling with ORAI, leading to calcium entry into the cytosol. Also shown in the figure, SERCA refills the store by pumping calcium from the cytosol to the ER (Yeung et al., 2020).

SOCE impairment and dysregulation have been implicated in various disease pathologies (Lacruz et al., 2015). In fact, patients with inherited mutations in the genes encoding ORAI1 (Prakriya et al., 2006) or its activator STIM1 are immunodeficient and prone to chronic infection by various pathogens (Desvignes et al., 2015), including Mycobacterium tuberculosis (Mtb). STIM1-deficient T cells exhibited markedly reduced IFNγ production during the early phase of Mtb infection and reduced numbers of induced regulatory T cells (iTregs). STIM1 and STIM2 deletion impairs the function of Th1 and Th17 cells (Ma et al., 2010). $CD4^+$ and $CD8^+$ T cell-dependent antiviral immunity requires STIM1 and STIM2 (Shaw et al., 2014).

SOCE has also been observed in cells of the innate immune system such as macrophages and dendritic cells (DCs) and may thus be expected to provide Ca^{2+} signals required for their function. In line with this assumption, STIM1 ablation was recently described to impair DC migration and local and global calcium signaling with effects on maturation and phagocytosis (Nunes-Hasler et al., 2017). However, the specific role of SOCE in macrophages and its contribution to innate immunity are not well defined. Macrophages surprisingly did not show any defect associated with STIM1 and STIM2 deletion when assayed for M1 polarization-specific properties such as cytokine production and phagocytosis (Vaeth et al., 2015). The same study also revealed that intracellular Ca^{2+} signaling is important for phagocytosis, and the general blocking of Ca^{2+} signals might have adverse effects. Moreover, activation of macrophages by type 1 interferon (IFNγ) was shown to be Ca^{2+}-dependent. Specifically, activation of STAT1 by phosphorylation (on S727 and Y701) downstream of IFNα was suppressed when Ca^{2+}/calmodulin-dependent Kinase (CamK) was inhibited or when the calcium chelator BAPTA was applied (L. Wang et al., 2008). Recently, Ca^{2+} entry through TRP Canonical 1 (TRPC1) has been reported to regulate the pro-inflammatory polarization of macrophages (Chauhan et al., 2018). Interestingly, TRPC1 was activated by IFNγ induced store depletion, i.e., formally representing a mode of SOCE. Corroborating a role of TRPC1-mediated Ca^{2+} entry in macrophage activation, respective knockout mice showed diminished expression of pro-inflammatory response-related molecules (iNOS/NOS2, IL-6, and TNF-α)

after infection with *Klebsiella pneumoniae* (Chauhan et al., 2018). As another target of regulation by Ca^{2+}, NLRP3 inflammasome activation and IL-1β release, a hallmark of pro-inflammatory macrophage, have been identified (Ainscough et al., 2015).

Anti-inflammatory (M2) polarization of macrophages has also been linked to calcium. A recent report suggests that ORAI1 mediates the activation of STAT6 and, thus, the M2 response (Nascimento Da Conceicao et al., 2021). It has also been found that mitochondrial Ca^{2+} uptake through mitochondrial calcium uniporter (MCU) is instrumental in M2 polarization, and consequently, knocking out MCU impairs this process (Tedesco et al., 2019). Though multiple reports suggest the involvement of Ca^{2+} in M2 polarization, the complete picture remains elusive.

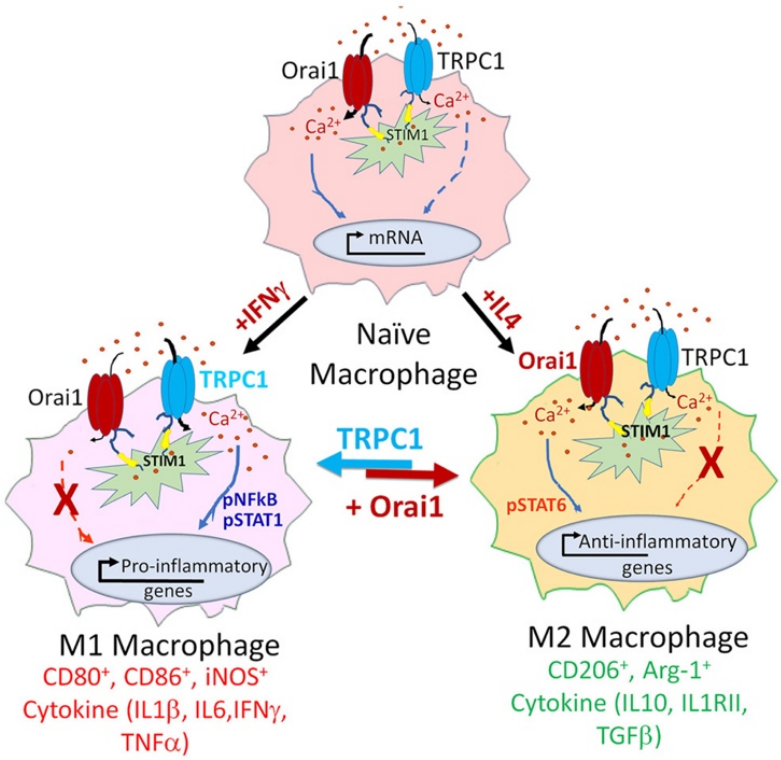

Figure 6: **Role of calcium in macrophage polarization**. Ion channels like TRPC1 are reported to regulate M1 polarization of the macrophages, whereas ORAI1 is known to be a major facilitator of calcium influx during M2 polarization (Nascimento Da Conceicao et al., 2021).

1.5 Control of Calcium homeostasis by Plasma Membrane Calcium ATPase and Neuroplastin:

To maintain intracellular calcium homeostasis, cells need to expel calcium from the cells through pumps and exchangers like Plasma Membrane Calcium ATPases (PMCA) and/or Na^+/ Ca^{2+} exchangers (NCX). In contrast to the latter, PMCAs are present ubiquitously in eukaryotic cells. Like SERCAs, they are ATP-driven and are well-regulated to cope with tissue-specific functions and they may be compartmentalized along the plasma membrane to fulfill localized roles (Korthals et al., 2017; Krick et al., 2021; Quintana et al., 2011). In vertebrates, PMCAs are encoded by 4 genes, and each has multiple splice variants, which may exhibit different levels of enzymatic activity. Whereas PMCA1 and 4 are expressed in all cell types, isoforms 2 and 3 are predominantly expressed in neurons and/ or muscles. All PMCA isoforms comprise 10 TMDs. The N and C terminals and two large loops between TMDs 2, 3 and TMDs 4, 5, respectively, from the intracellular body of PMCAs, including the active center and the ATP binding side. While various modes of isoform-specific regulations of PMCA activity have been described, autoinhibition via the C-terminal tail and its release by binding of Ca^{2+}/calmodulin to a respective C-terminal binding motif is encountered in all PMCA isoforms (but except for a few splice variants) (Krebs, 2015).

a. b.

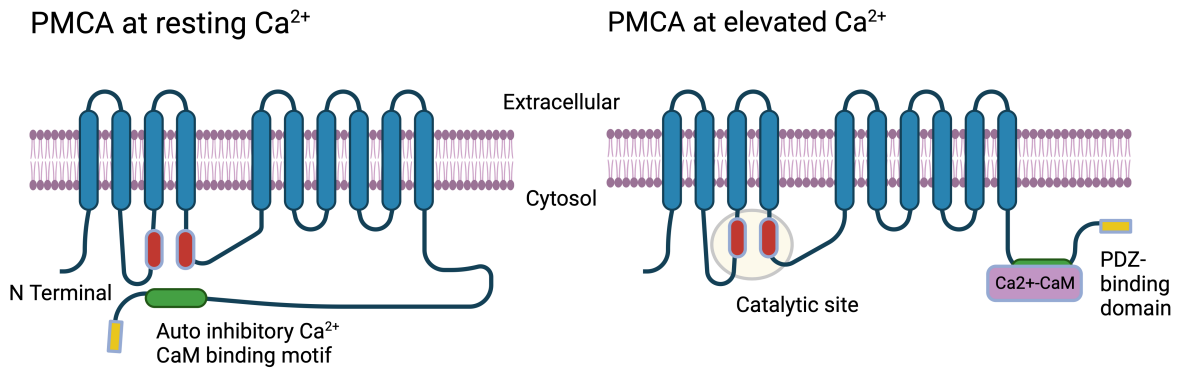

Figure 7: **Topology of PMCA during resting levels and elevated calcium levels.** The scheme depicts an a. autoinhibitory Ca^{2+}/CaM-binding domain motif and b. upon elevation of cytoplasmic Ca^{2+}, the inhibition is lifted, and the channel is rendered functional.

Recently, PMCAs have been found to be tightly associated with Neuroplastin (gene name *Nptn*), a small single-pass transmembrane protein of the immunoglobulin superfamily. Basigin (*Bsg*)/ CD147, a paralog of *Nptn*, may also be associated with PMCAs. In fact, both *Nptn* and

Bsg may be considered auxiliary subunits of PMCAs that are crucial for PMCA stability and activity (Gong et al., 2018; Herrera-Molina et al., 2017; Korthals et al., 2017; Schmidt et al., 2017). Neuroplastin has been most intensively studied in neuronal cells, and its involvement in synaptic plasticity, learning, and memory is well established (Herrera-Molina et al., 2017; Smalla et al., 2000). Loss of Neuroplastin in both neuronal and non-neuronal cells (viz. immune cells) leads to a substantial reduction in PMCA levels. Splice variation gives rise to *Nptn* with two or three immunoglobulins (Ig) domains, often called Np55 and Np65, respectively, according to their apparent molecular weight detected by immunoblots on brain samples. While the 3 Ig domain variant Np65 is mainly, if not exclusively, expressed in neurons, Np55 is expressed in a wide range of cell types, including immune cells (Korthals et al., 2017; Langnaese et al., 1997).

Loss of *Nptn* in T cells has been associated with elevated nuclear localization of NFAT, increased cytokine production, and impaired post-stimulation clearance of Ca^{2+}. Complete loss of *Nptn* is largely phenocopied by loss of one copy of PMCA1, indicating that complete loss of PMCA1 leads to a more severe outcome than loss of *Nptn*. Indeed, loss of PMCA1 during early T cell development leads to abrogation of thymic development (Beckmann et al., 2023).

a.

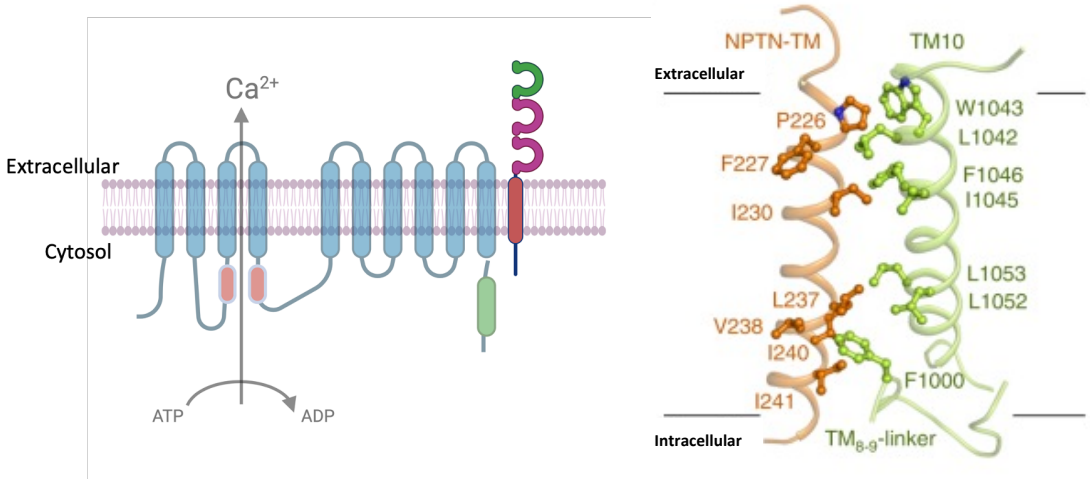

b.

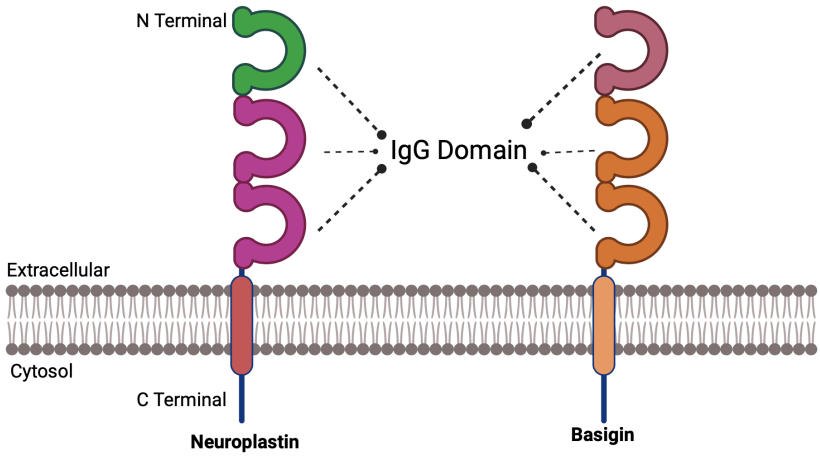

Figure 8: **a.** Neuroplastin-PMCA interaction- Neuroplastin (both isoforms) and PMCA and closely localized with the TM10 domain of PMCA interacting with Neuroplastin along with the TM8-9 linker domain (Gong et al., 2018). **b.** Neuroplastin and Basigin as paralogues- Neuroplastin and Basigin contain 2 (or 3) IgG domains where short isoforms are ubiquitous and long isoforms are tissue-specific.

Basigin, also known as EMMPRIN or CD147, is present on various cell surfaces like RBCs, endothelial cells, and neurons. Apart from its interaction with PMCA, Basigin is well known to be associated with Monocarboxylate transporters (MCTs), which facilitate the passage of lactate across cell membranes. MCTs belong to the superfamily of solute carrier transporters (SLCs) and act as uniporters for protons together with metabolites like lactate, pyruvate or ketone bodies. Basigin acts chaperone-like for MCTs, supporting their proper folding and transport to the cell membrane (Halestrap et al., 2012; Philp et al., 2003).

Neuroplastin has been well-studied in neuronal cells, and its involvement in synaptic plasticity, learning, and memory is well-established (Herrera-Molina et al., 2017; Smalla et al., 2000). Moreover, it involves roles like regulating receptor trafficking (Empson et al., 2006) and interacting with intracellular adaptor molecules like TRAF6 (Vemula et al., 2020).

1.6 Goals of the thesis:

The principal goal of this thesis is to analyze phenotypes in mouse macrophages predominantly, bone marrow-derived macrophages and peritoneum macrophages with putative chronic disruption in Ca^{2+} homeostasis caused by deletion of Neuroplastin or PMCA1. Elevated cytosolic Ca^{2+} levels have been shown to occur in neurons and T cells from the mutants mentioned above, but phenotypes in macrophages remain to be characterized. Disturbed Ca^{2+} homeostasis not only could mean altered levels of cytosolic Ca^{2+} but could also affect Ca^{2+} handling upon stimulation (TLR, IFNGR), thus affecting the kinetics of signaling viz phosphorylation of transcription factors (STAT, NF-κB) and expression of corresponding genes, polarization, and so on.

Specifically, the following goals are being addressed in the thesis: -

1. Characterization of PMCA isoforms and Basigin in Neuroplastin-deficient macrophages as well as characterization of Neuroplastin in PMCA1-deficient macrophages:

   A quantitative analysis of PMCAs in Neuroplastin isoforms as proof of principle shows that Neuroplastin loss destabilizes PMCA. On the other hand, the impact of loss of PMCAs on Neuroplastin (especially on the plasma membrane) is assessed as a novel observation. Basigin is assessed not only as a putative source for compensation of Neuroplastin but also as an interaction partner and subunit for molecules like MCTs.
2. Comparative analysis of signal transduction in Neuroplastin and PMCA1 knockout macrophages:

   Using the biochemical approach, signaling transduction downstream of TLR and interferon-gamma signaling, viz. phosphorylation and nuclear localization of transcription factors, has been analyzed. It's an important part of a study aimed at revealing the role of chronic disruption of calcium homeostasis on canonical signaling pathways of macrophages.
3. Measuring cytokine production, ROS, and metabolism in Neuroplastin deficient and PMCA1-deficient macrophages:

   Cytokines and ROS production by macrophages are key phenotypes of inflammation. This justifies the necessity to measure and analyze the above-mentioned parameters, to shed more light on how calcium handling by macrophages can affect these parameters. Also, macrophages are known for switching their metabolic phenotype

between mitochondrial-based OXPHOS to Glycolysis upon stimulation. Using seahorse-based assays, metabolic parameters have been analyzed in both genotypes to study the effects of disruption in calcium homeostasis on metabolism and metabolic switching.

4. RNA seq and analysis:

   For a global comparative analysis of transcripts and Gene Ontology Pathways in a *PMCA1* KO mutant RNAseq has been performed. The outcome provides a broad picture of events related to Calcium overload in macrophages.

2. Materials and Methods:

2.1 Mice:

Neuroplastin knockout mice (from here on, *Nptn*$^{-/-}$ or *Nptn* KO) were described in (Herrera-Molina et al., 2014). Heterozygous (*Nptn*$^{+/-}$) mice were crossed to obtain Neuroplastin-deficient (*Nptn*$^{-/-}$) and wild-type *(Nptn*$^{+/+}$*)* littermates as homozygotes males were sterile. The knockout here is a complete knockout that conveniently deletes both the isoforms of Neuroplastin from the mice.

PMCA1 (gene name: *Atp2b1*) complete knockouts are embryonically lethal, so conditional knockouts (PMCA1-cKO) were needed. For this purpose, *Atp2b1*$^{tm1a(KOMP)Wtsi}$ mice had originally been obtained from the UC Davis Knockout Mouse Project (www.komp.org; project ID CSD77635) and had first been crossed with an FLPo deleter mouse (*B6.Cg-Tg(Pgk1-flpo*)10Sykr/J, The Jackson Laboratory) to obtain *Atp2b1*$^{tm1c(KOMP)Wtsi}$, referred to as *PMCA1*$^{f/+}$ mice (Beckmann et al., 2023; Korthals et al., 2021). The latter mice were crossed with *LysMcre* mice (B6N.129P2(B6)-*Lyz2*$^{tm1(cre)Ifo}$/J, Jackson Stock 018956) to generate PMCA1-cKO mice with *PMCA1* deleted in the myeloid lineages (including bone marrow-derived macrophages) used here (Mice Facility: Uniklinikum Magdeburg).

2.2 Cell Culture:

Material	Supplier/Manufacturer
DMEM with Glutamax Supplementation	Gibco™ (Thermo Fisher Scientific™)
Fetal Bovine Serum	Gibco™ (Thermo Fisher Scientific™)
Penicillin-Streptomycin 100X	Gibco™ (Thermo Fisher Scientific™
RPMI 1640 with Glutamax supplementation	Gibco™ (Thermo Fisher Scientific™)
T-25, T-75 and T-175 Easy Flasks	Nunc™ (Thermo Fisher Scientific™)
Falcon® 15mL and 50mL tubes	Corning®
25 G Syringe Needles	BD
Disposable Scalpel	BD
70µm Cell Strainer	Corning®
Estradiol (10mM in Ethanol)	Sigma
1X PBS without Ca^{2+}	Gibco™ (Thermo Fisher Scientific™)
BRB-Flt3L cells derived medium supplement	A gift from Dr. Kristina Langnaese, IBZB

Macrophage Medium	DMEM Medium, 10% FBS, 1X PenStrep, 10% L929 conditioned medium

L929 medium: L929 fibroblast cells (ATCC no. CCL1) were gifted by Dr. Kristina Langnaese (IBZ, Uniklinikum Magdeburg). They were cultured in T-175 flasks until they were 75% confluent. The flasks were then filled up to 50mL medium and left undisturbed for seven days. Media was collected from the flasks and labeled as the 1st week. For the 2nd week, 50mL medium was put into the flasks again for a week and then collected. Media from both weeks were equally supplemented with macrophage differentiation medium, described in the material section.

Bone marrow-derived macrophage (BMDM) cultures: Mice were sacrificed, and hind limbs (from femur onward) were cut out. The legs were carefully cleaned with a scalpel to remove muscles and extract femur and tibia bones from the legs. These bones were then separated, and the top of the bones was removed with a scalpel to create an opening for needles. A 5 mL syringe with a 26G needle was used for flushing bone marrow out with medium into a 50 mL Falcon® tube. The bone marrow was then thoroughly resuspended in the medium with a Pasteur pipette to create a single-cell suspension and centrifuged at 300x g for 6 minutes.

Bone marrows from one femur and one tibia were resuspended in 5 Petri dishes, each with 10 mL of macrophage differentiation culture medium containing L929 cell-based supplements (see below). Cells were then plated in 100 mm bacterial culture dishes and placed in an incubator with humidity, 5% CO_2, and 37°C. Cells were supplemented with 5 mL medium on Day 4, and then a complete change of medium was done on Day 7. After Day 7, fully differentiated macrophages in the culture dish were obtained.

HoxB8 progenitors: HoxB8 Progenitors for *WT*, *Nptn*$^{-/-}$ and *PMCA1*-cKO were developed at IBZ courtesy of Dr. Kristina Langanaese and Prof. Dr. Klaus Dieter-Fischer, according to the protocol provided in literature (Redecke et al., 2013). These stem cell lines were cultured for propagation and later differentiation. For propagation, 1X10^5 progenitors/mL of medium were seeded in a T-25 flask in RPMI HoxB8 medium with estrogen (working concentration 1mM) and Flt-3 ligand (from BRB Flt3 cells), with cells being assessed and reseeded every third day to maintain a maximum of 80% confluency and avoid overcrowding of the cells.

To differentiate these cells into macrophages, they were centrifuged and washed in 1X PBS with 1% FKS, three times to remove the estrogen completely. The cells were reseeded with a density of $2X10^5$ cells in a Petri dish supplemented with 10 mL of macrophage differentiation medium. The process further is similar to that of culturing BMDMs, where 5mL medium is supplemented to the cells after three days and a complete change of medium on the seventh day.

2.3 Preparation of protein extracts for Western blot analysis:

Material	Supplier/Manufacturer
Mouse IFNγ	Miltenyi Biotec
Lipopolysaccharide (LPS)	Thermo Fisher Scientific™
Tris	Carl Roth
NaCl	Carl Roth
$MgCl_2$	Carl Roth
Benzonase	Sigma
cOmplete™ Protease Inhibitor cocktail	Roche
Bicinchoninic acid (BCA) kit	Pierce, Rockford
Rotiload I loading buffer	Roth®
RIPA lysis Buffer	Santa Cruz Technologies
Precast SDS-PAGE Gel	SERVA and Invitrogen
NuPAGE™ MES PAGE Running Buffer	Thermo Fisher
Amersham™ NitroCellulose Mebrane	Protran® MERCK
Non-Fat Dried Milk	Roth®
Tween® 20	Sigma-Aldrich
Triton X 100	Roth®
Western Transfer System	Pharmacia Biotech
HRP substrate	SERVA *Eos Ultra* and SERVA *Vega*
Electrophoresis System	SERVA
Triton Homogenization Buffer	20 mM Tris pH 7.5, 150 mM NaCl, 1% Triton-X-100, 2 mM $MgCl_2$, 750 U/mL Benzonase, and protease inhibitors (1 tablet/ 50 mL of cOmplete™ Protease Inhibitor cocktail)

Cells were seeded at a density of $1X10^6$ cells/well on a 6-well plate. For polarizing macrophages with M1 phenotype, cells were primed with IFNγ with a concentration of 150 U/mL for at least 6 hours, followed by LPS stimulation with a concentration of 50ng/mL overnight. Cell pellets were homogenized by incubation at 4°C for 30 min in a Triton-

homogenization buffer (120 mL per 5X10^6 cells) centrifuged at 15,000×g for 20 minutes, and the resulting supernatants were used for the analysis. The protein content in the supernatant was determined using a bicinchoninic acid (BCA) kit according to the manufacturer's instructions. The samples were denatured at 42° C for 20 min in a sample loading buffer at approximately 0.8–1.5 µg/µL concentrations. For the LPS and IFNγ time course, cells with similar density in 6-well plates were seeded. For every time point, from 15 minutes to 2 hours, LPS and IFNγ were supplemented separately, and the medium was subsequently added to the wells at the desired time points. Cells were first washed 2X with chilled 1X PBS buffer and then lysed in 100 µL RIPA lysis buffer from Santa Cruz technologies by incubating at 4°C for 10 minutes. Lysates were used after BCA-based quantification, and denaturing was done using a loading buffer as previously described.

Buffer	Composition/Supplier
10X TBS	200mM Tris-base, 1.37M NaCl in water, adjusted to pH 7.6
10X Western Transfer	0.25M Tris-base, 1.92M Glycine, 0.2% SDS (Supplemented with 15% methanol in 1X buffer)
Stripping Buffer	Thermofisher Scientific™

SERVA precast gels with a 4-20% acrylamide concentration were used for SDS-PAGE using Tris/Glycine Buffer system. Typically, two gels were run in an electrophoresis system with voltage set to 300V (constant). Samples were then electrotransferred at 200 mA for 90 mins onto nitrocellulose membrane (0.45 µm) in a wet transfer system using western transfer buffer. After blocking with 5% non-fat milk in TBS containing 0.1% of Tween 20 (TBST), blot membranes were probed overnight at 4°C in fresh blocking buffer with primary antibodies (see table below for antibody-specific dilutions). After washing 3 times with TBST, secondary antibodies conjugated to horseradish peroxidase were applied at 1:5000 for 1 hour at room temperature. After washing with TBS containing 0.1 % of Tween 20, blot membranes were visualized by ECL solution using Intas ECL system (Intas Chemocam ECL Imaging). ECL-blots were evaluated using a sequence of exposures (3-10 seconds per scan, up to 15 times). The blots were quantified by using Fiji ImageJ. For this, blot images were opened in Fiji software, and brightness/contrast was adjusted accordingly. Using the draw option, a rectangle is drawn around the line of bands of interest. Then, within the Analyse option, Gels and the first

lane option were selected. Once again, the Gels option was visited, but this type of Plot Lanes function was used. A graph appears with different peaks. On all peaks of interest, base to-base line was drawn and with a magic wand option area under the peak measured.

Antibodies (Species)	Catalog #. (Dilution)	Company
pan PMCA (Mouse)	ab2825 (1:1000)	AbCam
Neuroplastin (Sheep)	AF7818 (1:2000)	R & D System
GAPDH (Rabbit)	2118S (1:2000)	Cell Signaling Technologies®
iNOS (Rabbit)	13120S (1:2000)	Cell Signaling Technologies®
Phospho AKT (Serine 473) (Rabbit)	4060T (1:2000)	Cell Signaling Technologies®
Total AKT (Rabbit)	9272S (1:2000)	Cell Signaling Technologies®
Phospho NF-κB (Serine 536) (Rabbit)	3033S (1:2000)	Cell Signaling Technologies®
Total NF-κB (Rabbit)	8242S (1:2000)	Cell Signaling Technologies®
Phospho ERK1/2 (Threonine 202/Tyrosine 204) (Rabbit)	4370T (1:2000)	Cell Signaling Technologies®
Total ERK1/2 (Rabbit)	4695T (1:2000)	Cell Signaling Technologies®
Phospho STAT1 (Tyrosine 701) (Rabbit)	9167S (1:2000)	Cell Signaling Technologies®
Total STAT1 (Rabbit)	14994S (1:2000)	Cell Signaling Technologies®
Basigin (Rabbit)	AF772 (1:1000)	R & D Systems

2.4 Cytokine Measurement:

Material	Supplier
LEGENDPLEX™ Mouse Pro-inflammatory(13-plex) CBA kit	Biolegend®
LEGENDPLEX™ Software	Biolegend®
FlowJo v10.9.0	the BD®

Cytokine measurement was done using Cytometric bead analysis (CBA) using the Cytometric Bead Assay kit in combination with FACS. The CBA method uses the principle of sandwich ELISA. It utilizes beads pre-coated with antibodies for their intended target cytokines. With two bead sizes and distinct intrinsic levels of APC fluorescence, bead populations can easily be identified in the LEGENDplex™ complimentary software suite. A cocktail of biotinylated

antibodies is added once the analyte is bound to these beads. This is followed by PE-Streptavidin, which serves as the signal to help quantify cytokine concentrations alongside a standard curve in the software itself, followed by FlowJo-based analysis for more gating and quantification.

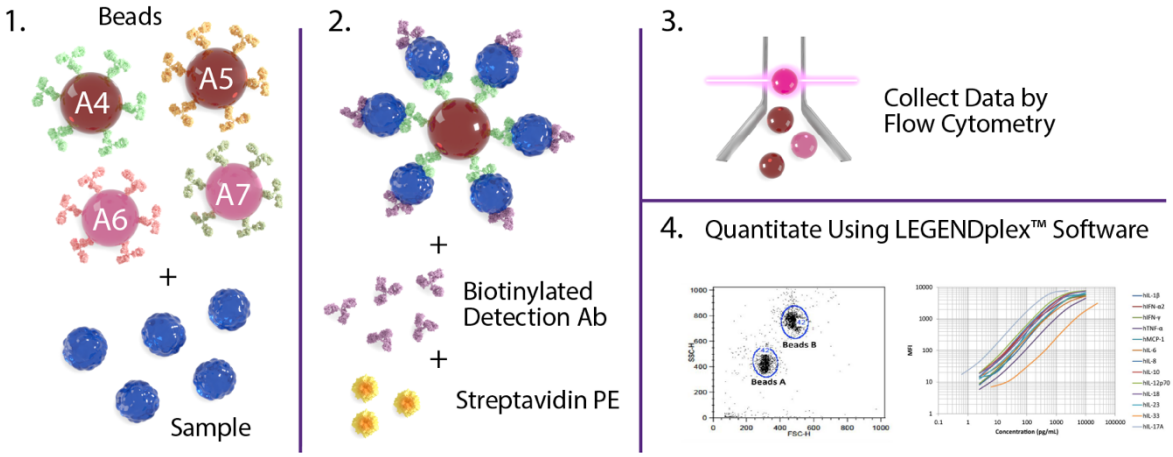

Figure 9: Principle of FACS-based CBA assay using Biolegend® LEGENDplexTM representing step-wise usage of pre-coated beads followed by biotinylated Detection Antibody and the Stretavidin PE. Flow Cytometry and then Quantification process is done using LEGENDplex™ and FlowJo software. *Source: Biolegend*

Macrophages were seeded on a 96-well plate at a density of 50,000 cells/well and left for at least 2 hours to adhere. Fresh medium was then supplemented to those wells where macrophages did not require activation. Wells with macrophages for M1 polarization were primed for 6 hours with IFNγ (150 U/mL) and then topped with LPS (50 ng/mL) in a way that the final volume in the well reached 200 μL. LPS stimulation lasts overnight. After 16 hours, the next day, roughly after 16 hours of LPS stimulation, the medium was collected to determine the amount of various secreted cytokines. The kit allows to assess the pro-inflammatory (M1-related) cytokines. The procedure was performed following the manufacturer's protocol (https://www.biolegend.com/Files/Images/media_assets/pro_detail/datasheets/76100_Mu_Inflammation_Panel_R8.pdf) with decent modifications:

The modified protocol uses the following amount of reagents that differ from the manufacturer´s protocol

- 12.5 μL of Assay Buffer was added to all wells.
- 12.5 μL of each standard was added to the standard wells.
- 12.5 μL of each sample was added to the sample wells.

Two to three technical replicates were used for every sample measured. CBA was performed on N=3 for all the genotypes of BMDM.

2.5 Calcium Measurement:

Material	Supplier/Manufacturer
Fluo-8 AM	Life Technologies® Thermofisher Scientific™
Fura Red AM	Life Technologies® Thermofisher Scientific™
EGTA	MERCK Millipore
FACS buffer	Thermofisher Scientific™
Thapsigargin	MERCK Millipore
Flow Cytometer	BD FACSCanto II
HBSS	Biochrome®

Calcium measurement was done as described in T cell study (Korthals et al., 2017).The cells were subsequently stained with a combination of two dyes 1.3 μg/mL of Fluo-8 and 2.7μg/mL of FuraRed in RPMI1640 medium for 30 minutes at 37°C/5% CO2, washed and resuspended in HBSS buffer, which was free of Ca^{2+} and supplemented with 1 mM EGTA. Before FACS acquisition of the cells, the cells were preincubated at 37°C/5% CO_2 for 15 min. The Fluo-8 and FuraRed fluorescence were acquired on a BD FACSCanto II flow cytometer at 1 μl/s (recording several hundreds of cells per second). For the baseline measurement of Ca^{2+}, the FACS recording was done for 2 minutes, the measurement was stopped, and 1 μM final concentration of Thapsigargin was added into the cell suspension. Recording was resumed for another 10 minutes. To further measure SOCE, cells were centrifuged, resuspended in a buffer with 2 mM of Ca^{2+}, quickly returned, and measured for 5 minutes. To measure the

clearance of Ca^{2+} from the cell, cells were again centrifuged down, resuspended in Ca^{2+}-free buffer (HBSS) with EGTA, and recorded over time.

The kinetics data were generated with the BD® FlowJo Kinetics Tool and then processed and plotted using GraphPad® Prism . Each time point represents the mean ratio of cells acquired in consecutive intervals of two or three seconds. To this end, the area under the curve (AUC) of the Fluo-8/FuraRed kinetics graph was calculated and divided by the respective time interval t. The data were then normalized by dividing each AUC/t value by the AUC/t value of the basal Ca^{2+} level of the respective *WT*/Control population.

2.6 Seahorse Assays:

Material	Manufacturer/Supplier
Seahorse XFe96 Analyzer	Agilent®
Calibrant medium	Agilent®
DMEM Assay medium Pack (with Glucose, Pyruvate and GlutaMax)	Agilent®
Cell Mito Stress Test Kit	Agilent®
Glycolysis Stress Test Kit	Agilent®
XFe96 Cell Culture Plate	Agilent®
XFe96 Sensor Cartridges	Agilent®

2.6.1 Mitostress Assay:

Seeding and activation parameters for the seahorse assay were similar to those of the Cytokine measurement assay, although this time cells were seeded in XFe96 plates provided for the assay by Agilent. Mitostress was performed to measure mitochondrial OXPHOS in resting macrophages. The assay utilizes Oligomycin, FCCP, and Rotenone/AA as modulators of the mitochondrial ETC (Electron Transport Chain) to evaluate various parameters related to OXPHOS. These drugs were loaded in multiple sensor cartridge ports that sit over the 96-well plate in the XFe96 Seahorse analyzer and microinjected sequentially to perform the assay.

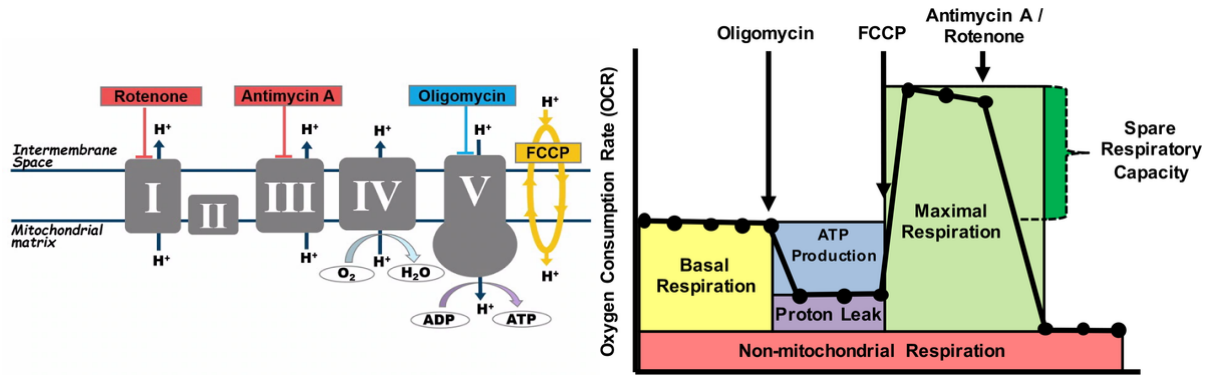

Figure 10. a. Agilent Seahorse Cell Mito Stress Test Modulators of Electron Transport Chain. b. Critical parameters of the mitochondrial function evaluated after ETC modulation. Adopted from Agilent®

Oligomycin inhibits ATP synthase (complex V) and was injected first in the assay following basal measurements. It decreases electron flow through the ETC, reducing mitochondrial respiration or Oxygen Consumption Rate (OCR). This decrease in OCR is linked to cellular ATP production. Carbonyl cyanide-4 (trifluoromethoxy) phenylhydrazone (FCCP) is an uncoupling agent that collapses the proton gradient and disrupts the mitochondrial membrane potential. It was injected following Oligomycin. As a result, electron flow through the ETC is uninhibited, and oxygen consumption by complex IV reaches the maximum. The FCCP-stimulated OCR can then be used to calculate spare respiratory capacity as the difference between maximal and basal respiration. Spare respiratory capacity is a measure of the ability of the cell to respond to increased energy demand or under stress. As a third injection, a mixture of rotenone, a complex I inhibitor, and antimycin A, a complex III inhibitor, was applied. This combination shuts down mitochondrial respiration and enables the calculation of non-mitochondrial respiration driven by processes outside mitochondria.

To perform the assay overnight, the sensor cartridge should be hydrated in Seahorse XF Calibrant at 37 °C in a non-CO2 incubator. The assay medium was prepared by supplementing Seahorse XF DMEM or RPMI medium with 1 mM pyruvate, 2 mM glutamine, and 10 mM glucose. The assay medium was warmed to 37 °C in a water bath. The same medium was used to dissolve ETC modulators; the working concentration for Oligomycin was 1.5 μM, FCCP 1 μM, and Rotenone/AA 0.5 μM, although the concentration prepared to be loaded in the sensor cartridge port is 10X. Seahorse XF Cell Culture Microplates were removed from the 37 °C CO_2 incubator, and the cells were examined under a microscope to confirm confluence. The assay medium was removed from the water bath. The cell culture growth medium in the

cell culture microplate was changed to a warmed assay medium using a multichannel pipette, and the cell culture microplate was placed into a 37 °C non-CO_2 incubator for 45 minutes to 1 hour prior to the assay. The assay was performed using the seahorse XFe96 analyzer machine, a method described in the URL in detail:

https://www.agilent.com/cs/library/usermanuals/public/XF_Cell_Mito_Stress_Test_Kit_User_Guide.pdf

2.6.2 Glycolysis Stress Test Assay:

Glycolysis Stress Assay was performed similarly to Mitostress assays, although with various modulations.

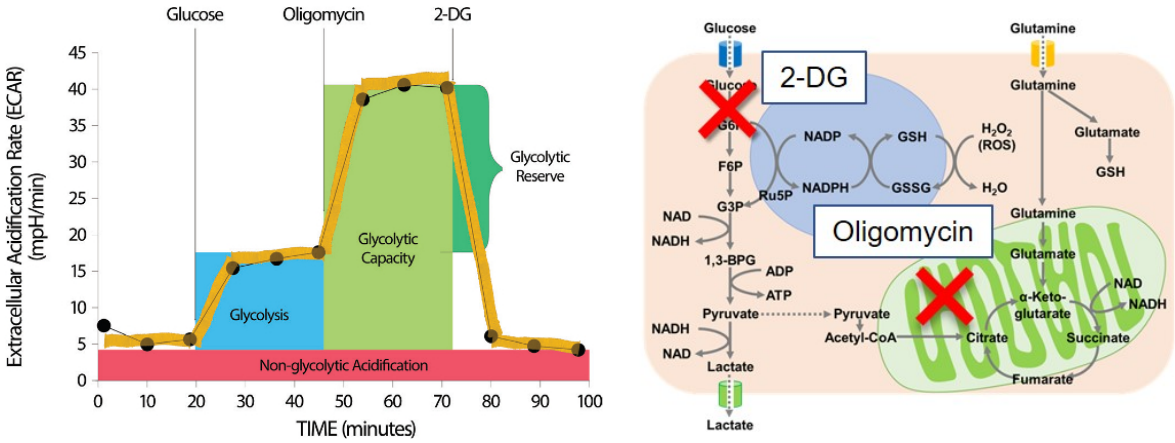

Figure 11: a. The Agilent Seahorse XF Glycolysis Stress Test profiles the essential parameters of glycolytic function. Sequential injections of compounds measure glycolysis and glycolytic capacity, enabling the calculation of glycolytic reserve and non-glycolytic acidification (Source: Agilent) b. The Agilent Seahorse XF Glycolysis Stress Test Modulators of Glycolysis diagram depicts a simplified version of glycolysis and highlights the sites of action of the kit components. Glucose serves as the fuel for glycolysis. Oligomycin inhibits ATP synthase in the mitochondria, leading to an increased reliance on glycolysis. 2-DG acts as a competitive inhibitor of glucose, effectively shutting down glycolysis. Adopted from Agilent®

One difference between the Glycolysis stress test and the Mito-stress test is that the former's medium initially lacks glucose, and cells are incubated in the glucose-free medium for at least one hour to stop glycolysis. This allows for the measurement of real-time glycolysis with the first injection of glucose. The final concentrations are 10 mM for glucose, 1 μM for

Oligomycin, and 50 mM for 2-DG, all loaded into the ports of sensor cartridges at 10X concentration.

A detailed protocol is provided in the URL below:

https://www.agilent.com/cs/library/usermanuals/public/XF_Glycolysis_Stress_Test_Kit_User_Guide.pdf

2.7 Inflammasome measurement:

Reagent	Manufacturer/Supplier
FAM-FLICA caspase Assay®	Biorad
6 well cell culture plate	Greiner
Micro-centrifuge tubes	Eppendorf

The inflammasome, previously described in the introduction chapter, is a multiprotein complex that mediates the activation of Caspase-1, IL-1β secretion, and the signature of macrophage activation. To analyze inflammasome activation, FAM-FLICA© dye was used. FLICA, or Fluorescence Labelled Inhibitor of Caspase, is a cell-permeable compound that efficiently diffuses in and out of all cells. An active caspase enzyme inside the cell (in this case, Caspase 1) will covalently bind with FLICA and retain the green fluorescent signal within the cell. Unbound FLICA usually diffuses out of the cell during the wash steps. Each FLICA probe contains a 3 or 4 amino acid sequence targeted by activated caspases. This target sequence is sandwiched between a green fluorescent label, carboxyfluorescein (FAM), and thus, cells fluoresce brighter than healthy cells.

FAM-FLICA caspase assay was performed to assess Caspase-1 activity according to the manufacturer's protocol provided in the URL (https://www.bio-rad-antibodies.com/static/uploads/ifu/ict096.pdf). Briefly, $1x10^6$ macrophages were cultured on to a 6-well plate and stimulated with 50ng/mL LPS for 8 h. Using a cell scrapper, the cells were taken off from the plate and centrifuged at 300 x g for 6 min. To make a stock concentration of 150X, FAM-FLICA was dissolved in 50 μl DMSO. Before use, a 30X working concentration of FAM-FLICA was prepared by diluting the stock solution (1:5) in PBS. Further, cells were stained with 145 μL of 30X FAM-FLICA in FACS tubes, incubated for 30 min at 37°C, 5% CO_2 incubator, and tubes were protected from light. After incubation, cells were washed with 2 ml 1x

apoptosis wash buffer and again centrifuged at 300 x g for 6 min. Cells supernatant were discarded and the cell pellet was re-suspended in 150 µl FACS buffer. Unstained cells served as a negative control and stained cells heated at 65°C for 20 min were used as a positive control. Cells were acquired using BD FACSCanto II flow cytometer. FAM-FLICA positive cells were further quantified using FlowJo.

2.8 Peritoneal Macrophage Culture and Labeling:

To assess Peritoneal Macrophages (*in vivo* differentiated macrophages), macrophages were isolated from the peritoneal cavity of control and PMCA1-cKO mice. For this, mice were euthanized in a CO_2 chamber, and the peritoneal cavity was filled with 5 mL 1X PBS with 5% Fetal Calf Serum and gently shaken. Using a 1 mL pipette, the medium was sucked out from the cavity and transferred into 15 mL falcon tubes. RBCs were lysed using erythrocyte lysis buffer (0.01 M $NaHCO_3$, 0.155 M NH_4Cl and 0.1 M EDTA) for 3 min at RT. The cells were then spun in a centrifuge at 300 x g for 6 min and washed with 1X PBS before counting and labeling with antibodies.

For flow cytometric measurements, $1x10^6$ peritoneal macrophages were used. Before labeling, cells were blocked with 20 µL Fc block solution for 20 min at 4°C. A cocktail of surface-staining antibodies was prepared in FACS buffer. For surface staining following anti-mouse antibodies were used:

Antibodies	Supplier/Manufacturer
CD11b APC-Cy7 clone M1/70	Biologend®
MHC class II PE-Cy7 clone AF6-120.1	Biologend®
CD86 V450	Biologend®
CD19 FITC	Biologend®
TCRβ FITC	Biologend®
Zombie Aqua™ dye	Biologend®

For compensation, Fluorescence minus one (FMO) control was used. Cells were stained with 50 µL of antibody cocktail in FACS tubes and incubated in the dark for 30 min at 4°C. Cells were washed with 1X PBS, resuspended in 150 µL FACS buffer and acquired by BD FACSCanto II flow cytometer. The analysis and quantification of surface expression were performed using FlowJo.

2.9 Lactate Assay:

The Lactate Assay using the Promega Lactate-Glo® assay kit was performed to quantify lactate both intra- and extracellularly (secretion in the medium as a by-product of glycolysis). Cells were seeded in a 96-well plate with a cell density of 50000/well. Cells were primed for 6 hours with IFNγ (150 U/mL) followed by overnight addition of LPS (50 ng/mL) incubation, with concentrations previously used. Before the experiment, the medium was pipetted in a fresh 96-well plate (this medium was used for measuring extracellular lactate), and cells were washed with chilled 1X PBS three times. 12.5 μL of 0.6N HCl was used to lyse the cells and later 12.5 μL of neutralizing solution (24.6 Trizma© base powder dissolved in 200 mL of water and pH 10.6) was added. The volume is made up to 50 mL by adding 1X PBS. The lysate is ready to be used with the Promega Lactate-Glo® assay kit. Kit components are provided in the URL, along with a detailed protocol.

https://www.promega.de/products/energy-metabolism/metabolite-detection-assays/lactate-glo-assay/?gad_source=1&gclid=CjwKCAjwwr6wBhBcEiwAfMEQsyu9erc_mrbjVgsqPxKnl_pg4-4sxS19eYGp_VRWVzFS99GhFEkarxoCX7QQAvD_BwE&catNum=J5021

For measuring extracellular lactate, the medium is diluted 1:50 in 1X PBS. For each well, 50 mL of a detection reagent is prepared. A 1:1 proportion of sample and lactate detection reagent is mixed and incubated at room temperature, shielded well from the light. The plate reader can read it directly with the optimum setting. Alongside samples, a standard curve is also prepared for quantifying the absolute amount of lactate with concentrations between 0 μM and 200 μM.

2.10 RNA extraction and RNA sequencing:

The RNeasy® Mini protocol (QIAGEN) for RNA extraction from cells was followed as described below:

Cells were seeded in a 6-well plate with a cell density of $1X10^6$ cells/well. Cells were polarized with a cocktail of IFNγ (150U/mL) and LPS (50ng/mL) for 4 hours. Cells were thoroughly washed in chilled 1X PBS buffer. 300 μL RLT buffer containing β-mercaptoethanol (10 μL of

per ml of RLT buffer) was added to the cells directly in the well. The mixture was gently vortexed or pipetted up and down to ensure thorough mixing. 300 µL of 70% ethanol was added to the homogenized lysate. The mixture was mixed well by pipetting. 600 µL of the sample, including any precipitate, was applied to a RNeasy column sitting in a 2 ml collection tube. It was spun for 30 seconds at 10,000 rpm. If the volume exceeded 700 µL, aliquots were successively loaded onto the RNeasy column and centrifuged again. The collection tube was reused, but the flow-through was discarded. 700 µL of Buffer RW1 was pipetted onto the RNeasy column and centrifuged for 30 sec at 14,000 rpm (once it reached the proper speed) to wash. The RNeasy column was transferred into a 2 mL collection tube. 500 µL Buffer RPE was pipetted onto the column, which was then centrifuged for 30 sec at 14,000 rpm to wash. The flow-through was discarded, and the collection tube was reused. 500 µL Buffer RPE was pipetted onto the RNeasy column. It was centrifuged for 2 min at 14.000 rpm to dry the RNeasy membrane. The spin column was placed in a new 2 mL or 1.5 mL collection tube and spun at 14,000 rpm for 1 minute. The RNeasy column was transferred into a new 1.5 mL collection tube, and 30 µL of RNAse-free water was pipetted directly onto the RNeasy membrane. It was centrifuged for 1 minute at 14,000 rpm to elute. The samples were frozen at -70°C and packed in dry ice before being transported to a collaboration partner at HZI Braunschweig for sequencing.

Quality and integrity of total RNA were controlled on Agilent Technologies 2100 Bioanalyzer (Agilent Technologies; Waldbronn, Germany). The RNA sequencing library was generated from 1000 ng total RNA using Dynabeads® mRNA DIRECT™ Micro Purification Kit (Thermo Fisher) for mRNA purification followed by NEBNext® Ultra™ II Directional RNA Library Prep Kit (New England BioLabs) according to the manufacturer's protocols. The libraries were sequenced on Illumina NovaSeq 6000 using NovaSeq 6000 S1 Reagent Kit (100 cycles, paired-end run) with an average of 5 $x10^7$ reads per RNA sample. Each FASTQ file gets a quality report generated by the FASTQC tool. Before alignment to the reference genome, each sequence in the raw FASTQ files was trimmed on base call quality and sequencing adapter contamination using fastq-mcf. Reads shorter than 15 bp were removed from the FASTQ file. Trimmed reads were aligned to the reference genome using the open-source short-read aligner STAR. A detailed methodology of data preprocessing and data normalization, along with various

spreadsheet files containing raw counts, normalized count per million, and differential expression of gene analysis, has been provided in the following URL.

file:///Users/nikhiltiwari/Desktop/23-0228-4/RNA_Seq_Report.html

Customized data visualization and further processing were done using R (scripts available in Bioconductor, open source), KEGG database, iDEP .96 and Shiny GO with URL provided (http://bioinformatics.sdstate.edu/idep96/) , (https://bioinformatics.sdstate.edu/go/) and Prism.

3. Results:

3.1 Nptn-KO macrophages display profound changes in PMCA and Basigin levels:

It has been shown previously that Neuroplastin acts as a stabilizing interaction partner of PMCAs in neuronal and non-neuronal cells, including macrophages (Korthals et al., 2017). In this work, this finding was re-visited by western blot assessment of PMCA expression in BMDM from *wild type* (*C57BL6*, hereupon referred to as *WT*) and constitutive *Nptn* KO mice or *Nptn*$^{-/-}$, complemented by the inclusion of IFNγ/LPS-stimulated BMDM from either genotype. To quantify total PMCA, a panPMCA antibody that recognizes all isoforms (i.e., PMCA1 and 4 in BMDM) was applied. Alongside, antibodies against Neuroplastin, its paralog Basigin, and iNOS, a marker for M1 polarization, were used in the analysis.

i) ii)

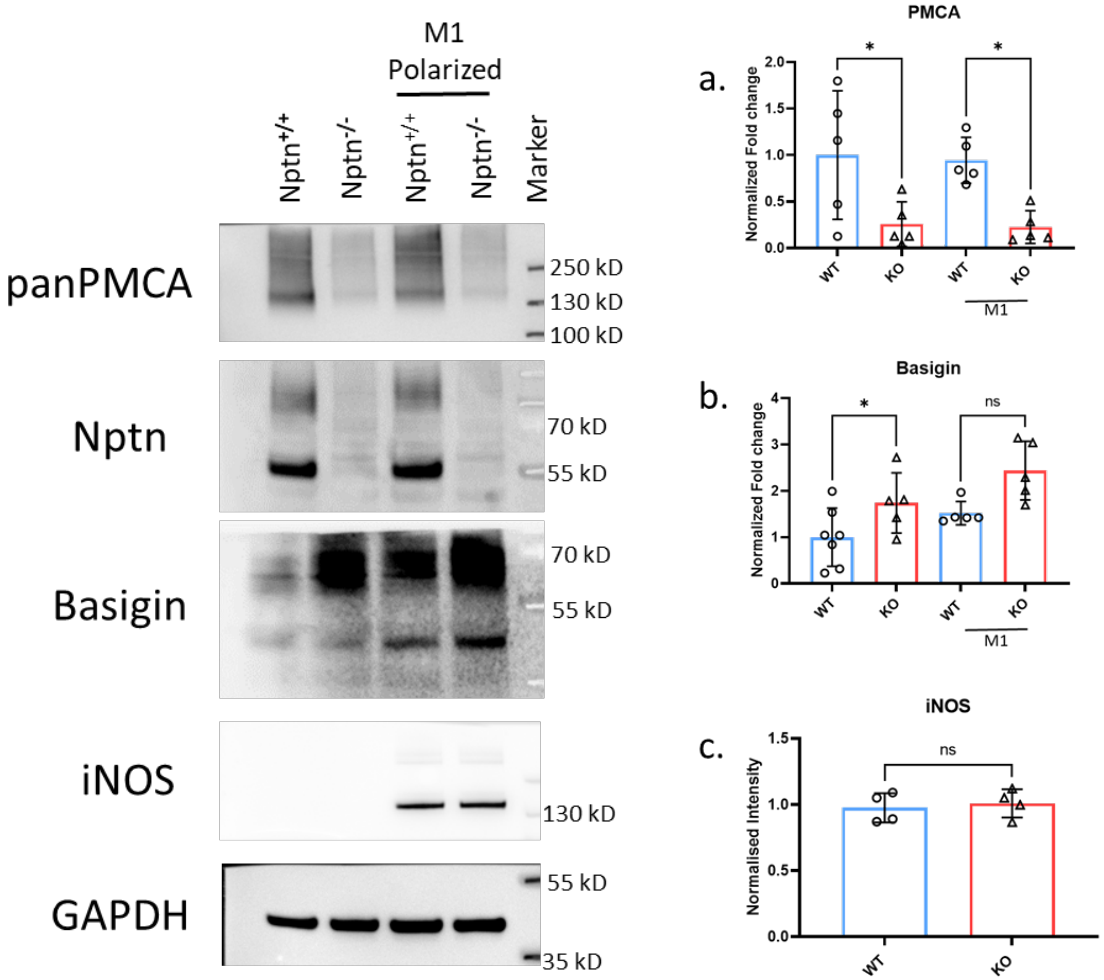

Figure 12: Expression of PMCAs, Neuroplastin, Basigin, and iNOS in *WT* and *Nptn*$^{-/-}$ BMDM before and after stimulation. (i) Image depicting unstimulated & IFNγ/LPS stimulated macrophages leading

to M1 polarization. Representative western blots probed for proteins as indicated. GAPDH immunoreactivity was used for normalization. Bands detected with anti-panPMCA span a range above the predicted MW (~ 135 kD) to > 250 kD. Detection of Neuroplastin reveals two major bands at 55 and 100 kD. Notably, both bands represent glycosylated variants of the shorter splice isoform Np55 (Korthals et al., 2017; Langnaese et al., 2024). Similarly, Basigin immunoreactivity splits into several bands, likely representing variations in glycosylation and/ or splicing. ii) Densitometric quantification of immunoreactive bands (N=4,5 for each protein; a. panPMCA; b. Basigin c. iNOS after stimulation (for a. and b. One way ANOVA was performed, and for c. t-test was performed for the test of statistical significance ns- non-significant, $*$ ≤ 0.05).

As expected, PMCA levels were found to be profoundly reduced in *Nptn*$^{-/-}$ macrophages as compared to *WT*. In contrast, Basigin levels were clearly elevated in the *Nptn*$^{-/-}$ macrophages (compared to *WT*: 241% or 204% before and after stimulation, respectively), presumably representing a compensatory effect that allows maintain some PMCA in the absence of Neuroplastin (Schmidt et al., 2017). Of note is that neither Neuroplastin nor PMCA levels showed a noticeable change in expression upon stimulation. This contrasts with earlier findings, where both proteins are significantly upregulated upon T cell receptor stimulation (Korthals et al., 2017). iNOS induction implied successful stimulation for both *WT* and *Nptn*$^{-/-}$, but there was no discernible difference between them. Basigin levels were increased in both genotypes following M1 polarization. However, the relative difference between Basigin levels in *WT* versus *Nptn*$^{-/-}$ remained apparent. The question of whether increased Basigin levels result from transcriptional upregulation or altered protein turnover will be addressed in Figure 40.

3.2 Neuroplastin-deficient macrophages display moderate effects on intracellular Ca^{2+}:

Given the severe reduction of PMCA in the absence of Neuroplastin, possible consequences for Ca^{2+} handling in macrophages were next addressed by a ratio metric Ca^{2+} measurement approach. To this end, BMDM were loaded with FuraRed and Fluo8 and subjected to FACS to measure baseline levels of free cytosolic Ca^{2+} ($[Ca^{2+}]_{cyt}$) for 2 minutes. This was followed by an assessment of Ca^{2+} levels in the endoplasmic reticulum (ER) after an irreversible inhibition of SERCA, which leads to the emptying of ER-Ca^{2+} into the cytosol.

a.

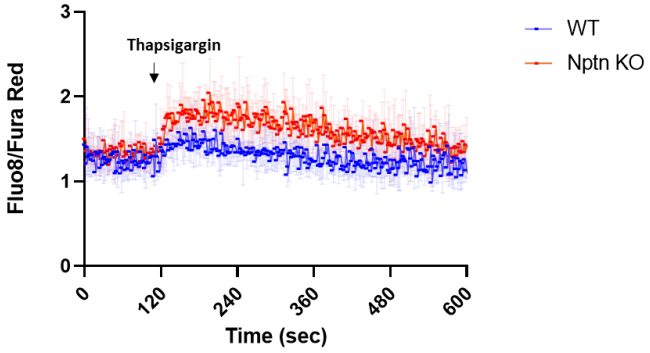

b.

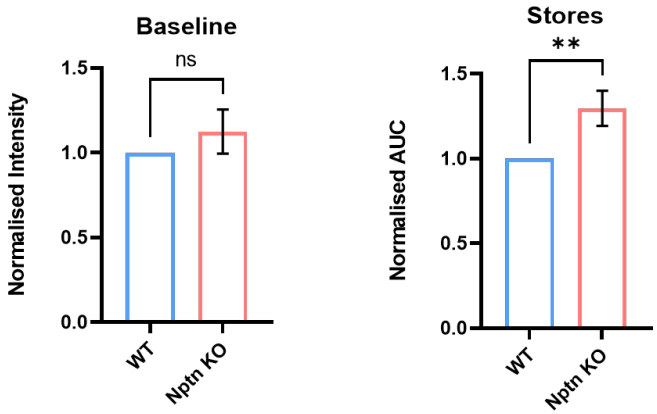

Figure 13: Ratio metric Ca^{2+} measurement of *WT* and *Nptn*$^{-/-}$ BMDM using FACS. a. Temporal profile of $[Ca^{2+}]_{cyt}$, monitored in the absence of extracellular Ca^{2+} for 2 minutes before and 8 minutes after the addition of the SERCA inhibitor Thapsigargin (1 µM). b. Quantification of Baseline and Store Ca^{2+}, the latter was quantified by determining the area under the curve (AUC), starting at 2 min., providing a read-out for ER-stored Ca^{2+} prior the SERCA inhibition. (ns- non-significant, ** ≤ 0.01, N=4, t-test).

As evident from Fig.13, *Nptn*$^{-/-}$ and *WT* BMDM displayed virtually the same free $[Ca^{2+}]_{cyt}$ level in baseline conditions. The Thapsigargin-treatment, however, revealed a significantly increased level of ER-Ca^{2+} for *Nptn*$^{-/-}$ versus *WT* BMDM. It may be speculated that this ER-Ca^{2+} overload could affect signaling in certain conditions.

3.3 Canonical signaling pathways remain unaffected in the absence of Neuroplastin:

M1 polarization of macrophages can be achieved through stimulation with IFNγ and LPS, which signal through well-established signaling pathways that lead to the activation of factors that control transcription, most notably STAT1, NF-κB, and ERK1/2 (Yunna et al., 2020) with the latter also affecting post-translational events. The activation of these proteins is typically brought about by phosphorylation of specific residues. To assess signal transduction

downstream of IFNγ alone, the phosphorylation of STAT1 on Tyr701 (pSTAT1), which fosters its dimerization and nuclear translocation (Platanias, 2005) was monitored before and after stimulation at different time points. Western blot analysis revealed peak levels of pSTAT1 between 15 and 30 minutes after stimulation. Quantification did not reveal significant differences between *WT* and *Nptn*$^{-/-}$ BMDM.

a. b.

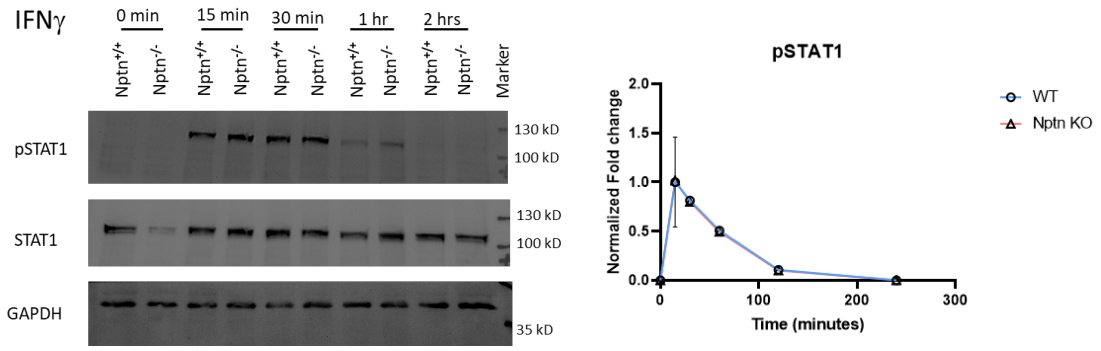

Figure 14 : Time course of IFNγ -induced STAT1 phosphorylation on Tyr701 in *WT* and Nptn$^{-/-}$ BMDM. (a.) Representative blots successively stained for pSTAT1 and total STAT1. GAPDH1 immunoreactivity was used as a loading control. (b.) Quantitative representation of densitometric quantifications based on N=3 blots. Total STAT1 intensities were used for the normalization of pSTAT1 intensities.

To further test *Nptn*$^{-/-}$ BMDM for possible abnormalities in signaling downstream of LPS stimulation, BMDM were subjected to western blot detection of NF-κB phosphorylated on Ser536 and ERK1/2, phosphorylated on Thr402/Tyr404. Like pSTAT1, phosphorylation of NF-κB or ERK1/2 leads to nuclear translocation of NF-κB or ERK1/2, respectively, clearly a prerequisite to exert their roles in gene expression. Again, phosphorylation was monitored before and after stimulation at several time points.

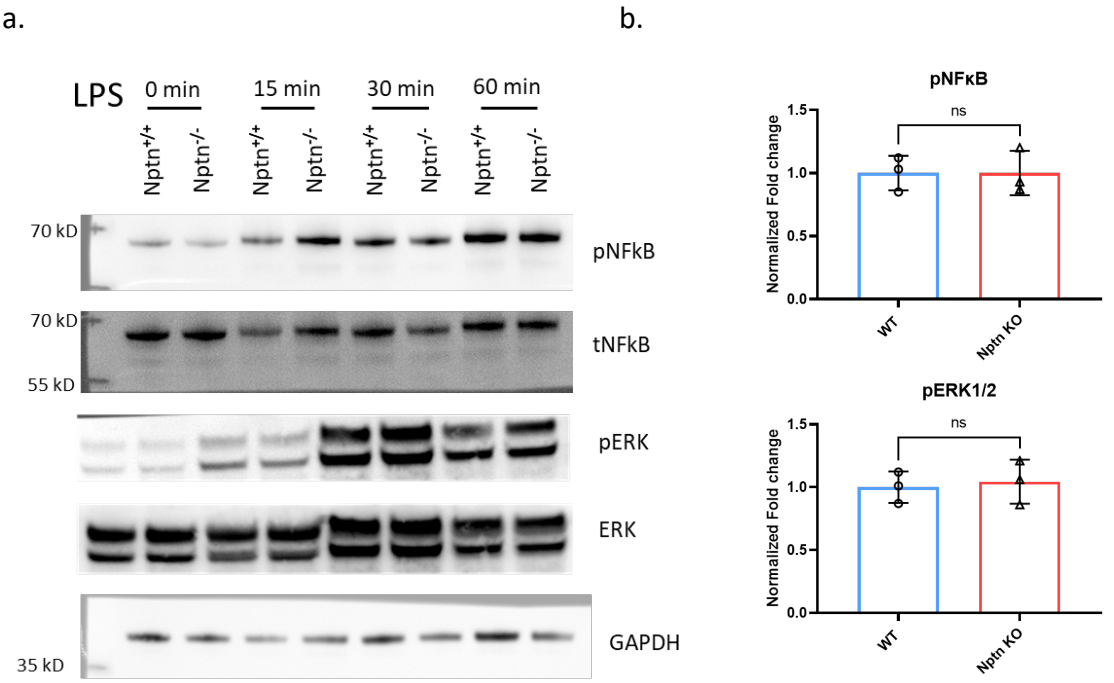

Figure 15: Time course of LPS-induced phosphorylation of NF-κB (pSer536) and ERK1/2 (pThr402, pTyr404) in *WT* and *Nptn*$^{-/-}$ BMDM. (a) Representative blots were successively stained for pNF-κB and total NF-κB or pERK1/2 and ERK1/2, respectively. GAPDH1 immunoreactivity was used as a loading control. (b) Quantitative representation of densitometric quantifications based on N=3 blots. The intensities for the phosphorylated forms were normalized to those of total NF-κB or pERK1/2, respectively at 15 minutes and 30 minutes, respectively.

As obvious from Figure 15, *Nptn*$^{-/-}$ BMDM did not display striking differences in NF-κB or ERK1/2 activation. This finding was corroborated by western blot analyses on macrophages differentiated from conditionally immortalized stem cell lines. Data from the analysis of this type of macrophage will be presented *en bloc* by the end of the results section. It thus seems that the moderately disturbed Ca^{2+} handling, as indicated by the overload of the ER-Ca^{2+} store, does not affect the canonical signaling pathways addressed here.

3.4 Cytokine measurements in *Nptn*$^{-/-}$ macrophages:

Despite the normal activation patterns of STAT1 NF-κB and ERK1/2, it cannot be ruled out that the altered Ca^{2+} handling associated with *Nptn*$^{-/-}$ impacts on the transcriptional and/ or post-transcriptional activity of these or yet other factors. The next approach was, therefore, to assess the downstream effects of macrophage activation. Macrophages produce and

release various cytokine signaling molecules to exert their crucial role in the immune response.

These cytokines act as messengers between cells, influencing their behavior and regulating immune responses. Understanding the regulation of cytokine secretion by macrophages is crucial for comprehending the immune response and developing therapeutic strategies for various diseases, including infections, autoimmune disorders, and inflammatory conditions.

Therefore, cytokine secretion was analyzed following combined stimulation by IFNγ and LPS by a Cytometric Bead Analysis (CBA) approach, which allows parallel assessment of multiple cytokines by FACS.

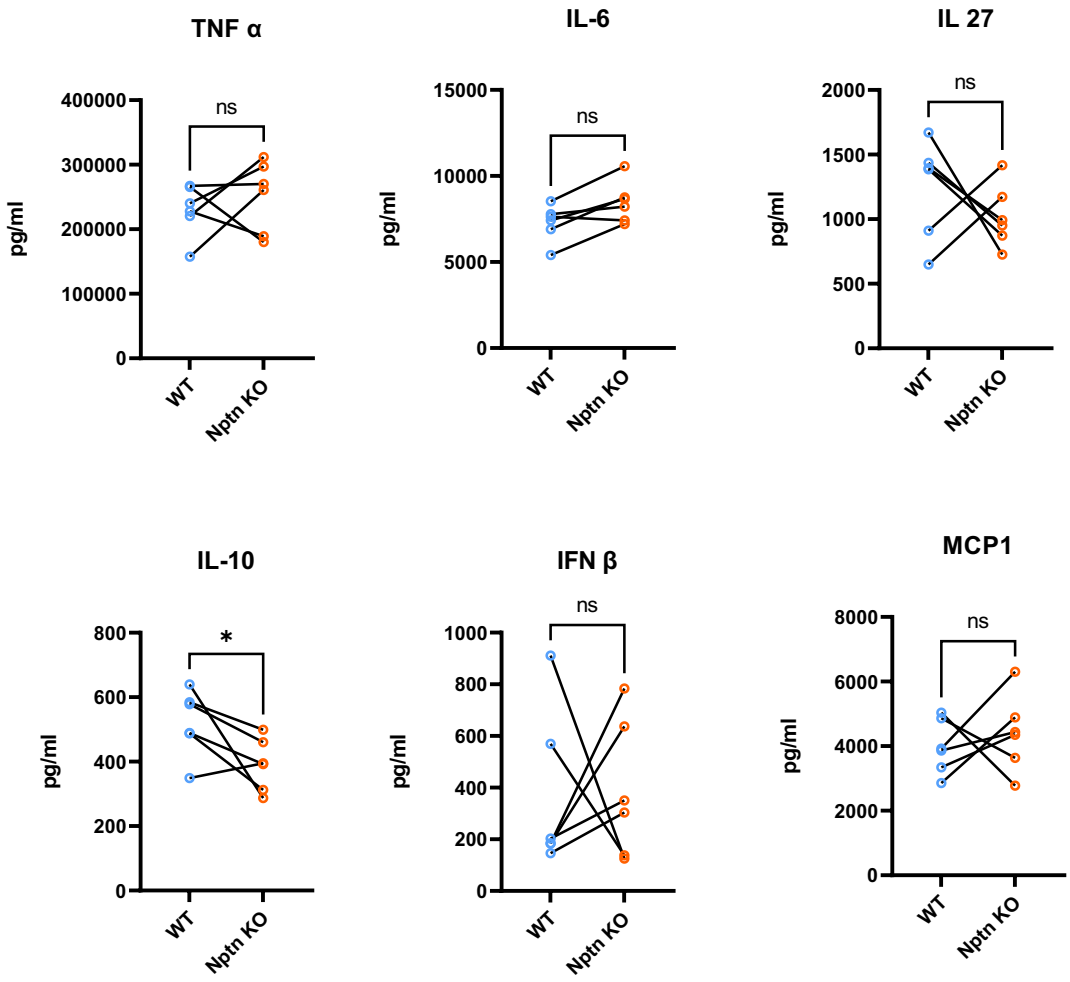

Figure 16: CBA analysis of typical cytokines produced by M1-polarized macrophages, comparing *WT* and *Nptn*$^{-/-}$. Results are from 5 or 6 biological replicates, each carried out with BMDM derived from a pair of one *WT* and one *Nptn*$^{-/-}$ mouse. Values for each such pair are connected by a line. Data points represent the mean value of 3 technical replicates. (ns = non-significant, * = p ≤.05, t-test).

For virtually all cytokines, this analysis showed strong inter-individual variation for both genotypes and consequently did not reveal significant differences between them, except for IL-10. This cytokine, considered anti-inflammatory and expressed at low levels, was found to be moderately reduced in the *Nptn*$^{-/-}$ BMDM.

3.5 Phagocytosis:

Phagocytosis is a functional hallmark of macrophages and was therefore evaluated in both *WT* and *Nptn*$^{-/-}$ using fluorescent beads, where both *WT* and *Nptn*$^{-/-}$ were incubated with fluorescent latex beads (Caymen Chemicals Limited) with 1:500 dilution.

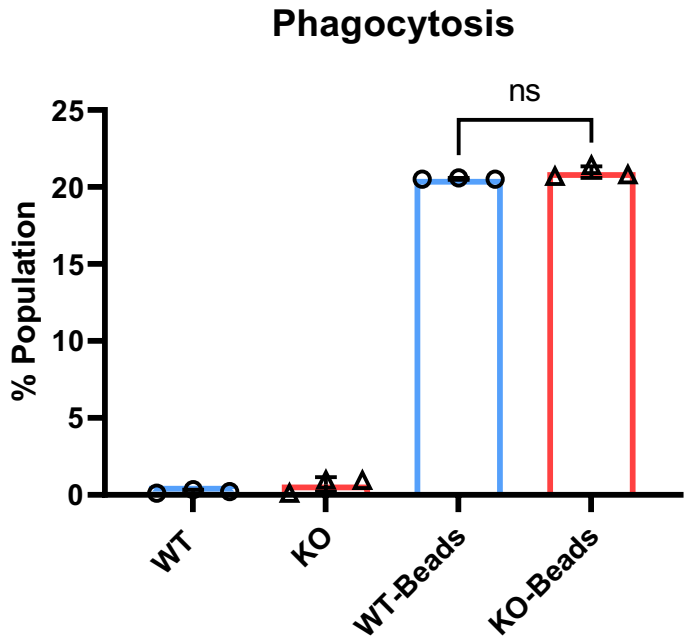

Figure 17: Phagocytosis bead assay performed on *WT* and *Nptn*$^{-/-}$ BMDM. Cells untreated with beads were used as a negative control. One-way ANOVA was used to test for statistical significance (ns, non-significant).

WT and *Nptn*$^{-/-}$ are not distinct in phagocytosis. The percentage of population cells positive for fluorescent beads after 3 hours of incubation does not differ.

3.6 PMCA1 in BMDM:

In summary, the above-presented data revealed mild primarily or even no phenotypes associated with loss of Neuroplastin in M1-polarized macrophages. Given the severe

reduction of PMCAs in macrophages, this could mean that Ca^{2+} handling by PMCA is hardly relevant for M1 polarization or that the remaining ~20% of PMCA expression is sufficient to warrant respective macrophage functioning. This raises the question of whether a complete lack of one or both PMCAs (isoforms 1 and 4) would affect macrophages. Transcriptomic data from the Immunological Genome Project (www.immgen.org) database reveal that PMCA1 is the predominant isoform in various subpopulations of macrophages (**Figure. 18**).

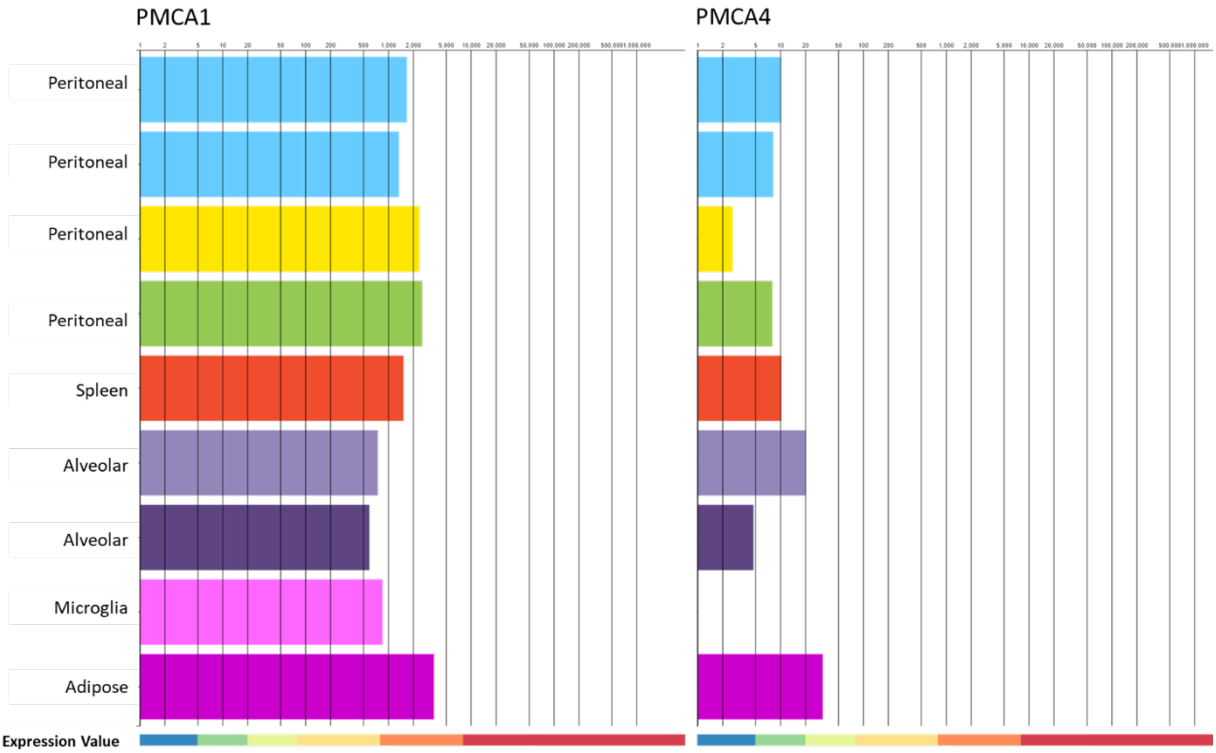

Figure 18: Expression levels of PMCA1 and PMCA4 in various macrophage populations. The vertical lines show the expression value normalized by Differential Expression Analysis (DESeq2) in increasing order (for example, 0, 2, 5, 10, 50, 100, 200, 500, 1000, and so on).

The recently introduced, inducible knock-out line *PMCA1*$^{fl/fl}$ (Beckmann et al., 2023) was employed to delete *Pmca1* specifically in macrophages by crossing it to a LysM Cre line. *Pmca1*$^{fl/fl}$ mice without LysM Cre served as controls (also represented as PMCA1$^{+/+}$ and *WT*). Western blots on BMDM confirmed efficient Cre-mediated KO (cKO) and aligned with the Immgen data, as loss of PMCA1 abolished almost all pan PMCA immunoreactivity. As for *Nptn*$^{-/-}$ (Figure 12), antibodies against Neuroplastin, Basigin, and iNOS were included in the analysis (Figure 19). Moreover, both resting and stimulated macrophages were analyzed.

a.

b.

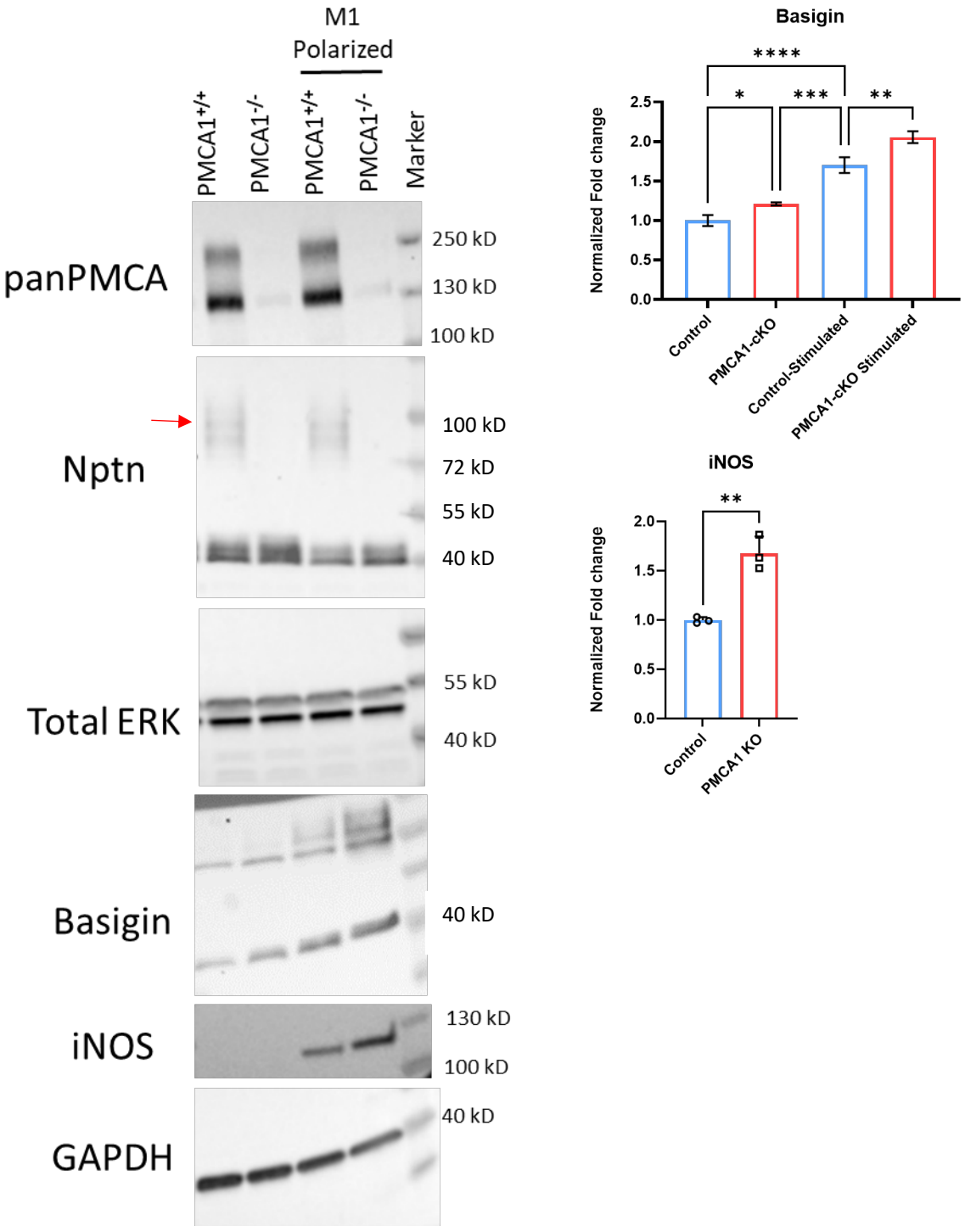

Figure 19: Expression of PMCAs, Neuroplastin, Basigin, and iNOS in *WT* and *PMCA1* cKO macrophages before and after IFNγ /LPS stimulation (a) Western blots on BMDM, representative for 4 biological replicates. Upon loss of PMCA1, very little pan PMCA immunoreactivity is left, indicating that PMCA4 is expressed at low levels only. Note the loss of the >100 kD band for Neuroplastin in the PMCA1-cKO samples and enhanced post-stimulation up-regulation of Basigin and iNOS in PMCA1-cKOs. (b) Densitometric Quantification of Western blots of Basigin and iNOS. Total ERK and GAPDH served as

loading controls for normalization of PMCA and Neuroplastin or iNOS and Basigin, respectively (N=4, t-test for iNOS and ANOVA for Basigin quantification, ns = non-significant, * = p ≤.05, ** = p ≤.01, *** = p ≤.001) The images were quantified with FIJI.

3.7 Calcium Measurement in *PMCA1*-cKO BMDM:

As the western blot approach on PMCA1-cKO BMDM revealed a clearly more severe reduction in total PMCA levels as compared to *Nptn*$^{-/-}$ (Figure 12), a stronger dysregulation of Ca^{2+} homeostasis may be anticipated. This hypothesis was addressed by ratio-metric Ca^{2+} measurement using FACS (Figure 20), following a diversified protocol that, compared to the one described in Figure 13, includes an additional step to assess SOCE and subsequent Ca^{2+} clearance from the cytosol. Specifically, after monitoring $[Ca^{2+}]_{cyt}$ in Ca^{2+}-free medium before and after Thapsigargin treatment, cells were supplied with a medium containing 2 mM Ca^{2+} for 2 minutes (check) to trigger Ca^{2+} entry via CRAC channels. Chelation of Ca^{2+} was then used to stop Ca^{2+} entry and to observe clearance.

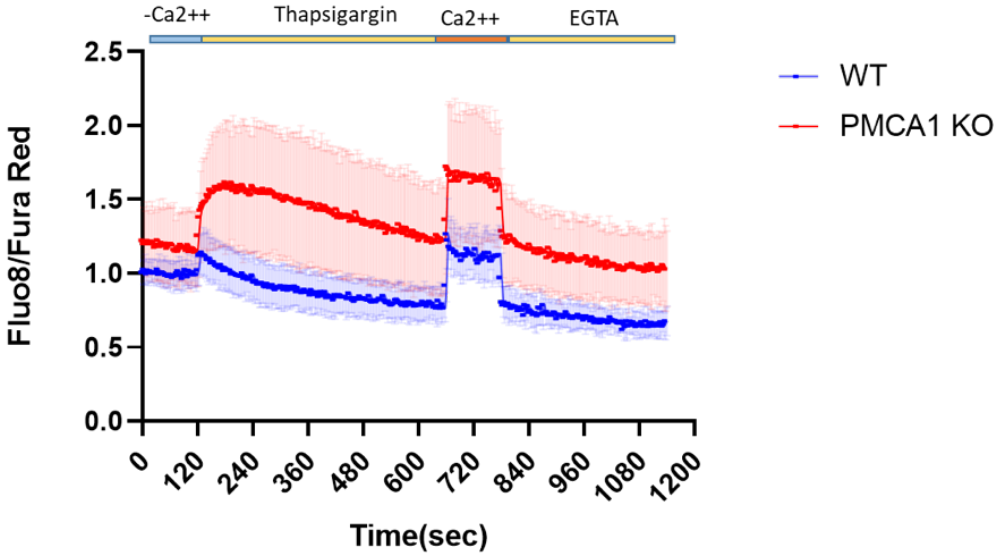

Figure 20: Ratio metric Ca^{2+} measurement of *WT* and *PMCA1*-cKO BMDM using FACS. Temporal profile of $[Ca^{2+}]_{cyt}$, monitored in the absence of extracellular Ca^{2+} ($[Ca^{2+}]_{ext}$) for 2 minutes before and 8 minutes after the addition of the SERCA inhibitor Thapsigargin (1 µM). $[Ca^{2+}]_{ext}$ was then raised to 2 mM for 2 minutes and again removed by EGTA to be monitored for 5 minutes. Note that initial peak levels after the initiation of SOCE are missed due to FACS-related handling constraints.

In contrast to unchanged baseline $[Ca^{2+}]_{cyt}$ in *Nptn*$^{-/-}$ BMDM, the *PMCA1*-cKO BMDM displayed an elevation of baseline $[Ca^{2+}]_{cyt}$ by almost 25% compared to controls. Moreover, ER Ca^{2+} overload as uncovered by Thapsigargin-induced raise in $[Ca^{2+}]_{cyt}$ was clearly much more

pronounced in the absence of PMCA1 than observed for *Nptn*$^{-/-}$. Both *WT* and *PMCA1*-cKO BMDM show SOCE, raising $[Ca^{2+}]_{cyt}$ by about the same degree relative to the respective pre-induction levels. Interestingly, the Ca^{2+} peak level elicited by Thapsigargin in the *PMCA1*-cKO BMDM exceeds the Ca^{2+} levels in control BMDM shortly after the triggering of SOCE (Figure 20). This suggests that in *PMCA1*-cKO BMDM, cytosolic Ca^{2+} signals due to IP_3R activation might entail responses like those downstream of SOCE in controls.

3.8 IFNγ and TLR4 Signaling in *PMCA1*-cKO BMDM:

The dysregulation of Ca^{2+} handling in BMDM lacking PMCA1 prompted the assessment of canonical signaling associated with M1 polarization, virtually as performed for *Nptn*$^{-/-}$ BMDM. Quantification of IFNγ-induced pSTAT1 levels did not reveal any difference between controls and the *PMCA1*-cKO, implying that this pathway is neither sensitive to the observed elevation of $[Ca^{2+}]_{cyt}$ nor to the striking ER Ca^{2+} overload (Figure 20).

a. b.

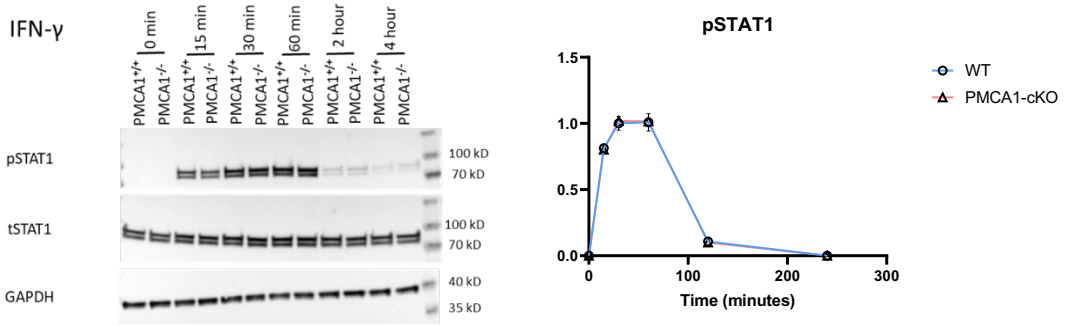

Figure 21: **Timecourse of IFNγ-induced STAT1 phosphorylation on Tyr701 in controls (*WT*) and *PMCA1*-cKO BMDM.** (a) Representative blots successively stained for pSTAT1 and total STAT1. GAPDH1 immunoreactivity was used as a loading control. (b) Quantitative representation of densitometric quantifications based on N=4 blots. Total STAT1 intensities were used for the normalization of pSTAT1 intensities.

Next, signaling downstream of LPS was assessed by probing western blots for the activation profiles of NF-κB and ERK1/2. In addition, phosphorylation of the non-receptor tyrosine kinase Akt on Ser473 occurs downstream of TLR4-mediated phosphatidyl inositol 3 kinase (PI3K) activation.

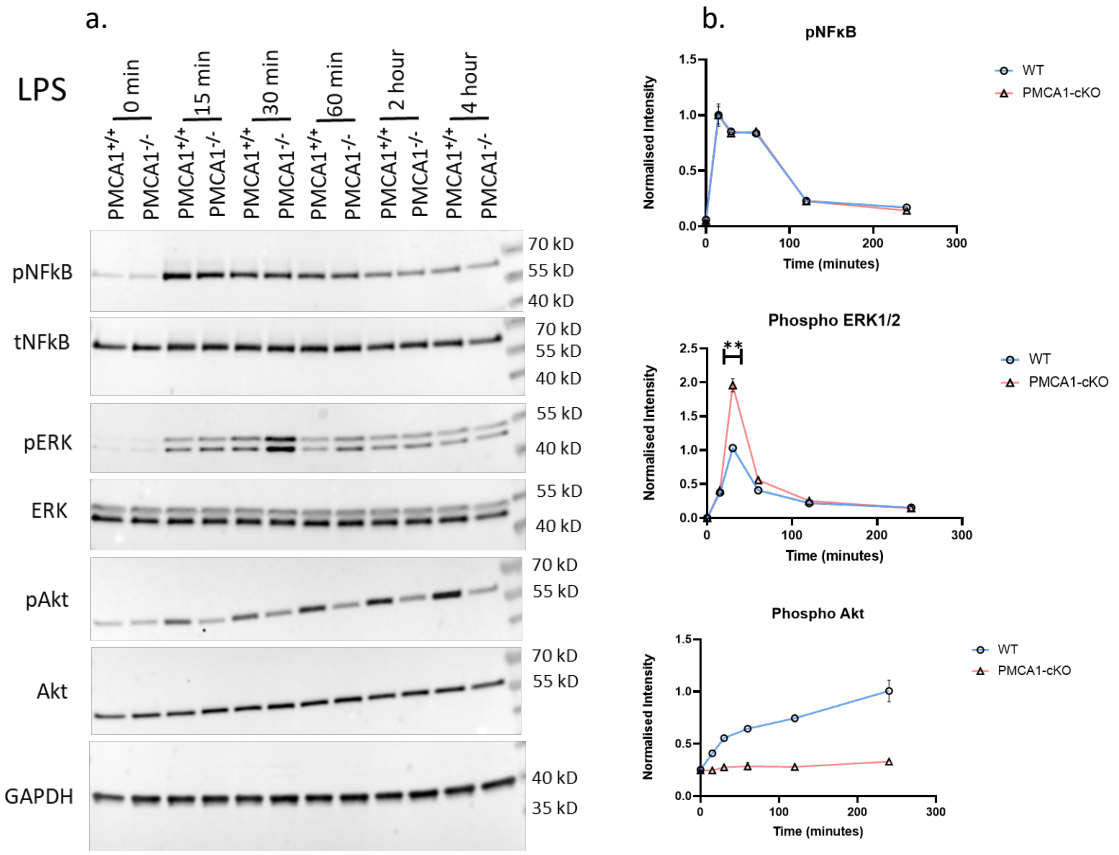

Figure 22: **Time course of LPS-induced phosphorylation of NF-κB (pSer536), ERK1/2 (pThr402, pTyr404) and Akt (pThr303) in controls (PMCA1$^{+/+}$) and *PMCA1*-cKO BMDM.** (a) Representative blots successively stained for pNF-κB and total NF-κB, pERK (phosphorylated ERK1/2) and ERK (total ERK1/2), and pAkt (phosphorylated Akt) and total Akt, respectively. GAPDH immunoreactivity was used as a loading control. (b) Quantitative representation of densitometric quantifications based on N=3 blots. The intensities for the phosphorylated forms were normalized to those of total NF-κB, ERK, and Akt, respectively. (N=3, paired t-test, ns = non-significant, ** = p ≤.01, Bars show Standard error of Mean) The images were quantified with FIJI.

The western blot analysis reveals that none of the addressed factors show pre-stimulation activation in the *PMCA1*-cKO BMDM. Moreover, the post-stimulation activation profile of NF-κB appeared unchanged in the absence of PMCA1. In contrast, ERK activation in the *PMCA1*-cKO BMDM clearly exceeded that in control BMDM 30 minutes after stimulation with LPS, and this effect was still apparent at 60 minutes. Before and after these time points there are no overt differences in pERK levels between the genotypes, indicating that *PMCA1*-cKO leads to a temporal rather than persistent hyperactivation of ERK. Interestingly, Akt activation as indicated by very slowly increasing levels of pAkt, was diminished in the *PMCA1*-cKO BMDM compared to controls at each time point. Thus, while the ~75% reduction of total PMCA in the *Nptn*$^{-/-}$ BMDM did not significantly affect the addressed pathways, a total loss of PMCA1 led to discernible changes in ERK1/2 and Akt activation.

3.9 Cytokine measurement in *PMCA1*-cKO BMDM:

To evaluate possible phenotypes associated with loss of PMCA1, cytokine release following IFNγ/LPS stimulation was addressed by CBA as delineated in Figure 23**.**

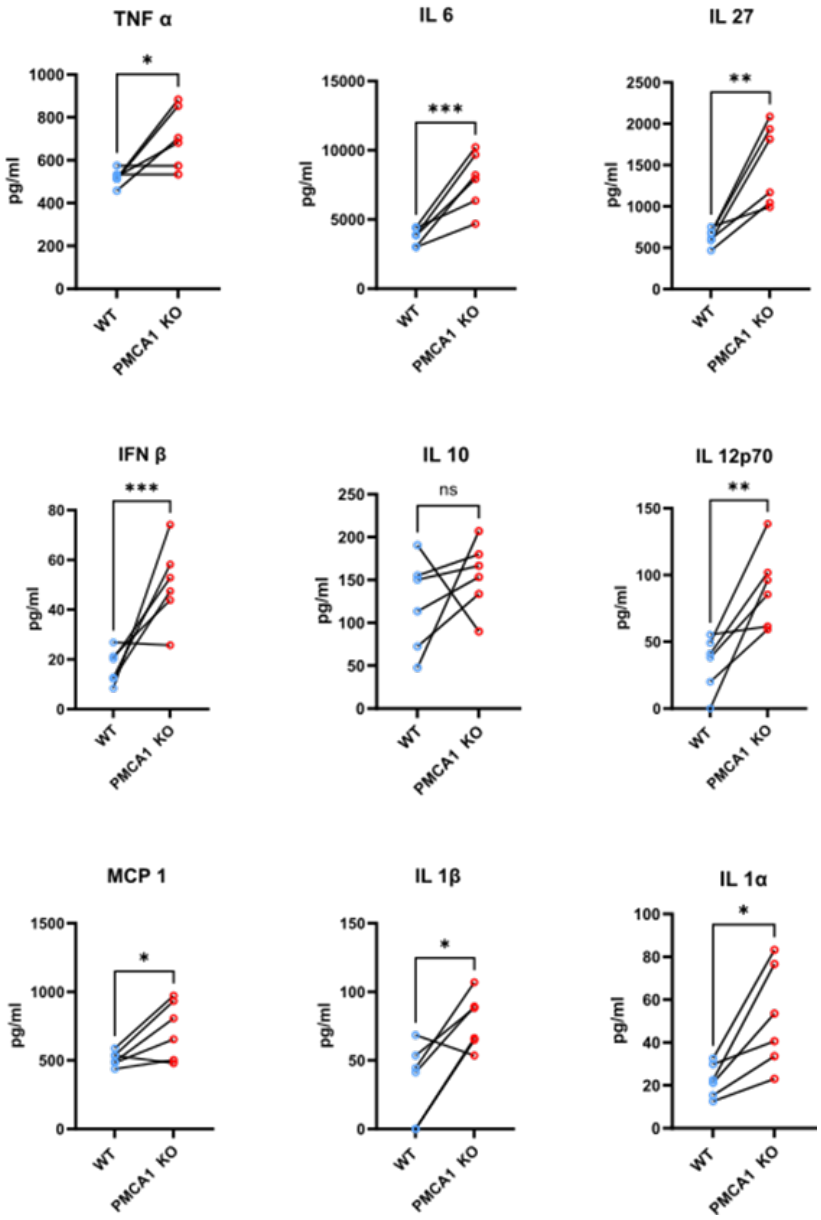

Figure 23: CBA analysis of typical cytokines produced by M1-polarized macrophages, comparing *PMCA1*-cKO and controls. Results are from 5 biological replicates, each carried out with BMDM derived from a pair of one control and one *PMCA1*-cKO mouse. Values for each such pair are connected by a line. Data points represent the mean value of 3 technical replicates. (ns = non-significant, * = p ≤.05, ** = p ≤.01, *** = p ≤.001 t-test).

CBA performed on *PMCA1*-cKO and control BMDM prior to stimulation revealed detectable amounts only for MCP-1. Except for IL10, every cytokine with a quantifiable amount within

the detection range showed significant upregulation in the *PMCA1*-cKO BMDM compared to controls. Such up-regulation of pro-inflammatory cytokines might result from the observed hyperactivation of ERK1/2 (Risco et al., 2012). It should be pointed out, however, that the latter was obtained already with LPS alone, whereas the above cytokine profile resulted from stimulation with both IFNγ and LPS, possibly leading to even more elaborate effects on signaling pathways.

3.10 FAM-FLICA Caspase Assay for Inflammasome Activation:

The principal effects of ERK1/2 phosphorylation during M1 polarization include priming and activating a protein complex known as inflammasome, which proteolytically processes IL1β, which can then be released from the macrophages. To assess the activation of the inflammasome, BMDMs were loaded with FAM-FLICA, a fluorescent reporter dye that is retained inside cells through covalent binding to inflammasome-activated Caspase-1. Without stimulation, about 10% of BMDM displayed an above-threshold fluorescence as determined by FACS, and there was no difference between the *PMCA1*-cKO and control BMDM. However, following stimulation with LPS, *PMCA1*-cKO BMDM showed a significantly increased inflammasome activity as compared to controls.

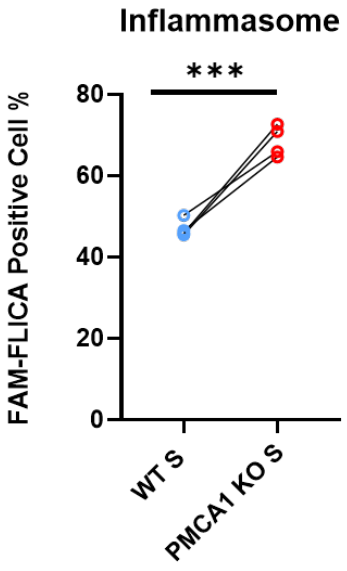

Figure 24: Inflammasome activity in BMDM after stimulation with LPS for 8 hours, revealed by FAM-FLICA fluorescence. An unpaired t-test has been performed to analyze statistical significance. (N = 4; ***: $p < 0.001$)

3.11 Metabolic phenotyping of *Nptn*$^{-/-}$ and *PMCA1*-cKO BMDM:

The shift between resting and proinflammatory states of macrophages involves changes at transcriptomic and proteomic levels, including cytokine profiles, and goes along with metabolic rewiring (Freemerman et al., 2014). The data presented so far indicate that loss of PMCA1 leads to excessive pro-inflammatory responses to respective stimuli, raising the question of whether this would be reflected at the level of metabolic parameters. On the other hand, loss of Neuroplastin showed largely normal M1 polarization as judged based on canonical signaling and cytokine release. However, it remained elusive whether this predicts normal metabolic performance as well. To address these questions, metabolic profiles for both *Nptn*$^{-/-}$ and *PMCA1*-cKO BMDM were acquired using Seahorse®, a metabolic flux analyzer that allows to monitor the extracellular acidification rate (ECAR) as a read-out for glycolytic activity and the oxygen consumption rate (OCR) as a measure for mitochondrial respiration, namely oxidative phosphorylation or OXPHOS (protocol described in Figure 10 and 11). As non-activated macrophages mainly rely on OXPHOS for fueling their metabolic needs, OCR was first monitored in BMDM without stimulation, yet including manipulations to determine parameters associated with separate steps or hallmarks of this metabolic process (Figure 25 onwards for further details).

a. b.

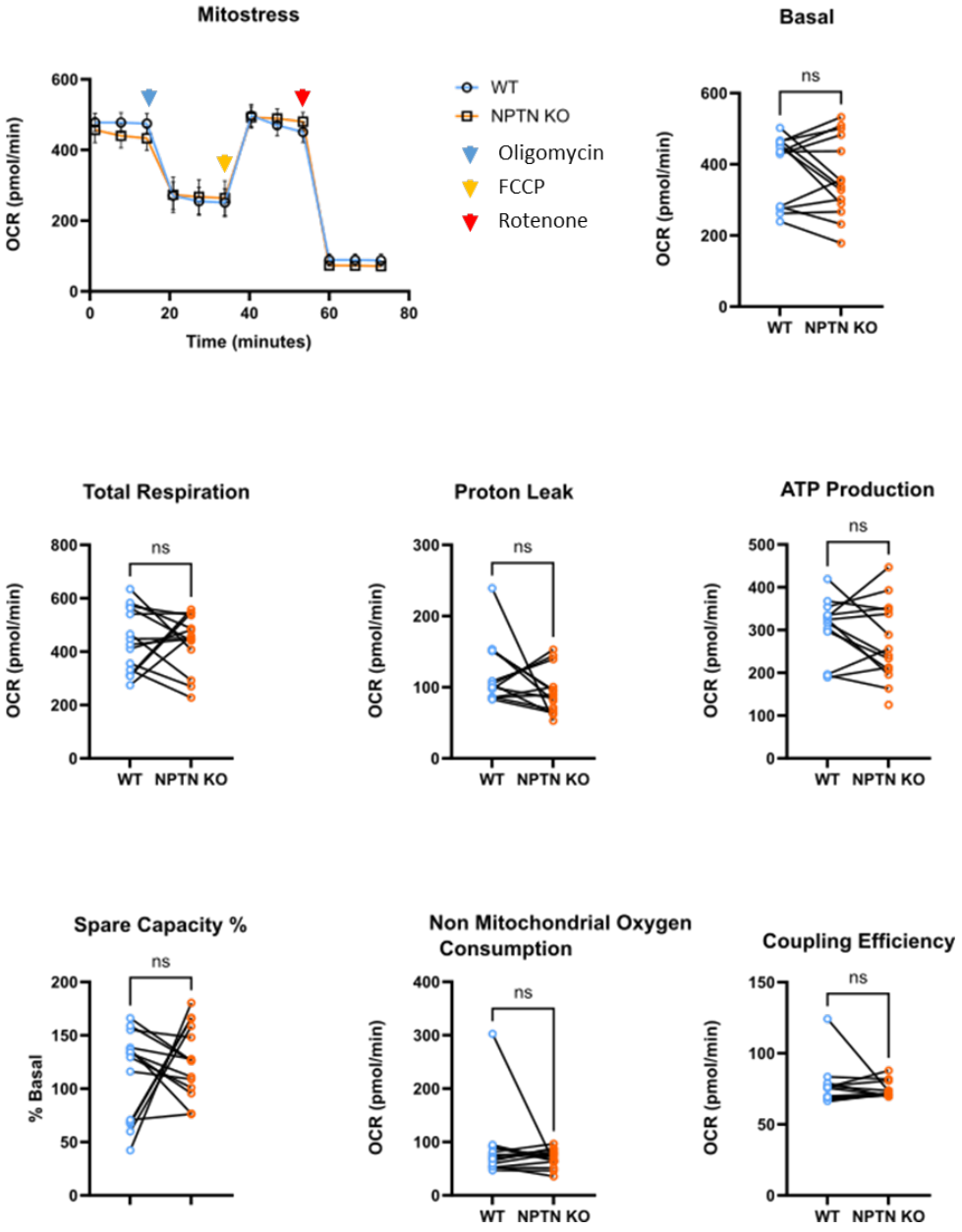

Figure 25: **OXPHOS in resting *WT* and *Nptn*$^{-/-}$ BMDM as revealed by Seahorse® Mitostress assay**. **(a)** OCR profile. Upon monitoring of baseline OCR, oligomycin was used to block complex V, leading to a decline though not complete block of OCR. Use of FCCP abrogates the proton gradient and entails elevated OCR. Rotenone blocks complex I and leads to a complete shutdown of OCR. **(b)** Various parameters deduced from the OCR profile are shown in separate plots. Results are from 4 or 5 biological replicates with 2 to 3 technical replicates for each. Values for each such pair are connected by a line. Error bars in (A) indicate SEM. t-tests did not reveal statistically significant differences between *WT* and *Nptn*$^{-/-}$. (ns = non-significant)

Following the trend observed for the other phenotypical parameters, *Nptn*$^{-/-}$ showed no significant deviation in the Mitostress assay compared with their control counterparts. Both

Nptn$^{-/-}$ and *WT* BMDM were next assessed for OCR and ECAR following IFNγ/LPS stimulation. Of note is that both mutants showed the virtual shutdown of OXPHOS (shown below), which is commonly associated with the metabolic switch as observed in stimulated *WT* murine BMDM.

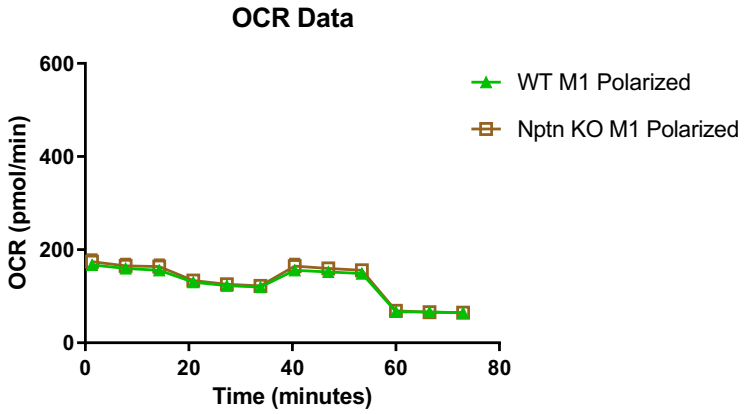

Supplement Figure: **Downregulation of OXPHOS in M1 polarized BMDM from *WT* and *Nptn*$^{-/-}$ cultures.** Evidently, after IFNγ and LPS stimulation, the OXPHOS is downregulated, and cells fail to respond to mitochondrial complex modulators, hence showing downregulation in Spare Respiratory capacity and ATP production through ETC.

In contrast to *Nptn*$^{-/-}$ (as depicted in Figure 25.) *PMCA1*-cKO BMDM showed remarkable differences from controls when assayed for OXPHOS (Figure 26).

a. b.

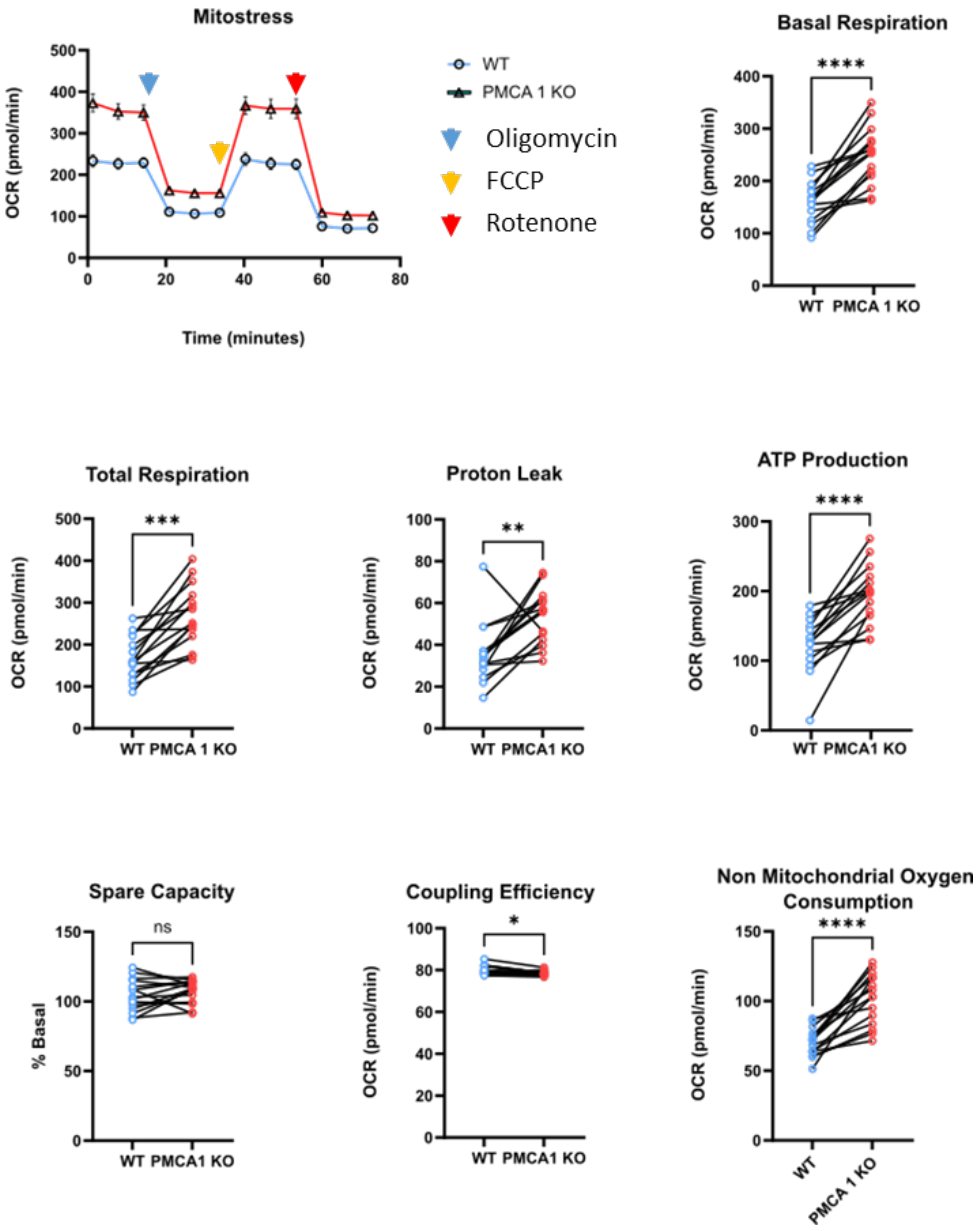

Figure 26: OXPHOS in resting *WT* and *PMCA1*-cKO BMDM as revealed by Seahorse® Mitostress assay. (A) OCR profile following the protocol as described in Figure 10. Please note that the absolute OCR values for the control group are reduced compared to those for *WT* in the *Nptn*$^{-/-}$ BMDM analysis. (B) Parameters deduced from the OCR profile are shown in separate plots. Results are from 4 or 5 biological replicates with 2 to 3 technical replicates for each. Values for each such pair are connected by a line. Error bars in (A) indicate SEM. (ns = non-significant, * = p ≤.05, ** = p ≤.01, *** = p ≤.001, paired t-tests)

The mutant BMDM showed significantly increased baseline OCR, which affected most parameters except spare capacity and coupling efficiency. ATP production was also increased. The OCR as measured in this assay is based mainly but not exclusively on the electron transport chain (ETC) underlying OXPHOS. In addition, however, the so-called proton leak

adds to OCR and may account for by-products like superoxide anions and peroxides like O_2^- and H_2O_2. In fact, a significantly increased proton leak in the mutant BMDM pointed to a possible increase in the level mitochondrially generated ROS (mtROS).

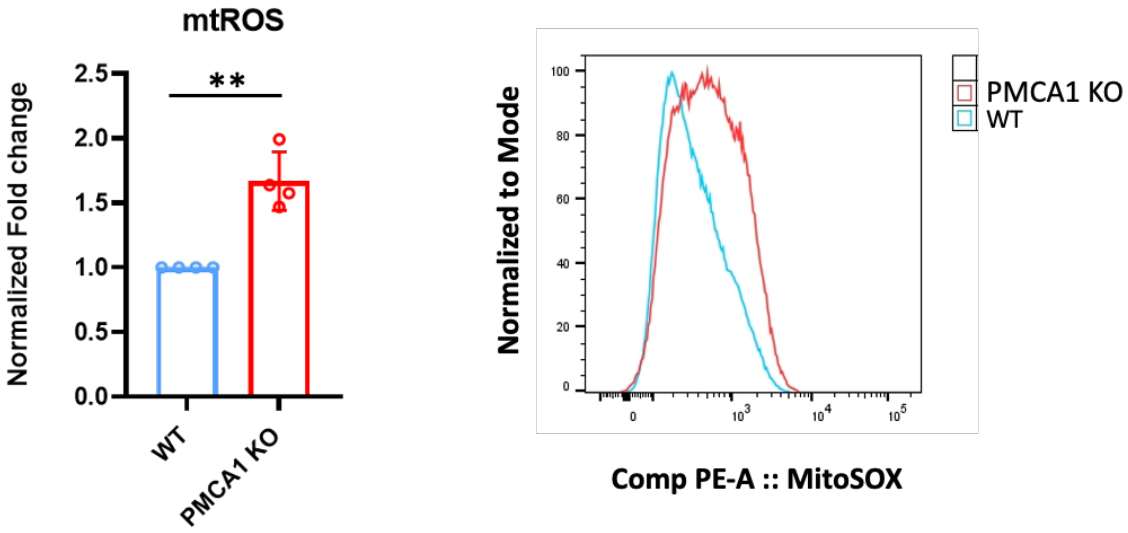

Figure 27 : Mitochondrial ROS, determined by FACS measurement of the fluorescent mitoSOX dye. (A) FACS histogram displaying fluorescent intensities on the X-axis and fractions of cells normalized to the most frequently occurring value (mode = 100) on the Y-axis. (B) Bar graph deduced from FACS analysis showing an ~1.63 fold increase of mtROS in PMCA-cKO BMDM. An unpaired t-test was done to look for statistical significance. (ns = non-significant, * = p ≤.05, ** = p ≤.01, *** = p ≤.001, paired t-tests)

Interestingly, a striking reduction of ECAR was observed in M1-polarized *Nptn*$^{-/-}$ *versus WT* BMDM, pointing to an impaired metabolic switch from OXPHOS to oxidative glycolysis in the mutant macrophages.

a.

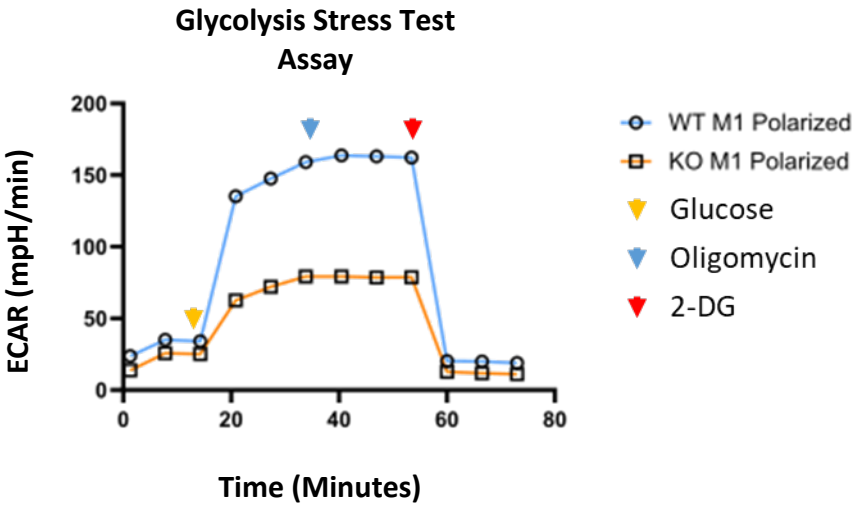

b.

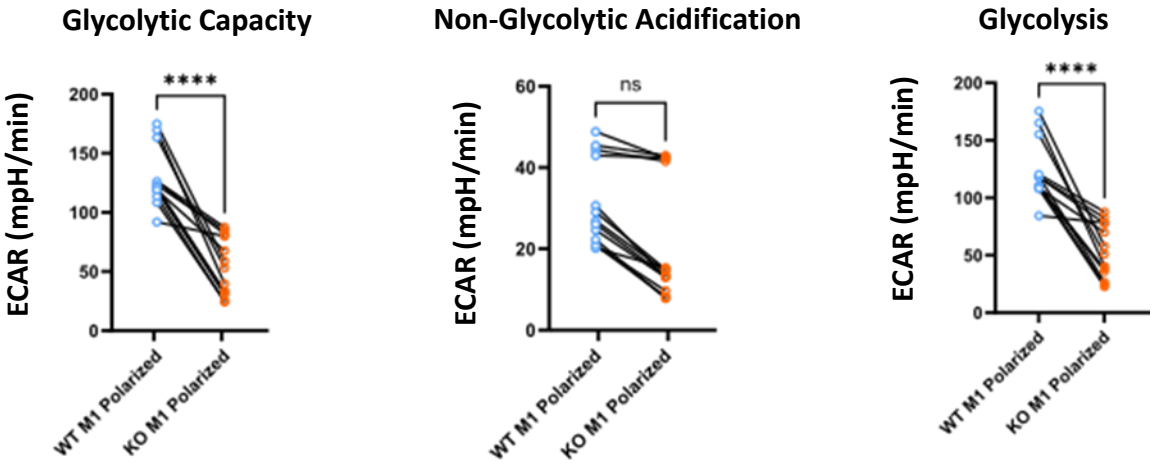

Figure 28: Glycolytic activity in M1-polarized *WT* and *Nptn*$^{-/-}$ BMDM. (a) A Seahorse® glycolysis stress assay was used to analyze the glycolytic phenotype. The glycolytic activity was induced in cells glucose-deprived for 1 h by adding 5 mM glucose. Oligomycin was used to block mitochondrial activity to measure the glycolytic capacity. 2-deoxyglucose blocks glycolysis with little non-glycolytic acidification left. (b) Parameters deduced from the ECAR profile are represented in separate plots. (ns = non-significant, * = p ≤.05, ** = p ≤.01, *** = p ≤.001 t-test paired)

In accordance with the metabolic switch and as revealed by an oligomycin-induced block of OXPHOS, M1-polarized BMDM generally shows little increase in glycolytic activity, i.e., low glycolytic reserve. The total glycolytic capacity, however, was found to be reduced in the mutants, whereas non-glycolytic activity was not significantly different. *Nptn*$^{-/-}$ (KO M1 polarized) macrophages have reduced glycolysis and glycolytic capacity, although there was no change in non-glycolytic acidification.

The glycolysis stress assay on M1-polarized *PMCA1*-cKO BMDM painted a different picture in showing significant upregulation in glycolytic activity.

a.

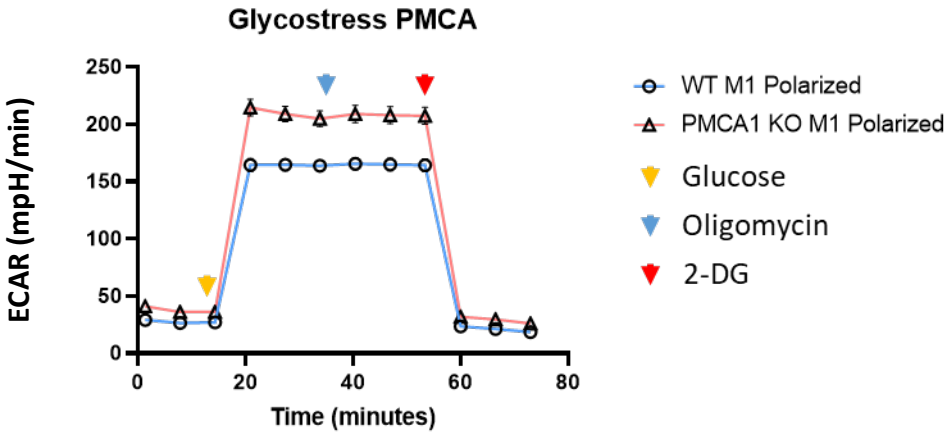

b.

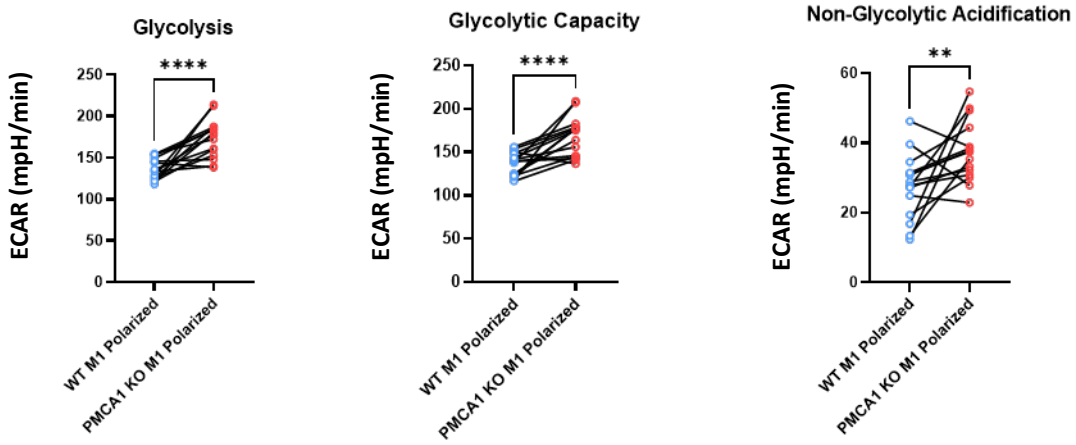

Figure 29: Glycolytic activity in M1-polarized controls (labeled *WT*) and *PMCA1*-cKO BMDM. (a) A Seahorse® glycolysis stress assay was used to analyze the ECAR profile upon LPS/IFNγ stimulation. Stepwise manipulations were performed as described in Figure 11. (b) Parameters deduced from the ECAR profile represented in separate plots. (ns = non-significant, * = p ≤.05, ** = p ≤.01, *** = p ≤.001 t-test paired)

The finding that M1-polarized *Nptn*$^{-/-}$ BMDM displayed considerably reduced glycolytic activity contrasts with the lack of phenotype with regard to other M1-related parameters but also with the fact that loss of PMCA1 led to the opposite, i.e., increased glycolytic activity. This striking difference could point to a role of Neuroplastin that is independent of its

interaction with PMCA. Glycolysis results in the generation of lactate, which is shuttled across the plasma membrane via monocarboxylate transporters (MCTs). Next to Basigin, which has been established as a *bona fide* interactor of MCTs, Neuroplastin has also been found to interact with MCTs ((Wilson et al., 2013) K. Langnaese, personal communication). Therefore, it seemed conceivable that loss of Neuroplastin could affect lactate transport and thus intra- and or extracellular lactate levels. To address this possibility, lactate was measured.

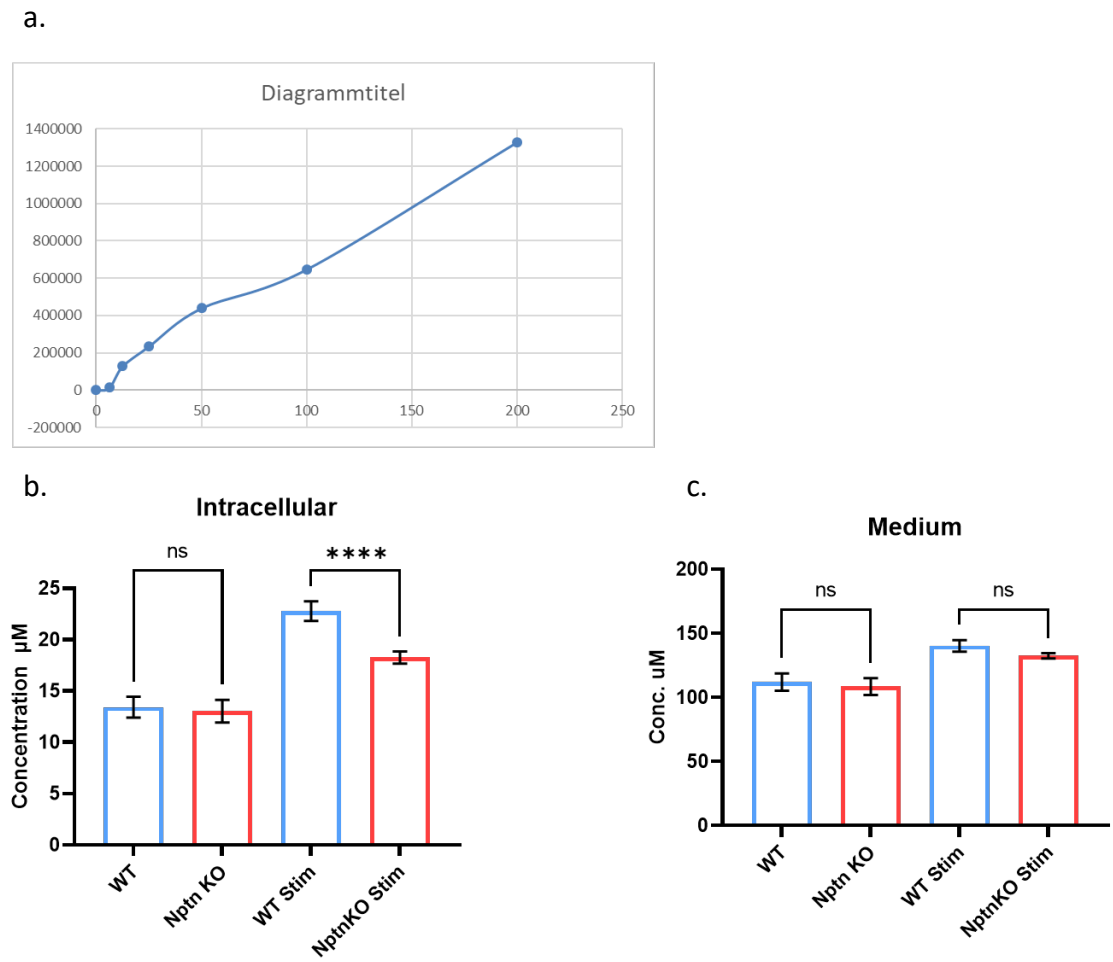

Figure 30: Lactate assay was performed on *WT* and *Nptn*$^{-/-}$ BMDM using the Promega ® Lactate-Glo™ kit. Figure a. represents a standard curve made using various concentrations of lactate provided in the kit, plotted against luminescence intensity on the Y-axis. Figures b. and c. represent intracellular and medium(secreted) lactate concentrations, respectively, in both genotypes and stimulations.(ns = non-significant, * = p ≤.05, ** = p ≤.01, *** = p ≤.001 t-test paired)

Intracellular lactate in *Nptn*$^{-/-}$ macrophages is low after stimulation, which fits with ECAR measurement on *Nptn*$^{-/-}$ macrophages, although the secreted lactate measured in the medium does not differ across genotypes.

While intracellular lactate increased upon stimulation in both *WT* and *Nptn*$^{-/-}$ BMDM, the latter did not reach the levels observed in the *WT* controls, consistent with restricted glycolysis in the mutant BMDM. Lactate also increased in the medium, yet without significant difference between the genotypes. This result supports a role for Neuroplastin in glycolysis but leaves open how this role is executed, when cells are forced to enter glycolysis after starvation as in the Seahorse® glycolysis stress assay.

3.12 HoxB8 Progenitors Derived Macrophages:

A continued generation and use of BMDM from *Nptn*$^{-/-}$ and *PMCA1*-cKO mice was repeatedly hampered by breeding problems associated with both mutants. To circumvent this problem, BM-derived stem cells from *WT, Nptn*$^{-/-}$ and *PMCA1*-cKO mice were turned into clonal stem cell lines (performed by Dr. K. Langnaese), which can be differentiated into macrophages (Redecke et al., 2013). Western Blot analyses confirmed loss of Neuroplastin or PMCA1 in respective clones upon differentiation. A select few clones of these progenitors were used to evaluate findings made for BMDM. It should be noted that while for the BMDM analyses true biological replicates (i.e. samples from individual animals) were employed, the replicates for the HoxB8 progenitors derived macrophages represent cells derived from one clone but differentiated in separate batches. The data acquired on HoxB8-based macrophages (hereupon just HB8M) will be presented in the same order as for the regular BMDM.

3.13 Canonical signaling in *WT* and *Nptn*$^{-/-}$ HB8M:

As for BMDM, *Nptn*$^{-/-}$ HB8M compared to *WT* HB8M did not show obvious changes in the phosphorylation of Tyr701 in STAT1 upon IFNγ treatment over time nor did they show differences in the phosphorylation profiles for NF-κB (pSer536) and ERK1/2 (pTyr404, pThr402) upon LPS treatment (Figure 31 and 32).

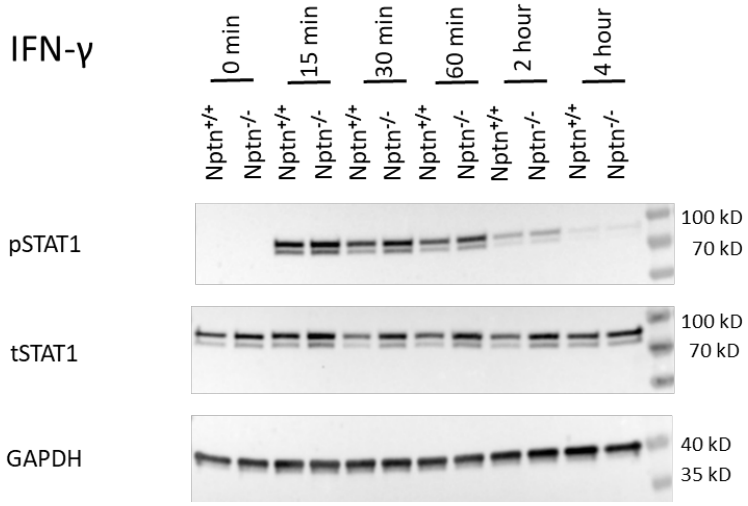

Figure 31: Time course of IFNγ -induced phosphorylation of STAT1 in *WT* and *Nptn*$^{-/-}$ HB8M . No apparent differences were seen in pSTAT1 levels throughout the time course of measurement after IFNγ stimulation.

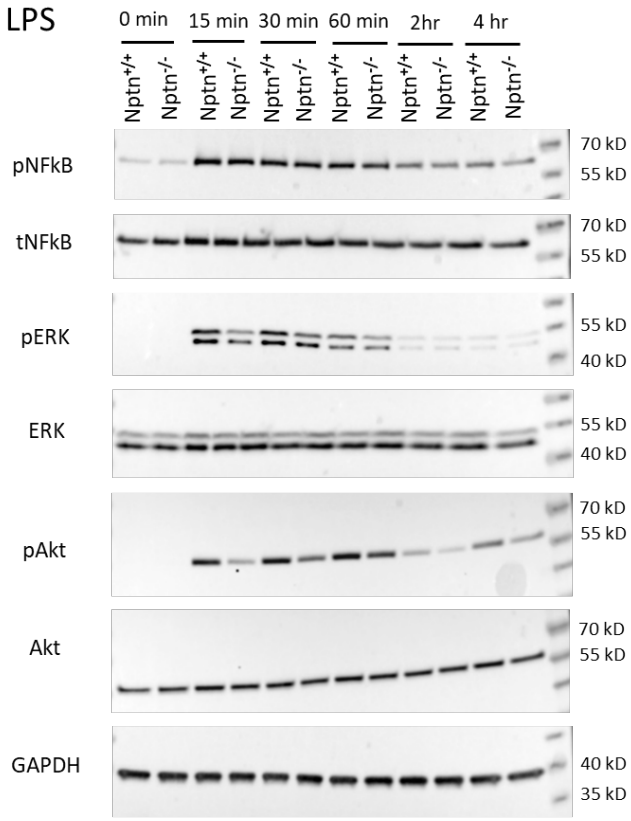

Figure 32: Time course of LPS-induced phosphorylation of NF-κB and ERK1/2 in *WT* and *Nptn*$^{-/-}$ HB8M. Like pSTAT1, NF-κB and pERK1/2 not vary, although pAkt shows some variation (downregulation in the knockouts), although it is subject to of further exploration and analysis.

3.14 Cytokine release from stimulated *WT* and *Nptn*$^{-/-}$ HB8M

The HB8M were also assessed for secreted cytokines using the CBA assay. The results were similar as for BMDM, although a few deviations are to be mentioned. Specifically, while TNF-α, IL-6 and IL-10 showed little if any difference between the genotypes, IL-27 and IFNγ showed significant upregulation only in the *Nptn*$^{-/-}$ HB8M but not in the *Nptn*$^{-/-}$ BMDM. IL-1α, which remained undetectable in the CBA on BMDM showed a moderate downregulation in the *Nptn*$^{-/-}$ HB8M as compared to *WT*. In general, the cytokine data showed less variability between replicates for HB8M than for BMDM, presumably due to the abovementioned fact that the tested HB8M originated from a single clonal stem cell line.

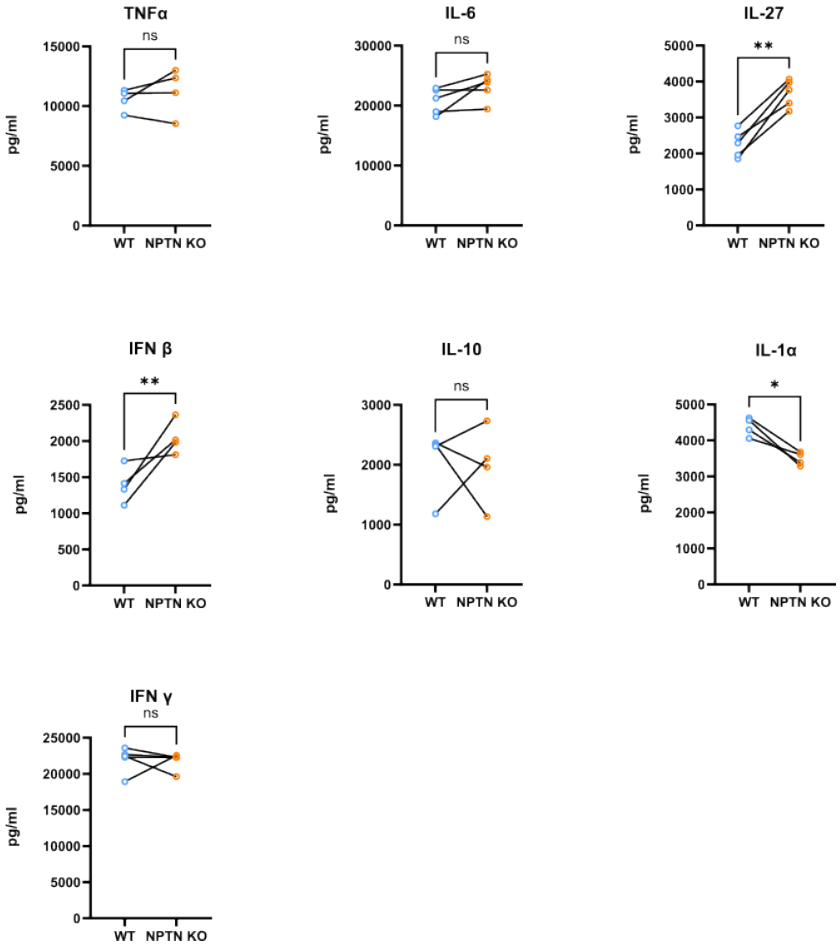

Figure 33: CBA analysis of some critical cytokines produced by macrophages, comparing *WT* and *Nptn*$^{-/-}$ HoxB8 macrophage results. TNF-α and IL-6, which are primary pro-inflammatory cytokines, do not show a difference across genotypes, whereas IL-1a is downregulated. IL-27 and IFNγ beta show upregulation. A t-test was used to test for statistical significance (ns = non-significant, * = p ≤.05, ** = p ≤.01, *** = p ≤.001 paired t-tests).

3.15 Signaling in *PMCA1*-deficient HB8M:

IFNγ and LPS-stimulated signaling was analyzed in the same manner as for BMDM and for *Nptn*$^{-/-}$HB8M.

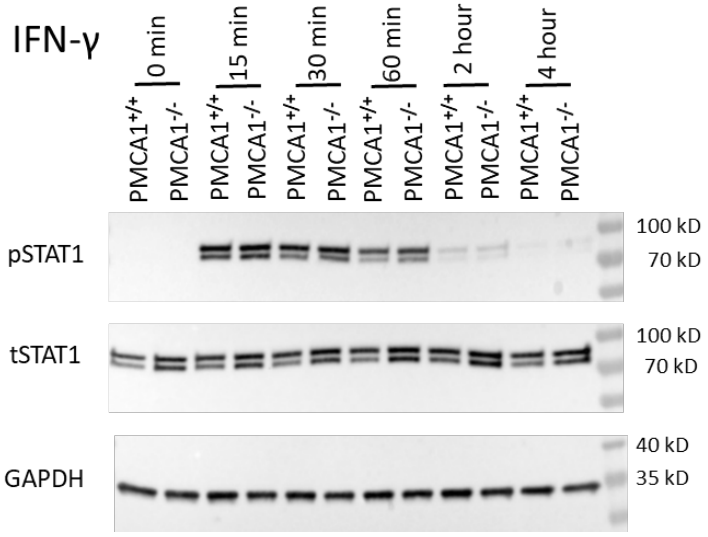

Figure 34: Timecourse of IFNγ -induced phosphorylation of STAT1 in *PMCA1*-cKO and control HB8M. As observed for *PMCA1*-cKO BMDM, loss of PMCA1 did not affect STAT1 phosphorylation in HB8M.

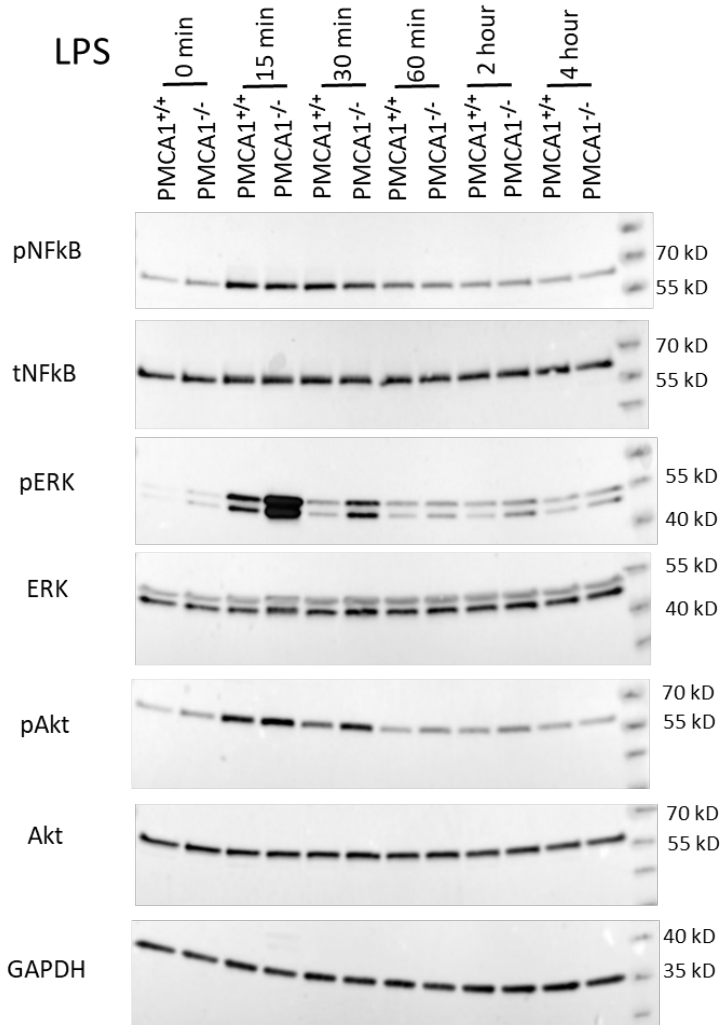

Figure 35: Time course of LPS-induced phosphorylation of NF-κB and ERK1/2 in *PMCA1*-cKO and control HB8M

LPS-induced signaling in *PMCA1*-cKO HB8M showed the same pattern for NF-κB as for controls, thus confirming the finding in BMDM. Also, like BMDM, compared to controls, excessive ERK1/2 phosphorylation was observed in HB8M lacking PMCA1. Notably, this effect was particularly observed at 15 min, i.e. earlier and more pronounced than in BMDM (30 minutes). Akt phosphorylation was found to be slightly upregulated in the mutant HB8M after LPS stimulation time points in contrast to what was observed in BMDM (Figure 35).

3.16 Cytokine measurement in *PMCA1*-cKO HB8M:

Further along the route as for BMDM, cytokine profiling was done for HB8M lacking PMCA1 and for respective controls. The results represented by the graphs in Figure 36 largely agree

with those from the measurements on BMDM-derived cytokines. IL-10, which was not found significantly increased for *PMCA1*-cKO BMDM, showed a moderate and statistically significant increase in the *PMCA1*-cKO HB8M. IL1α, which was not detectable in CBA on BMDM, was increased in the *PMCA1*-cKO HB8M. All other cytokines were found significantly increased. This assay, therefore, strongly supports the finding on BMDM that revealed an exaggerated M1 polarization response for macrophages lacking PMCA1.

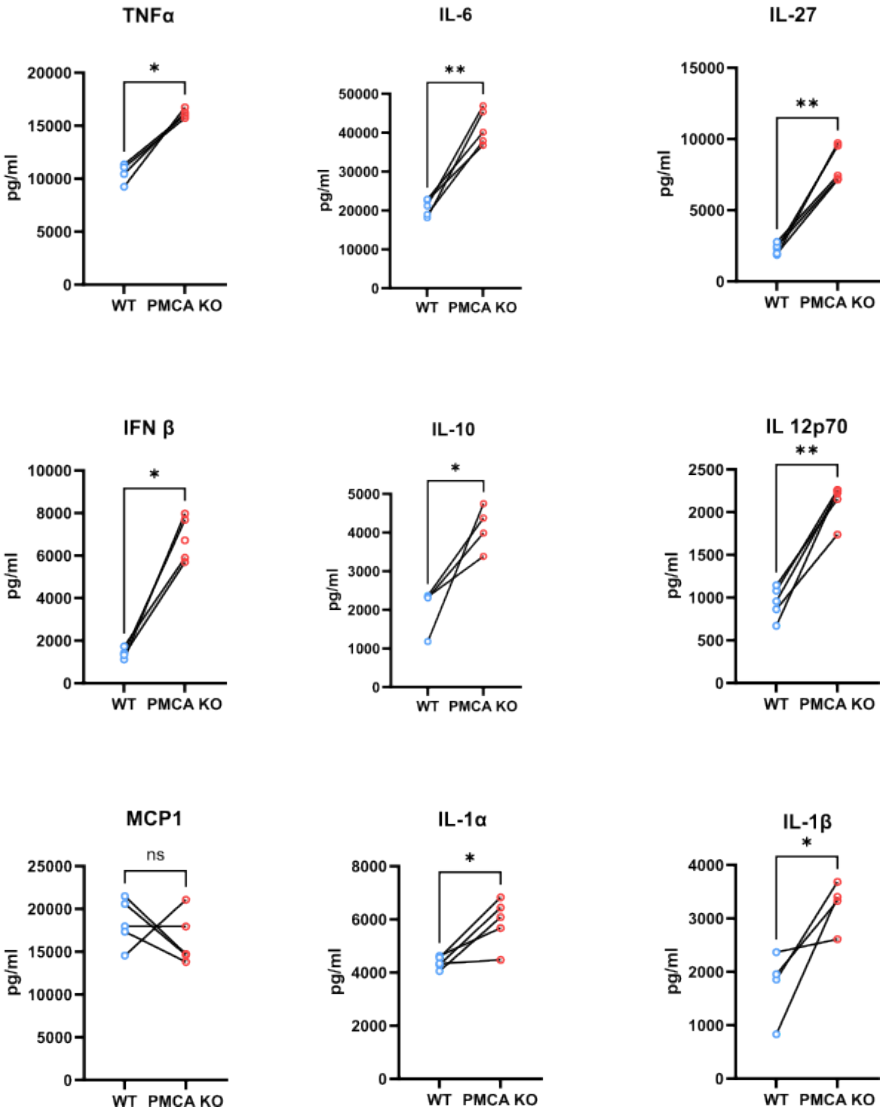

Figure 36: CBA analysis of HoxB8 macrophages from *WT* and *PMCA1*-cKO HoxB8 culture medium. Most cytokines upregulated in bone marrow-derived knockouts are also upregulated in HoxB8 knockouts. However, cytokine levels (represented in pg/ml) are higher in HoxB8 cells than in their bone marrow counterparts. (ns = non-significant, * = p ≤.05, ** = p ≤.01, *** = p ≤.001 t-test paired t-tests)

3.17 Metabolism in HB8M macrophages:

Sea-horse metabolic assays were also performed on HoxB8-derived macrophages. A Mito-stress assay on non-stimulated macrophages was performed, and a Glycolysis stress test assay on stimulated, M1-polarized macrophages was performed.

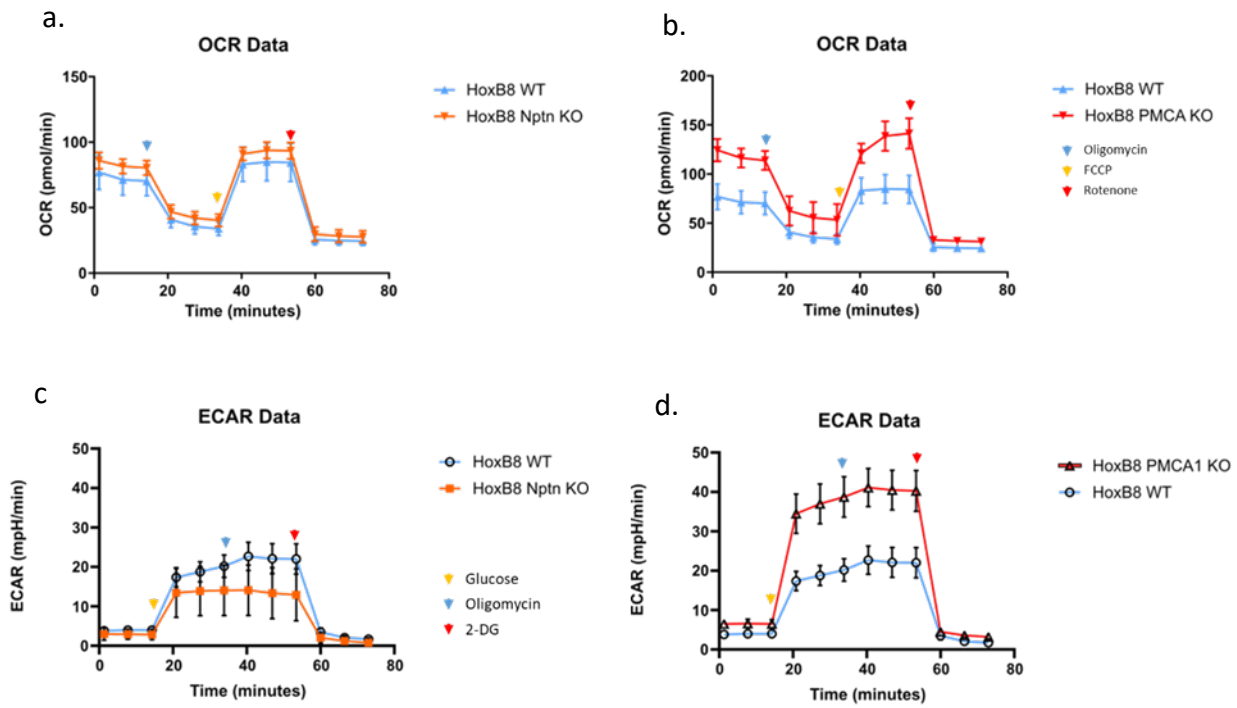

Figure 37: Metabolic analysis of HoxB8 macrophages. a. A comparative analysis of OXPHOS between HoxB8 *WT* and HoxB8 *Nptn* KO macrophages. **b**. A comparative analysis of OXPHOS between HoxB8 *WT* and HoxB8 *PMCA1*-cKO macrophages. **c**. A comparative analysis of glycolysis in HoxB8 M1 polarized macrophages *Nptn* KO and *WT* and **d**. A comparative analysis of glycolysis in HoxB8 M1 polarized macrophages *PMCA1*-cKO and *WT*. (ns = non-significant, * = p ≤.05, ** = p ≤.01, *** = p ≤.001 paired t-tests)

HoxB8 cells, in their phenotypes and metabolism, mostly align with their bone marrow counterparts. Like their bone marrow counterparts, HoxB8 *Nptn*$^{-/-}$ macrophages have reduced glycolysis after polarization; conversely, glycolysis is increased in *PMCA1*-cKO polarized macrophages.

As mentioned before, macrophages could turn glycolytic from mitochondria-based metabolism, namely OXPHOS. This switch happens relatively quickly and can be observed in relative change in extracellular acidification rate or ECAR values. We tried to look at this

switch through acute stimulation of these cells with LPS and looking at ECAR, following it over a period.

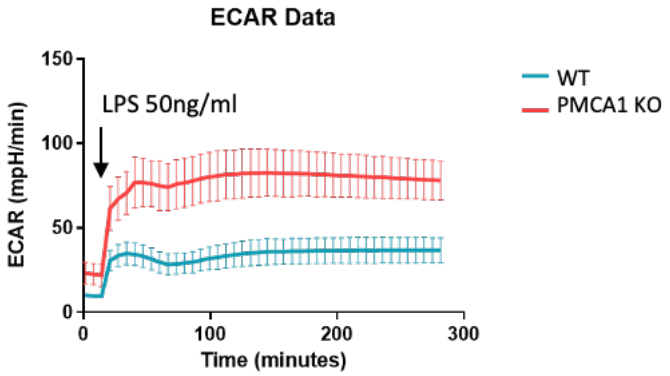

Figure 38: Acute micro-injection of LPS in a seahorse-based assay to measure the change in ECAR levels. *PMCA1*-cKO demonstrates the ability to turn glycolytic quickly, measured by the change in extracellular acidification, compared to their *WT* counterparts.

The above results suggest that *PMCA1*-cKO is more prepared for the metabolic switch. Hence, right after TLR ligation with LPS, they switch quickly to glycolysis. The readiness of *PMCA1*-cKO can be attributed to the proteome responsible for glycolysis that Ca^{2+} could regulate, though this proposition needs to be rigorously tested.

3.18 RNAseq Analysis of *PMCA1*-cKO macrophages:

PMCA1-cKO macrophages provide us with an excellent model to study macrophages with chronic disruption in Ca^{2+} homeostasis. The above experiments have revealed striking phenotypes concerning ERK signaling, cytokine production, and metabolism when PMCA1 is missing. To further characterize and unravel changes in gene expression associated with these phenotypes, BMDM were analyzed at the transcriptome level by bulk RNA sequencing (RNAseq). Specifically, $polyA^+$ RNA isolated from non-stimulated as well as M1-polarized (4 h IFNγ /LPS) control and *PMCA1*-cKO BMDM (n=3 for each) was used. Gene expression profiling across the genotypes and activation states was then performed using bioinformatics tools. The first thing was to perform a "Principal Component Analysis" (PCA), which resulted in a clear discrimination of the four groups (Figure. 39 a), i.e. the latter were found in separate clusters based on robust transcriptomic differences between them. Next, the number of

differentially expressed genes with a significance level of p<0.05 in the various groups was determined and compared pairwise for all conditions (Figure. 39 b).

a. b.

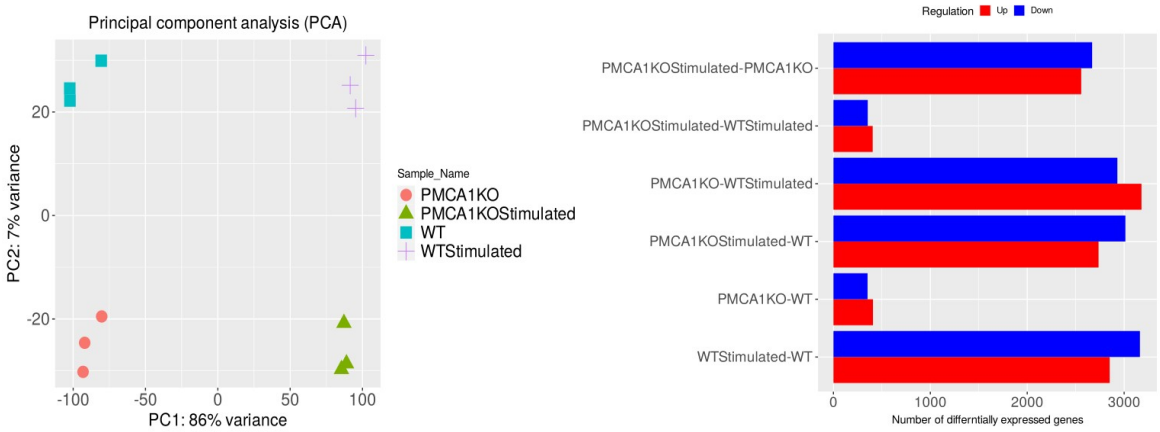

Figure 39: **a. PCA of seq data shows the comprehensive difference between different groups. b. Bar graphs compare the number of genes differentially expressed in different groups**. The number of genes that were up or downregulated for any given pair was similar. Surprisingly, stimulation caused higher gene expression dynamics for control BMDM (~3000 genes up-/downregulated) compared to *PMCA1*-cKO, with ~2500 genes up-/downregulated. This could reflect a predisposition of the mutant BMDM towards M1 polarization at the gene expression level.

It should be stressed that the above analysis considers just the number of differentially expressed genes without addressing the fold changes in transcript levels. To elaborate on the latter, expression levels were included in the analysis. Results are depicted in Fig. 40 as volcano plots, commonly used to visualize differential expression as deduced from RNA-Seq data analysis. It simultaneously displays the statistical significance (usually represented by p-values) and the magnitude of change in gene expression between two conditions or groups. To compare *PMCA1*-cKO vs. control in non-stimulated and stimulated cells, volcano plots were generated using VolcanoseR, a web-based plotting software.

(https://huygens.science.uva.nl/VolcaNoseR2/)

a.

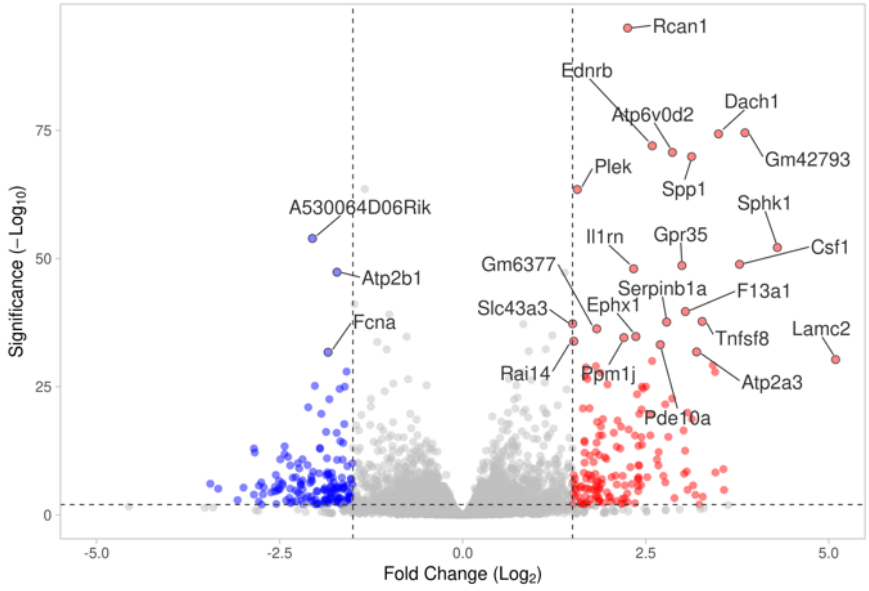

b.

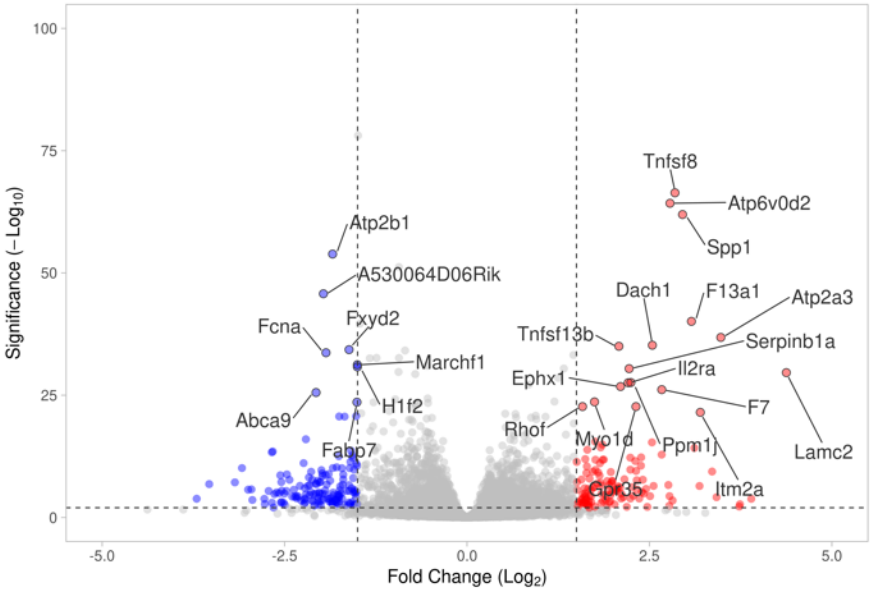

Figure 40: Volcano plot representation of differential gene expression. a. *PMCA1*-cKO vs. control macrophages, non-stimulated. b. *PMCA1*-cKO vs control macrophages, stimulated. The threshold set for the X-axis was $\log_2$ 1.5 ($2^{1.5}$) -times fold change, and The Y-axis had a significance level of $p < 0.05$.

While virtually all genes are represented in the volcano plots, various genes that showed changes above threshold levels can be easily identified. For starters, PMCA1 (*Atp2b1*), as expected, showed profound downregulation in both the volcano plots. The fact that the *PMCA1*-cKO does not affect transcriptional initiation *per se* and that some transcripts may

have endured the ~3-day phase since LysM-Cre-induction of the KO can explain the persistence of some PMCA1 mRNA. Among the many transcripts that show a considerable difference in their abundance between *PMCA1*-cKO and control BMDM before and/or after stimulation, two are mentioned here explicitly because of their well-established roles in Ca^{2+}-signaling or homeostasis. Transcripts for *Rcan1*, a negative regulator of calcineurin, show striking upregulation in non-stimulated *PMCA1*-cKO BMDM, possibly reflecting a predisposition, thereby suppressing nuclear translocation of NFAT, is significantly upregulated. SERCA3 (*Atp2a3*) was another such hit, showing significant upregulation in *PMCA1*-cKO versus control, yet both before and after stimulation by ~8 fold. It is conceivable that the upregulation of *Rcan1* and SERCA3 represent negative feedback mechanisms to counteract the dysregulation of Ca^{2+} homeostasis in conditional knockouts. To mention again, Basigin transcripts show upregulation across genotypes and after stimulation (not marked in Figure 40).

KEGG (Kyoto Encyclopedia of Genes and Genomes) and GO (Gene Ontology Resource) are two widely used bioinformatics resources for functional annotation and analysis of genes and gene products. KEGG integrates genomic, chemical, and systemic functional information and includes information on pathways, diseases, drugs, and biological relationships. It also provides information on metabolic pathways, regulatory pathways, and other cellular processes. A series of molecular interactions, such as enzymatic reactions or signaling cascades, represent each path. Here, the RNAseq data were used to uncover KEGG categories that are enriched for genes with altered expression in the *PMCA1*-cKO versus control BMDM before or after stimulation, respectively (Figures 41 and 42). At first, KEGG enrichment analyses were performed for genes upregulated in non-stimulated and stimulated *PMCA1*-cKO BMDM.

a.

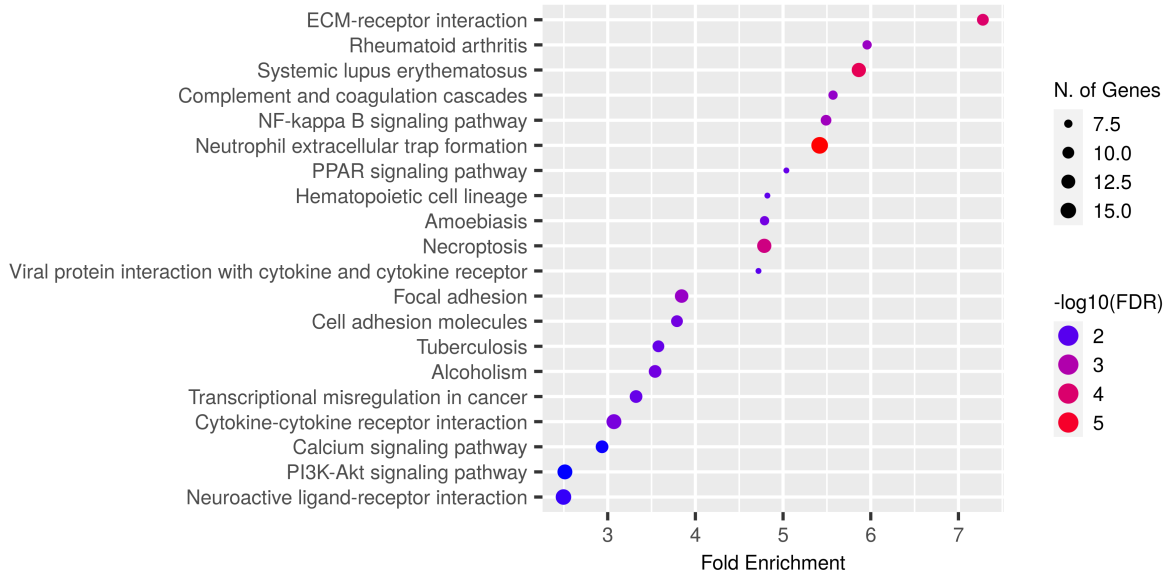

b.

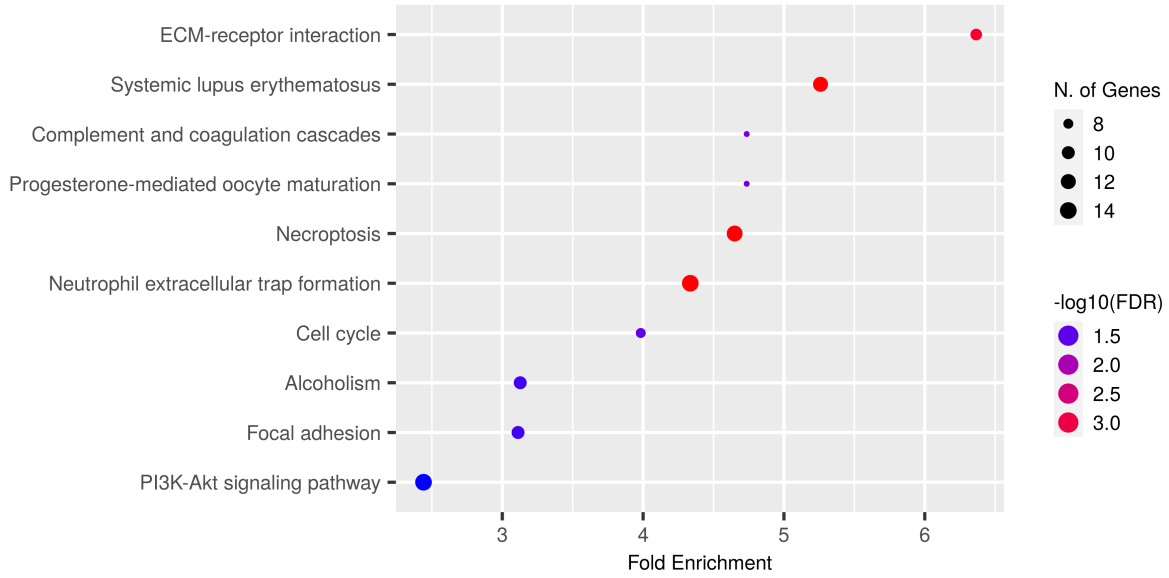

Figure 41: Dot plot showing KEGG pathway enrichment analyses performed on upregulated genes in *PMCA1*-cKO a. before and b. after stimulation. The enrichment measures the number of genes with altered expression relative to the total number of genes within a given KEGG pathway/category. The dot size represents the number of genes participating in a particular KEGG pathway, fold enrichment defined above, and FDR is the false detection rate used to determine statistical significance.

As for the list of genes upregulated after stimulation in the knockouts, KEGG enrichment analysis was performed for downregulated genes.

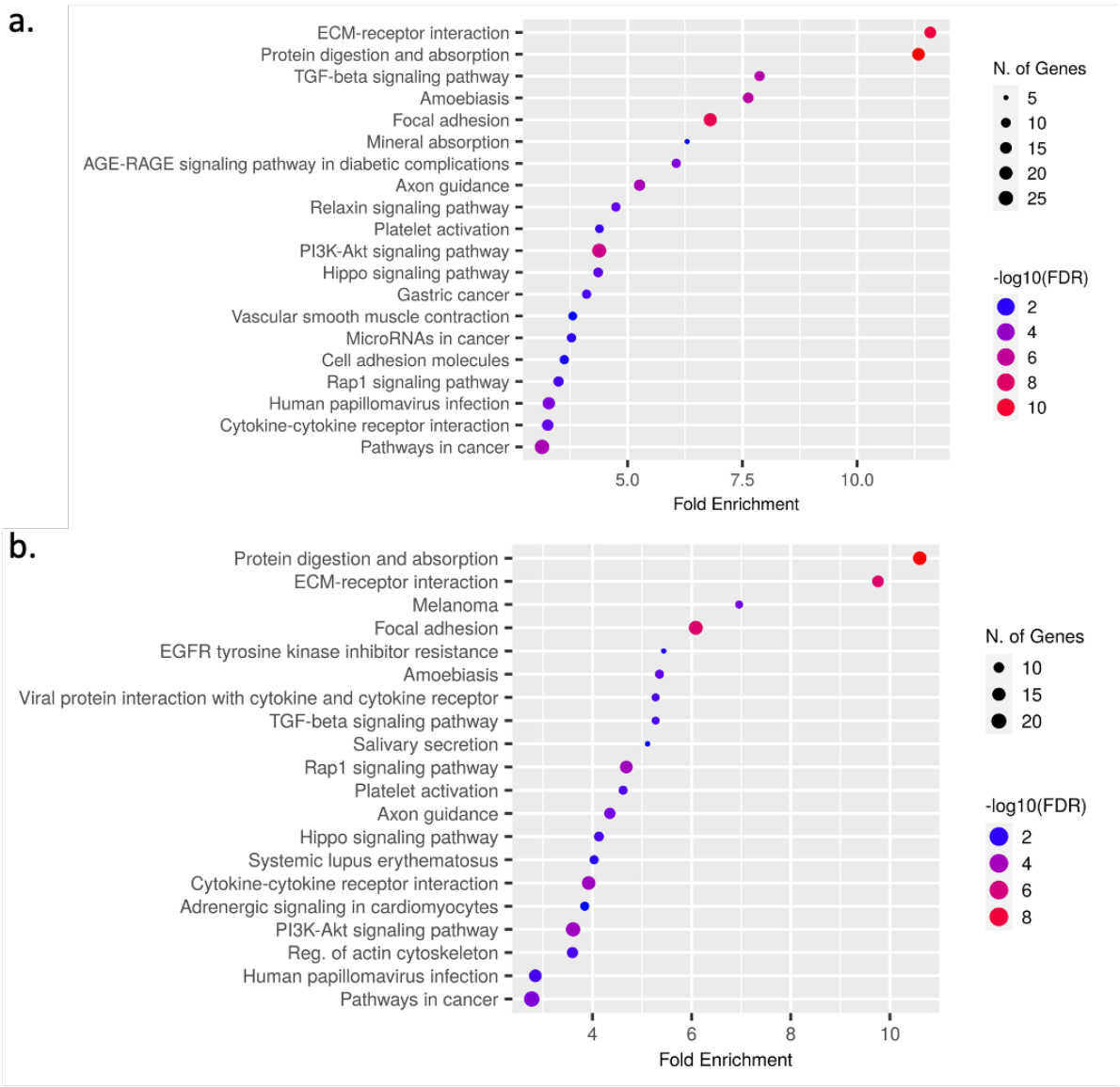

Figure 42: Dot plot showing KEGG pathway enrichment analyses performed on downregulated genes in *PMCA1*-cKO a. before and **b**. after stimulation.

For some pathways that are peculiar in terms of high enrichment or their relation to the phenotypical analyses in this study, lists of genes, along with their normalized counts per million (CPM), were created and plotted as heatmaps (Figure 43 onward). In addition to the genes found in the respective KEGG pathway clusters, some more were hand-picked, cytokines in particular, chemokines, and ion channels relevant to previous reports on Ca^{2+} handling in macrophages.

Genes related to ECM-receptor interactions as well as genes related to the PI3K-Akt pathway, were found enriched in all four plots, whereas pathways/categories such as the NF-κB pathway, PPAR signaling, and calcium signaling showed enrichment specifically in the set of

upregulated genes. In contrast, TGF-β signaling, which is typically related to M2 polarization, was found enriched for downregulated genes.

The CBA assay measuring secreted cytokines revealed that *PMCA1*-cKO macrophages, after M1 polarization, showed several cytokines that were significantly upregulated. The RNAseq data were used for a comparative heatmap representation of such cytokines and of various chemokines in controls and *PMCA1*-cKO BMDM after stimulation.

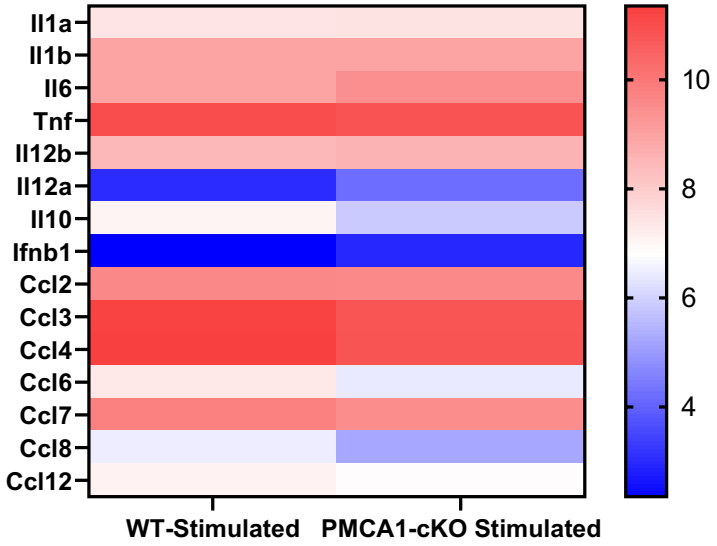

Figure 43: Heatmap displaying transcript levels for selected cytokine and chemokine transcripts produced by BMDM after stimulation. The gradient color scale bar represents counts normalized across the whole RNAseq sample data as $\log_2$ (increasing from dark blue to red with white representing the mean count within the group; note that even blue may represent robust expression).

After stimulation, most cytokines and chemokines were well represented at the transcript level, and none of the cytokines showed big differences between controls and the knockouts, as opposed to what was revealed by the CBA analysis. This suggests that the observed increase of various cytokines secreted by *PMCA1*-cKO versus controls involves post-transcriptional mechanisms. Moderate downregulation was evident for IL-10 and most of the tested chemokines.

The Mitostress Assay revealed a change in mitochondrial OXPHOS in non-stimulated macrophages, showing *PMCA1*-cKO to have elevated levels of mitochondrial function (OXPHOS). Genes involved in OXPHOS via the five distinct complexes in the inner

mitochondrial membrane were clustered in respective groups to display their transcript levels as heat maps (**Figure 44**)

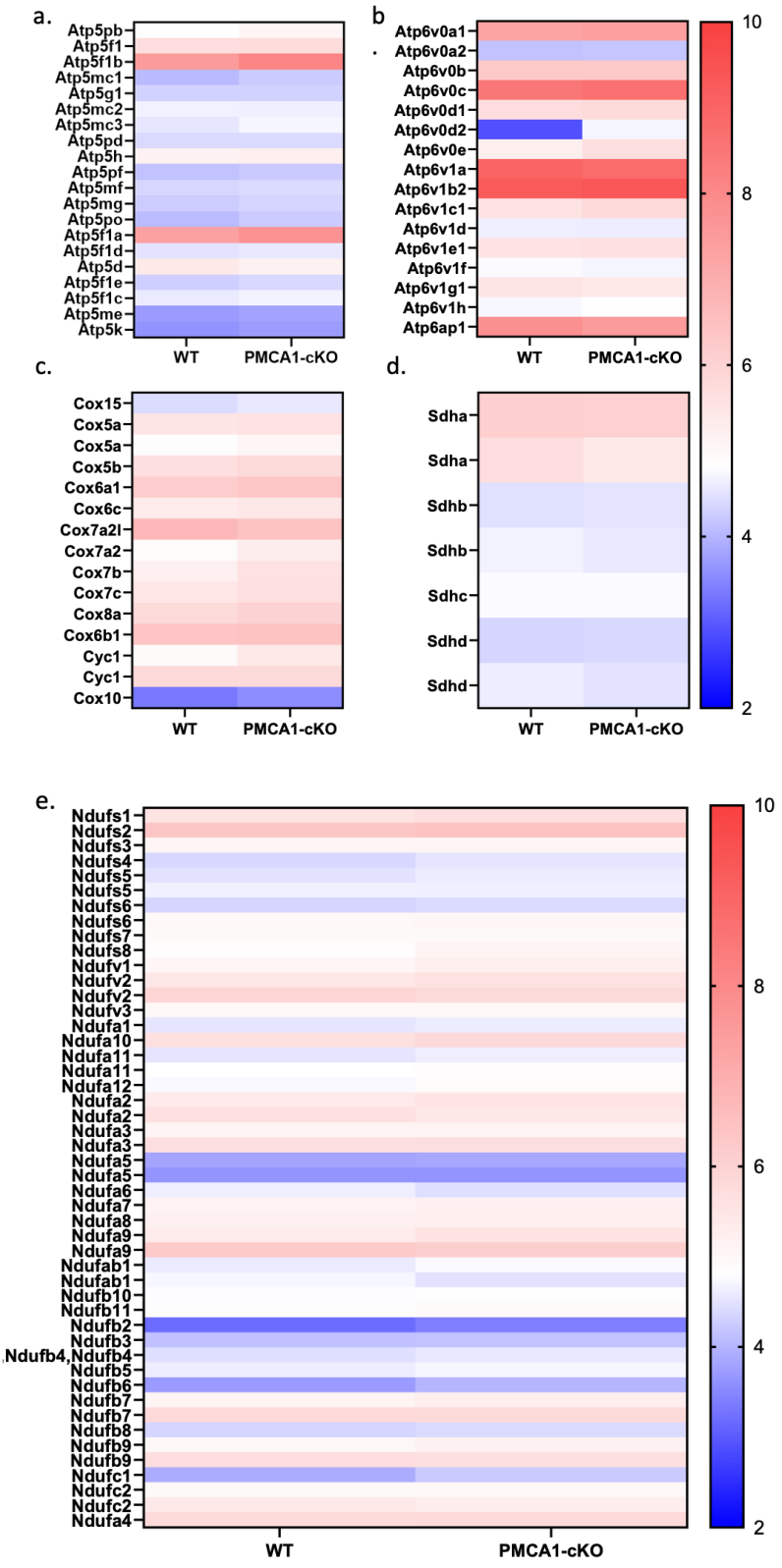

Figure 44: Heatmap showing genes from OXPHOS in non-stimulated control and *PMCA1*-cKO BMDM. The different clusters of genes correspond to: a. ATP synthase subunit 5 and b ATP synthase subunit 6 (complex V); c. Cytochrome Oxidase (complex III/IV); d. Succinate dehydrogenases (complex II); e. NADH:Ubiquinone Oxidoreductase (complex I). The gradient color scale bar represents counts normalized across the whole RNAseq sample data as log_2

While several genes from the clusters show quite moderate changes in their transcript levels in one or another direction, it remains rather questionable as to whether these alterations account for the observed increase of OXPHOS in non-stimulated *PMCA1*-cKO. The transcript level was elevated for only one gene, *Atp6v0d2* (see also the volcano plot in Figure 40). It should be noted, however, that the respective protein is not only part of subunit 6 in complex V but is also present in the lysosomal ATPase.

Glycolysis was found elevated after stimulation in *PMCA1*-cKO compared to control BMDM. Hence, genes involved in glycolytic function were also analyzed.

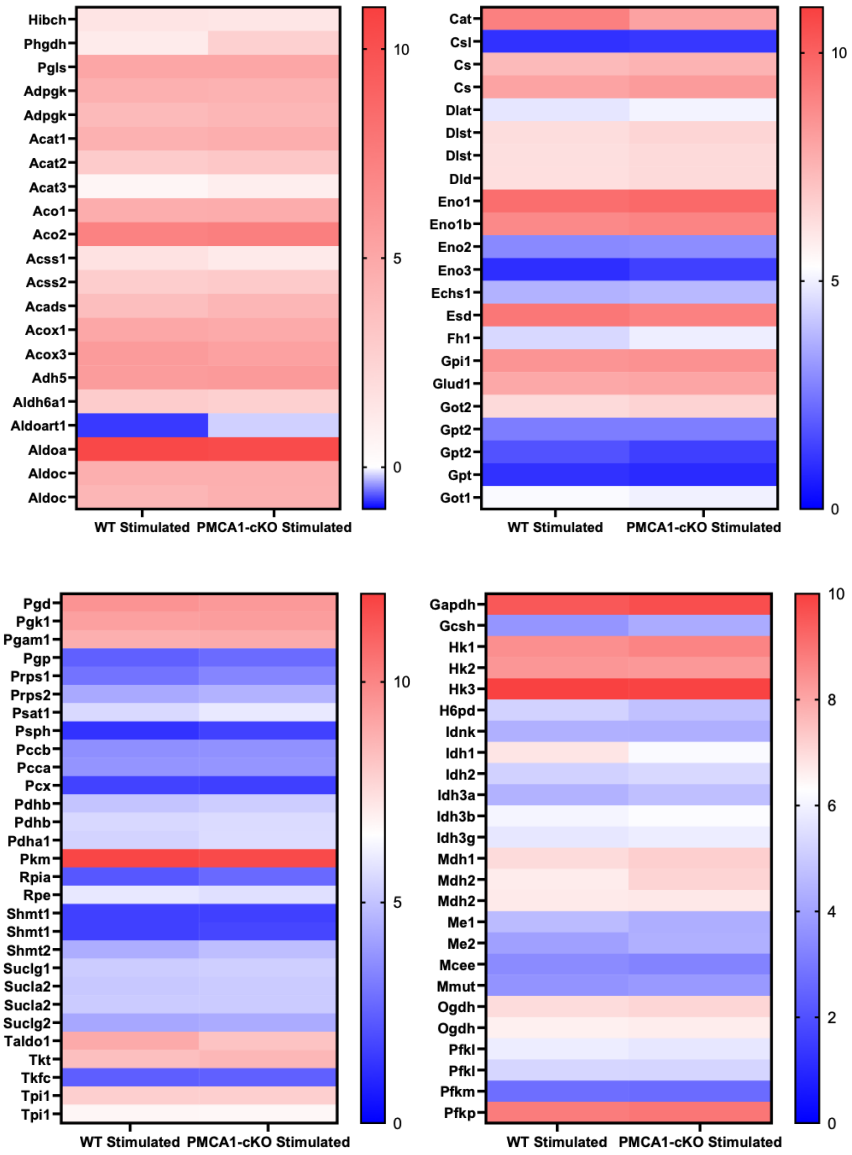

Figure 45: Heatmap showing genes related to glycolysis (carbon metabolism as listed in KEGG) in stimulated *WT* and *PMCA1*-cKO macrophages. Genes are represented in split clusters for the ease of viewing. The gradient color scale bar represents counts normalized across the whole RNAseq sample data as $\log_2$.

As for OXPHOS-related genes, most genes involved in glycolytic function did not significantly differ between controls and *PMCA1*-cKO. This was confirmed using the analysis underlying the volcano plots (Figure 40). The only two exceptions are the *Aldoart1* gene, which is involved in fructose bisphosphate metabolism, and the *Hk1* (Hexokinase 1) gene, which is moderately upregulated with statistical significance.

The KEGG database was also used to group genes involved in Ca^{2+} signaling. For heat maps, these genes were further sorted into various subgroups based on the cellular localization of their gene products; for example, genes expressing proteins that are localized on the plasma membrane would be grouped.

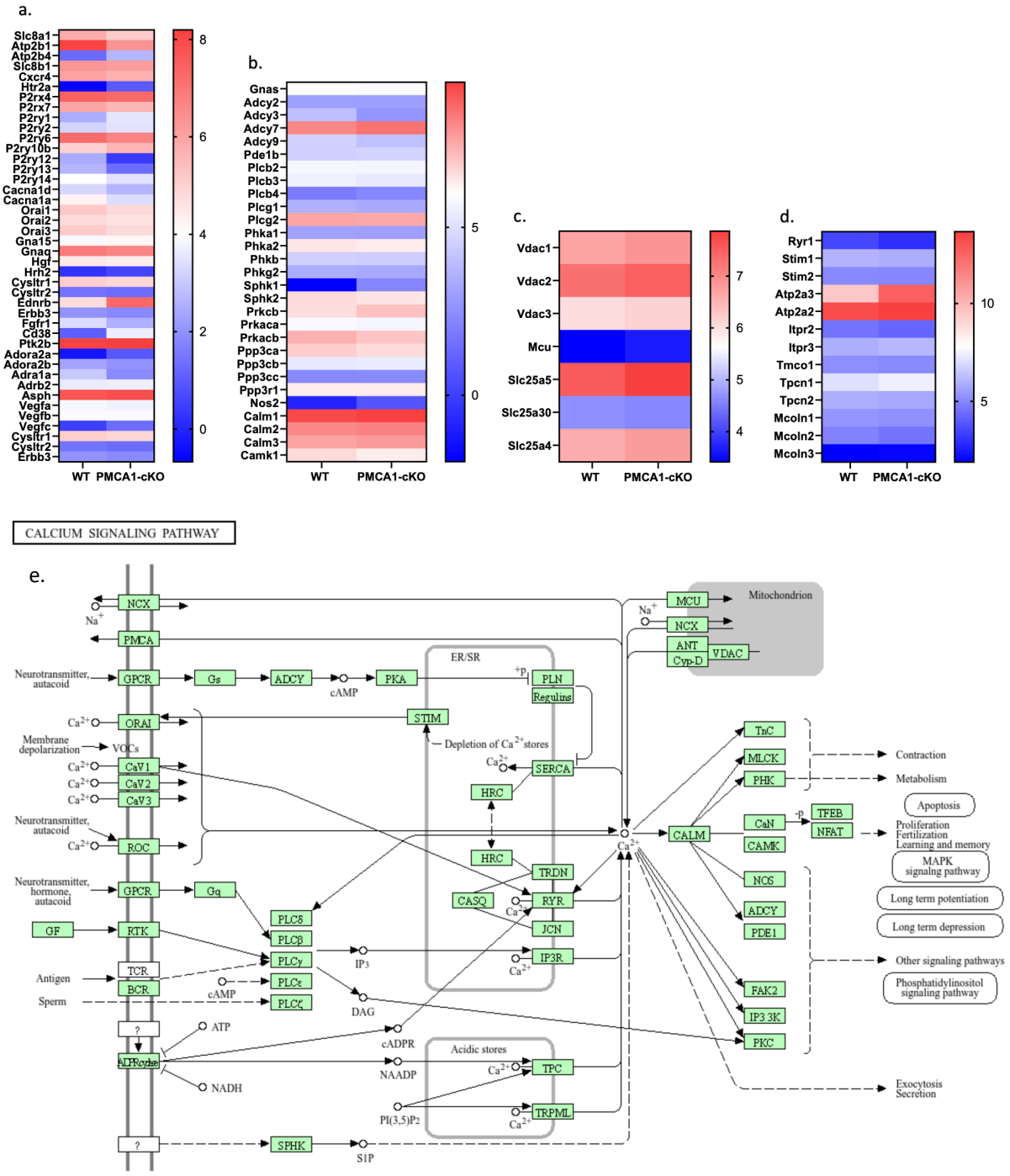

Figure 46: Heatmap of genes related to calcium signaling pathways; genes encoding proteins are localized to a. Plasma membrane, **b**. Cytoplasm **c**. Mitochondria **d**. ER-Lysosome. The color gradient for each heatmap shows normalized log2 change from high (red) to low (blue). **e**. KEGG database description of Ca^{2+} signaling.

Next to the downregulation of *Atp2b1* transcripts, PMCA4 was found to be slightly upregulated in the knockouts (Figure 46a). Of note, a few genes encoding plasma membrane resident proteins (Figure 46a) directly involved in Ca^{2+} influx, including ORAI1 and 3, the L-type channels Cacna1a and Cacna1d, and the P2X channels P2rx4 and P2rx7, where found to be moderately downregulated with statistical significance. Interestingly, transcripts for CD38 and the endothelin receptor B (Ednrb), which both have been implicated in the mobilization of Ca^{2+} from internal stores (Jouneaux et al., 1994; Lee et al., 2022) displayed robust elevation. Among genes with products assorted to the cytosolic compartment (group b), no strong up- or downregulation was observed. Moderate downregulation of some adenylate cyclase or CaM-dependent Kinase 1 (Camk1) transcripts may nonetheless affect Ca^{2+} signaling. Significant upregulation of the gene for sphingosine 1 (*Sphk1*) could account for the modulation of Ca^{2+} influx (Pulli et al., 2018). The gene for iNOS (*Nos2*) displayed mild and statistically non-significant upregulation, and it therefore remains elusive as to whether it adds to the significant increase in iNOS levels observed in stimulated *PMCA1*-cKO BMDM compared to controls. Genes with products assorted to mitochondria (group c), such as the mitochondrial uniporter (MCU) or the sodium-calcium exchanger (NCX), showed no significant change. The outcome was similar for genes related to the ER-lysosome compartment (group d), except for the profound upregulation of transcripts for SERCA3 (*Atp2a3*).

In light of data in the literature that point to roles for distinct TRP ion channels for Ca^{2+} influx into macrophages (Chauhan et al., 2018; Nascimento Da Conceicao et al., 2021; Schappe et al., 2018), another exploratory grouping was based on the expression levels of various well-known TRP ion channels. Some of these ion channels have been reported to regulate immune cell function through Ca^{2+} influx.

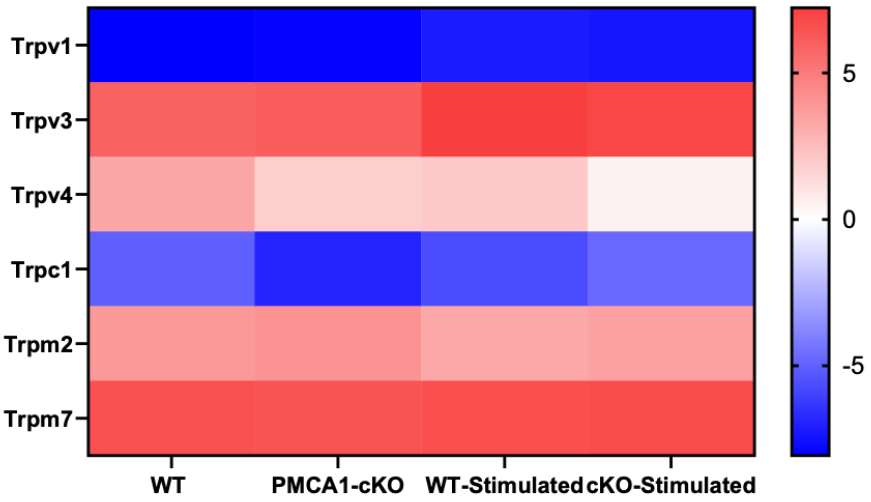

Figure 47: Heatmap for previously reported TRP ion channels in macrophages, previously reported to have vivid function in macrophages.

Although previously characterized in macrophages, TRPV1 and TRPC1 remained significantly downregulated (or undetected) in the BMDM samples analyzed here, both with and without stimulation across both genotypes. Instead, TRPV4 was found robustly downregulated with high statistical significance in *PMCA1*-cKO compared to controls, both before and after stimulation. TRPV3, although not showing any change across genotypes, was found upregulated after stimulation. TRPM2 and TRPM7 are highly expressed in both genotypes before and after stimulation.

Gene Ontology is a standardized system for annotating the functions of genes and gene products. Where KEGG focuses primarily on pathways and network interactions, GO terms provide a structured vocabulary to describe gene function using three ontologies: Molecular Function, Biological Process, and Cellular Component. As for the KEGG analysis, a GO enrichment analysis was performed for the sets of up- or downregulated genes in *PMCA1*-cKO, both before and after stimulation. The first plot depicts GO terms enriched in non-stimulated *PMCA1*-cKO versus controls.

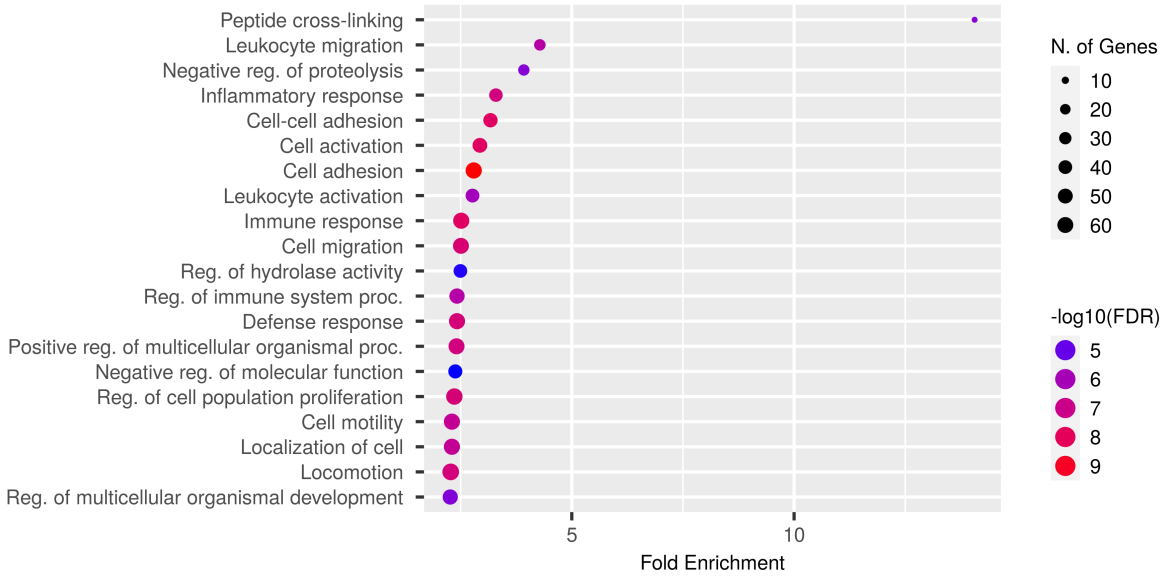

Figure 48: Dot plot showing GO enrichment analyses performed on upregulated genes in *PMCA1*-cKO. Genes related to adhesion and migration functions were found to be enriched. Other examples include genes involved in the inflammatory response and immune response, which were enriched by ≥ 2-fold.

3.19 Analysis of Peritoneal Macrophages from *PMCA1*-cKO:

Peritoneal macrophages, as the name suggests, are macrophages present in the peritoneal cavity. They play a crucial role in maintaining tissue homeostasis and mediate both pro and anti-inflammatory responses during pathogenic infection and tissue injuries, respectively (Cassado et al., 2015). For us, they provided us with an opportunity to analyze macrophages that have developed *in vivo* and assess the effect of PMCA1 deletion in these cells.

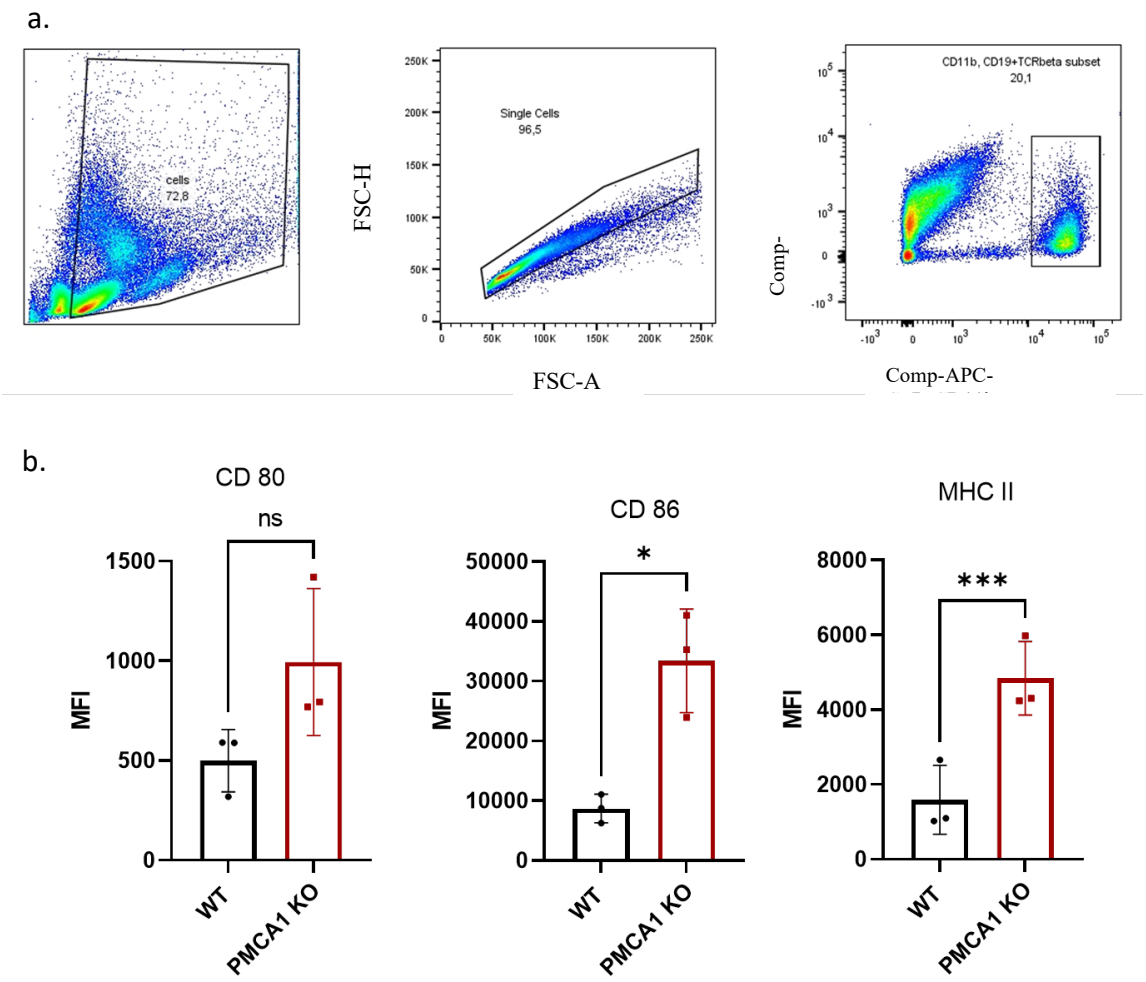

Figure 49: Analysis of markers associated with activation of peritoneal macrophages. a. Gating strategy for gating peritoneal macrophage specific population from peritoneal lavage, described in methods. b. Mean Fluorescent intensity displaying expression patterns of markers, CD 80 CD 86 and MHC II specifically. (paired t-test was performed; ns = non-significant, * = p ≤.05, ** = p ≤.01, *** = p ≤.001)

CD 86 and MHC II, known to be upregulated in activated monocytes have fairly elevated in expression in *PMCA1*-cKO peritoneal macrophages. CD 80 though shows upward trend does not have a statistical significance. Above results show an ongoing inflammation in the animals with PMCA1 knockouts without any external stimuli, although a comprehensive analysis is desired and could be a potential future direction of work on these knockout animals.

4. Discussion:

Macrophages are integral players in the immune system, and they orchestrate immune responses and inflammation. As described in the introduction to this thesis, the complex regulation of macrophage functions involves a delicate interplay of various molecular components. In this work, a major focus was placed on two proteins, Neuroplastin and PMCA1, that have recently been shown to physically interact and to be crucially involved in cellular Ca^{2+} handling (Gong et al., 2018; Herrera-Molina et al., 2017; Korthals et al., 2017; Schmidt et al., 2017). While Neuroplastin had been approved for its strong impact on PMCA stability in macrophages ((Korthals et al., 2017) and this work), the actual relevance of either Neuroplastin or PMCA1 for macrophage function had remained elusive. In fact, a comprehensive understanding of how Ca^{2+}-regulated processes participate in the control of macrophage polarization and function appears to be missing (Vaeth et al., 2015). This notion is supported by the surprising observation that the deletion of STIM1 and STIM2 is dispensable for M1 polarization (Vaeth et al., 2015). Few but interesting articles have since then put forward the idea that other routes of Ca^{2+} entry may be employed to trigger macrophage polarization (Chauhan et al., 2018; Schappe et al., 2018). In this work, by using mice with constitutive or conditional knock-out mutations for Neuroplastin or PMCA1, respectively, the importance of proper Ca^{2+} homeostasis was addressed independent of how Ca^{2+} actually enters macrophages. Despite the close interaction between both proteins, the respective mutants revealed clearly more severe phenotypes associated with loss of PMCA1 than with loss of Neuroplastin. The following discussion delves into the various levels of phenotypical analysis, putting particular emphasis on possible links to Ca^{2+} handling and disturbances thereof.

Neuroplastin has recently been characterized for its role in T cells. Here it was found that the protein is strongly upregulated upon TCR engagement. Loss of Neuroplastin in T cells resulted in about 75% reduction of PMCAs and entailed an about 60% increase in free cytosolic Ca^{2+} next to an overload of ER Ca^{2+}. These effects tightly correlated with increased nuclear NFAT levels, elevated levels of IL-2 and IFNγ and a bias towards Th1 polarization. Despite a similarly severe reduction in PMCA levels, the Ca^{2+} profile in Neuroplastin-deficient BMDM displayed only a moderate Ca^{2+} overload of the ER and was otherwise much less affected than in their

T cell counterparts. Also, no upregulation of Neuroplastin was observed after IFNγ/LPS stimulation. It may thus be not surprising that neither the addressed signaling parameters nor cytokine profiles nor other features, such as iNOS expression and phagocytosis of beads, showed abnormalities. The absence of Neuroplastin in BMDM was accompanied by significantly increased Basigin levels (Figure 12), which likely accounts for the stabilization of PMCA to a certain extent (Schmidt et al., 2017). Moreover, reduced PMCA levels may be compensated at least in part by Ca^{2+}/CaM-mediated release from autoinhibition of the ATPase activity (Lopreiato et al., 2014). While *Nptn*$^{-/-}$ BMDM displayed normal OXPHOS, glycolytic activity upon stimulation was reduced compared to controls, consistent with a moderate reduction of intracellular lactate. It may be speculated that this phenotype relates to the role of Neuroplastin or Basigin in controlling the surface expression of MCTs (MCT2 to be specific), i.e. the transport of lactate across the plasma membrane (Wilson et al., 2013), but a more concrete scenario remains elusive. Of note, a recent study by (Ren et al., 2022) reported that macrophages lacking the long splice isoform of Neuroplastin, Np65, displayed various deficits in response to E.coli infection and/or in *ex vivo* assays, including impairments of phagocytosis, lysosome function, and NO synthesis. These findings, however, are not only difficult to align with the here presented results but are also in conflict with the fact that Np65 is hardly, if at all expressed in macrophages (Langnaese et al., 2024).

In striking contrast to the *Nptn*$^{-/-}$ BMDM (and HB8M), BMDM (and HB8M) lacking PMCA1 displayed abnormalities for most phenotypical aspects addressed in this work. PMCA4 transcripts are clearly detectable in murine macrophages. However, PMCA1 transcripts are > 10 times more abundant as deduced from both microarray data at www.immgen.org and RNAseq data from this work. Given the virtual absence of PMCA2 and 3 transcripts, it is conceivable that PMCA1 is by far the predominant isoform in BMDM, consequently leading to the virtual absence of pan-PMCA immunoreactivity in Western Blot analyses on *PMCA1*-cKO BMDM (Figure 19). Therefore, PMCA4, despite some transcriptional upregulation and splice variation that may lead to increased pump activity (Corradi et al., 2021), can hardly compensate for the absence of PMCA1. A prominent mode of compensation was rather unraveled by the RNAseq approach, which demonstrated a tremendous upregulation of SERCA3 at the transcriptional level, which has been corroborated by Western blot analysis (K. Langnaese, personal communication) and which correlates with the Ca^{2+} overload of the ER.

Nonetheless, Ca^{2+} clearance after SOCE was still apparent in *PMCA1*-cKO BMDM, even though SERCA was irreversibly blocked (Figure 20), possibly involving NCX1 (SLC8A1), for which the RNAseq analysis revealed robust expression in BMDM. Thus, in this situation, Ca^{2+} homeostasis is distorted, though cell function and survival are apparently not compromised. Although PMCAs' dependency on Neuroplastin is now well established, the possibility of a vice *versa* dependency remains elusive. The western blot analysis on *PMCA1*-cKO BMDM showed that the overall abundance of Neuroplastin is not affected. However, Neuroplastin bands running at higher molecular weights due to extensive glycosylation were hardly detectable. Since such modified Neuroplastin is supposedly located on the plasma membrane (Korthals et al., 2017), it appears conceivable that the surface expression of Neuroplastin may be impaired.

In this work, four canonical signaling pathways involved in M1 polarization have been assessed at the level of their key components (STAT1, NF-κB, ERK1/2, Akt) in context with loss of PMCA1 and thus loss of almost all PMCA. Phosphorylation of STAT1 as a read-out for IFNGR-dependent priming and phosphorylation of NF-κB as a read-out for TLR4-dependent stimulation by LPS were both found to be unaffected. In contrast, Erk phosphorylation showed clear upregulation, largely following the normal time course upon LPS stimulation. In fact, ERK1/2 phosphorylation can occur via CaMKI-mediated activation of MEK, thus involving a Ca^{2+}-dependent step (Schmitt et al., 2004; Ueda et al., 1996). Akt activation, in turn, remained subdued, and currently, literature explaining this phenomenon is scarce.

A role for NFAT isoforms, for NFATc3 and 4 in particular has been proposed in macrophage responses to discrete stimuli (Vandewalle et al., 2014). In the course of this study, only brief confocal microscopy- and FACS-based inspections of NFATc1 in non-stimulated BMDM were performed and did not reveal striking differences between *PMCA1*-cKO and controls regarding expression levels and nuclear localization. However, in light of the substantial changes in gene expression as revealed by RNAseq, the possibility of hyperactivated NFAT isoforms due to increased Ca^{2+} levels should be addressed in further detail. The involvement of Ca^{2+} in the activation process that leads to M1 polarization has remained obscure as compared, for instance, to the well-established role of SOCE-related Ca^{2+} signaling in T cell activation.

Macrophages, as part of the immune system, are crucial for detecting and responding to pathogens and other foreign materials, along with other stimuli from within the body, e.g., various chemical signals like interferons. They have several mechanisms for sensing, e.g., macrophages express various PRRs on their surface, such as Toll-like receptors (TLRs), NOD-like receptors (NLRs), and RIG-I-like receptors (RLRs). These receptors can recognize specific molecular patterns associated with pathogens, known as pathogen-associated molecular patterns (PAMPs). These receptors carry the signal to the nucleus through various signal transduction molecules, namely STAT1, NF-κB, ERK, and others, through phosphorylation (dephosphorylation) events. The quantification of phosphorylation may help us judge the extent of signaling in the cells. Activation of macrophages by IFNγ and LPS stimulates the production and release of pro-inflammatory cytokines, this way reflecting the successful execution of signaling events and their integration at transcriptional, post-transcriptional, and post-translational levels. *PMCA1*-cKO macrophages showed upregulated cytokine release into the medium, although these cells did not show any difference in stimulated NF-κB and STAT1 phosphorylation. Even at the transcript level, as revealed by RNAseq, most of the cytokines showed little if any difference between PMCA-cKO and control macrophages. Of note, however, activated ERK1/2 has not only been implicated in the transcriptional regulation of some cytokines but also in transcription-independent steps of cytokine release. Specifically, it can phosphorylate TNF-α -converting enzyme (TACE), which cleaves transmembrane TNF-alpha's extracellular domain to release the fully functional form (Sabio et al., 2014; Soond et al., 2005). Similarly, elevated levels of activated ERK may account for transcription-independent priming of NLRP3 inflammasome assembly (Ghonime et al., 2014). The active inflammasome, in turn, is necessary for the maturation and secretion of the pro-inflammatory cytokine IL-1β involving activated caspase-1. Both inflammasome and secreted IL-1β (rather than IL-1β transcripts) were found to be increased in *PMCA1*-cKO *versus* control macrophages. It is tempting to hypothesize that in this context, increased levels of Ca^{2+} could mimic an otherwise ATP-dependent Ca^{2+} influx through P2X receptors that foster inflammasome-dependent activation of caspase-1 (Ghonime et al., 2014; Zumerle et al., 2019). During M1 polarization, murine macrophages switch from OXPHOS to glycolysis, that provides a rapid source of ATP and metabolic intermediates (e.g., NAD^+) for inflammatory responses (Soto-Heredero et al., 2020). Enhanced glycolytic activity involves the upregulation

of the transcription factor HIF-1α , which promotes increased expression of glycolytic enzymes like Hexokinases (HK) and lactate dehydrogenases (LDH) and of glucose transporters (Frede et al., 2006; Hayashi et al., 2004; Vaeth et al., 2020). The RNAseq analysis in this work confirms robust upregulation of HIF-1α HK and LDH transcripts in stimulated BMDM, yet without noticeable or with only mild difference between *PMCA1*-cKO and controls (but see discussion below on time-dependent aspects of transcription). The shutdown of OXPHOS is at least partially due to the strong increase in NO, which competes with oxygen for binding to cytochrome c oxidase (Complex IV) heme and thus blocks the ETC's final electron transfer step (Sarti et al., 2012; Van den Bossche et al., 2016). At the transcript level (RNAseq), stimulation-dependent expression of iNOS was found to be unaltered between *PMCA1*-cKO and controls. However, a substantial increase in iNOS levels in *PMCA1*-cKO BMDM over their control counterparts was found after overnight exposure to LPS and IFNγ (Figure 19). Preliminary data imply that this difference manifests in NO production (Dr. Gayatri Jagirdar, pers. communication). As OXPHOS was virtually shut off in both genotypes after stimulation, excessive NO in the *PMCA1*-cKO may rather be expected to foster defense against pathogens and/or exert cytoprotective or unwanted cytotoxicity against other host cells (Kröncke et al., 1997). Whereas OXPHOS shut-off was unaffected in the absence of PMCA1, non-stimulated *PMCA1*-cKO BMDM showed elevated OXPHOS levels as compared to controls. RNAseq, however, did not demonstrate any significant differences in the expression of genes involved in OXPHOS in *PMCA1*-cKO compared to the controls (Figure 44). Neither did the KEGG analysis show any enrichment of OXPHOS-related gene sets. Of note, however, is that Ca^{2+} itself is known to stimulate OXPHOS by activating key dehydrogenases in the mitochondrial matrix (Dejos et al., 2020). Moreover, the malate aspartate cycle that acts as an accelerator for OXPHOS can be positively regulated by cytosolic Ca^{2+} (del Arco et al., 2023). Hence, links between elevated Ca^{2+} levels in non-stimulated *PMCA1*-cKO BMDM and elevated levels of OXPHOS can easily be proposed. Interestingly, the non-stimulated *PMCA1*-cKO BMDM also displayed higher than normal glycolytic activity, a phenotype that got even more pronounced after stimulation.

As for elevated OXPHOS in the non-stimulated *PMCA1*-cKO BMDM, KEGG analysis of the RNAseq data for M1 polarized *PMCA1*-cKO BMDM did not reveal an enrichment of gene sets related to the observed increase in glycolytic activity. Nonetheless, a closer inspection

identified a few genes with altered expression (Figure 45), e.g. reduced expression of Idh1 or upregulation of HK1. Moreover, as for OXPHOS-related enzymes, Ca^{2+} can modulate glycolytic enzymes. For example, the activity of one of the key glycolytic enzymes, 6-phosphofructo-2-kinase/fructose-2,6-bisphosphatase 3 (PFKFB3), can be blocked by intracellular chelating of Ca^{2+} (Sneyers et al., 2023).

In light of the close association of PMCAs and Neuroplastin, it came as a surprise that in contrast to *PMCA1*-cKO BMDM, *Nptn*$^{-/-}$ BMDM displayed subdued glycolytic activity after long-term stimulation and M1 polarization. No effects related to decreased glycolytic activity became obvious for these macrophages and the mechanism behind this outcome remains poorly understood. At present, it cannot be ruled out that it reflects a function of Neuroplastin that is not directly related to its association with PMCAs but rather with other proteins, including MCTs and TRAF6 (Herrera-Molina et al., 2014; Vemula et al., 2020; Wilson et al., 2013).

The phenotyping of PMCA1-depleted BMDM was complemented by an RNAseq analysis restricted to mRNA. This provided snapshots of the transcriptomes before and 4 hours after LPS/IFNγ stimulation. While assays like cytokine measurements, metabolic analysis, and inflammasome detection were performed only after an extended period of stimulation (16 hours), the 4-hour time point was chosen to meet the profiles of canonical signaling with a certain delay to allow for downstream transcriptional activity. Later post-stimulatory time points of RNAseq analysis could have added to a more detailed understanding (Das et al., 2018b) but were thus far unaffordable. Proteomic analysis may also be envisaged to complement this expression study. The aforementioned overproduction of iNOS in stimulated *PMCA1*-cKO, which was not predicted by RNAseq, provides an example, of where long-term transcriptional and/ or post-transcriptional mechanisms may be involved (Kleinert et al., 2003).

Comparing RNAseq data from resting and stimulated BMDM clearly pointed to the successful onset of M1 polarization (Figure 39) in both *PMCA1*-cKO and control BMDM, with about one-tenth of all genes showing differential expression. Whereas KEGG pathway enrichment analyses failed to uncover a transcriptomic basis for changes in cytokine production and

metabolism, it revealed several other categories with expected or yet obscure relation to the experimental conditions. The former included the "Calcium signaling pathway", "NF-kappa B signaling pathway", or "PI3K-Akt signaling pathway" when *PMCA1*-cKO and control BMDM were compared in both resting and stimulated conditions. Likewise, "Systemic Lupus erythematosus" (SLE) was identified as a KEGG category, which displayed an enrichment of genes that are upregulated in the *PMCA1*-cKO cells, suggesting a possible involvement of reduced PMCA1 in this autoimmune disease. Alignment of published data on the role of macrophages in SLE (S. Yang et al., 2023) with the genes included in the respective KEGG category will be needed to evaluate such a putative link, a notion that similarly applies to the majority of identified KEGG categories. NF-κB signaling was identified by the KEGG pathway enrichment analysis, although NF-κB itself was found unchanged between *PMCA1*-cKO and control BMDM in western blots, again exemplifying that thorough disentangling is required to substantiate KEGG results for their meaning in regard to the analyzed conditions. A preliminary inspection reveals that downstream factors of NF-κB, mostly cytokines and chemokines, account for detecting this pathway in the KEGG enrichment analysis as KEGG is biased towards well-studied signaling pathways.

Two genes closely related to Ca^{2+} signaling were among the genes that showed prolific upregulation in *PMCA1*-cKO before and/or after stimulation: *Rcan1* and SERCA3. *Rcan1* suppresses the Ca^{2+}-dependent activity of the phosphatase calcineurin and thereby diminishes the activation of NFAT. SERCA3 transcripts were found to be highly above control levels in *PMCA1*-cKO before stimulation and did not increase further thereafter. In controls, SERCA3 transcripts did not show significant upregulation even after stimulation, suggesting that the high levels of SERCA3 may result from increased cytosolic Ca^{2+} *per se*. In contrast, RCAN1 transcripts were clearly upregulated in control BMDM after stimulation yet did not fully reach the level that was found in *PMCA1*-cKO already before stimulation. RCAN1 thus stands for a number of genes that are normally upregulated only upon stimulation but were found to be increased in *PMCA1*-cKO without stimulation. This might imply that resting *PMCA1*-cKO BMDM display features of primed and/ or activated macrophages, but it should be noted that currently this is not yet supported by the phenotypical analysis. Ongoing research, however, addresses the idea that priming by IFNγ might be (partially) dispensable

to induce M1 polarization in the absence of PMCA1. For instance, whereas synergy between IFNγ and LPS is usually required for strong upregulation of iNOS (Dell'Albani et al., 2001), this hallmark of M1 polarization can be achieved by LPS alone in *PMCA1*-cKO BMDM.

The RNAseq data set also allowed to assess a number of "hand-selected" genes that are potentially involved in Ca^{2+} entry and intracellular Ca^{2+} handling, e.g. in order to evaluate their potential impact on macrophage function. This included various genes encoding TRP ion channels. TRPV1 has previously been implicated in macrophage differentiation to osteoclasts (Chakraborty et al., 2022; Chauhan et al., 2018). Elevated Ca^{2+}-influx through TRPC1 has been proposed to be crucial for M1 polarization (Chauhan et al., 2018). TRPM2 has been shown to play a role in macrophage polarization during *H. Pylori* infection (Beceiro et al., 2017) and TRPM7 has been found to carry LPS-mediated Ca^{2+} influx and endocytosis, leading to Macrophage activation (Schappe et al., 2018). Interestingly, the RNAseq analysis points to negligible levels of TRPC1 and TRPV1 transcripts in all tested conditions, questioning the impact of these TRP channels on macrophage function. Transcripts for TRPM2 and TRPM7, on the other hand, were found to be quite abundant, yet without noticeable differences between conditions. In contrast, transcripts for TRPV4, a thermosensitive TRP channel, were found to be robustly expressed in resting control BMDM but downregulated upon stimulation and even more so in *PMCA1*-cKO BMDM. It may be speculated that this serves to restrict Ca^{2+} entry. Another group that has been repeatedly implicated in Ca^{2+} entry into macrophages are purinergic P2X receptors, in particular P2X4 and P2X7 (Kawano et al., 2012; Zumerle et al., 2019). Both display robust expression at the transcript level with moderate downregulation in resting *PMCA1*-cKO BMDM, i.e., reminiscent of TRPV4 transcripts (Masuyama et al., 2008).

The phenotyping presented in this work has been oriented almost exclusively towards non-polarized macrophages and proinflammatory M1 polarization. Ca^{2+}, however, might also have an implicit role in the M2 polarization of macrophages (Nascimento Da Conceicao et al., 2021). *PMCA1*-cKO, as a model for dysregulated Ca^{2+} homeostasis, provides an opportunity to evaluate the potential role of Ca^{2+} in the polarization and functioning of M2 macrophages. In a study on HoxB8-derived macrophages, they were polarized to the M2 phenotype with IL-4 and IL-13 treatment. Activity of Arginase as a hallmark of M2 polarization was measured in the cell lysates of *PMCA1*-cKO, *Nptn* KO, and *WT*.

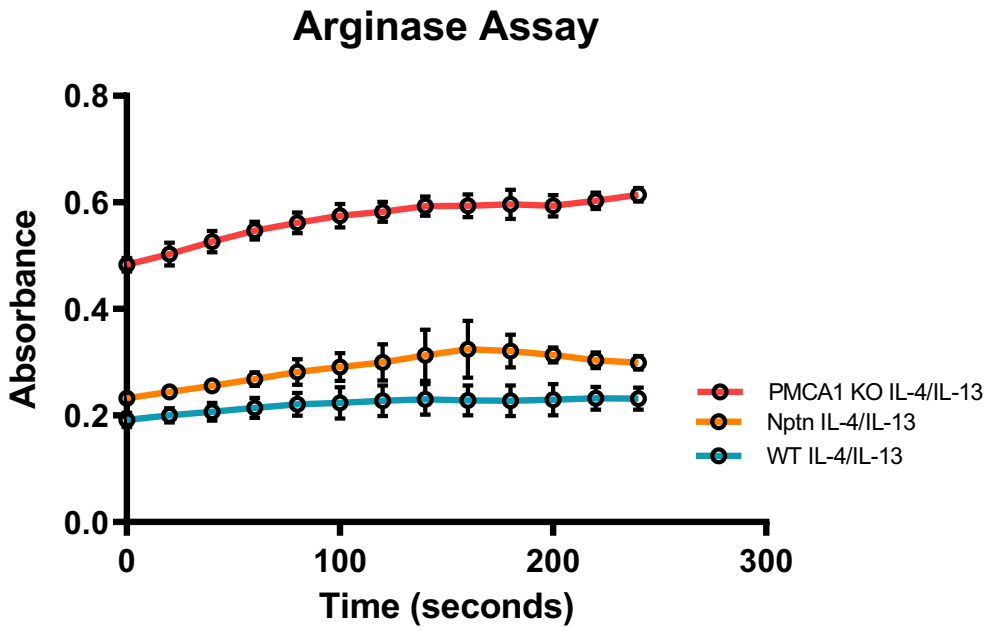

Figure 50: **Arginase Assay performed on HoxB8 macrophages**. 50,000 cells/well of a 96-well plate were seeded and polarized with a 20ng/ml cocktail of IL-4 and IL-13 overnight (15 hours). Cells were lysed by a reagent provided by Abcam® manufacturer and subjected to detection reagents to determine arginase activity. Absorbance at 570nm was recorded for 240 seconds.

PMCA1-cKO HB8M (in red) showed more than 2 times higher absorbance than control and *Nptn*$^{-/-}$ cells

The data pointed to high arginase activity in *PMCA1*-cKO HB8M compared to that of *WT* and *Nptn*$^{-/-}$ HB8M. This suggests that Ca^{2+} overload due to the absence of PMCA1 can also promote M2 polarization of macrophages. While this result awaits approvement in BMDM, it should be stressed that the use of HB8M in various assays throughout this study has largely confirmed results obtained from BMDM and may thus be considered as a promising alternative to using *ex vivo* cultured BMDM. On the other hand, the *in vivo* diversity of macrophages demands assessments of tissue-specific macrophages, for which results on BMDM and HB8M may serve as a basis. This line of action is exemplified by the analysis of antigen-presenting and co-stimulatory factors in peritoneal macrophages (Figure 49), which was prompted by RNAseq data.

A decline in PMCA activity has repeatedly been linked to aging and disease in various cell types (Stafford et al., 2017). While excitable cells, most notably neurons, are probably most

prone to this, the here presented findings suggest a possible involvement of impaired PMCA function in pathologies related to hyperactive macrophages. On the other hand, this work, within the range of addressed phenotypical parameters, uncovers an unexpected robustness of proinflammatory M1 polarization to a severe reduction of PMCAs as observed in the absence of Neuroplastin. However, in combination with additional impairment of proper Ca^{2+} handling, e.g. in human hereditary gain-of-function mutations that increase Ca^{2+} entry through CRAC channels (Feske, 2019), reduced PMCA function may be expected to lead to more severe disease phenotypes. In fact, the characterization of macrophages lacking Neuroplastin or PMCA1 is to be extended towards cellular phenotypes such as phagocytic properties, cellular morphology, and migration as well as to possible abnormalities at the systemic level.

References:

Adler, B., & Adler, H. (2021). Type I interferon signaling and macrophages: a double-edged sword? *Cellular & Molecular Immunology*, *19*(9), 967–968. https://doi.org/10.1038/s41423-020-00609-0

Ainscough, J. S., Gerberick, G. F., Kimber, I., & Dearman, R. J. (2015). Interleukin-1β Processing Is Dependent on a Calcium-mediated Interaction with Calmodulin. *Journal of Biological Chemistry*, *290*(52), 31151–31161. https://doi.org/10.1074/jbc.M115.680694

Arpa, L., Batlle, C., Jiang, P., Caelles, C., Lloberas, J., & Celada, A. (2023). Distinct Responses to IL4 in Macrophages Mediated by JNK. *Cells*, *12*(8), 1127. https://doi.org/10.3390/cells12081127

Awasthi, D., Nagarkoti, S., Sadaf, S., Chandra, T., Kumar, S., & Dikshit, M. (2019). Glycolysis dependent lactate formation in neutrophils: A metabolic link between NOX-dependent and independent NETosis. *Biochimica et Biophysica Acta (BBA) - Molecular Basis of Disease*, *1865*(12), 165542. https://doi.org/10.1016/j.bbadis.2019.165542

Baardman, J., Verberk, S. G. S., Prange, K. H. M., van Weeghel, M., van der Velden, S., Ryan, D. G., Wüst, R. C. I., Neele, A. E., Speijer, D., Denis, S. W., Witte, M. E., Houtkooper, R. H., O'neill, L. A., Knatko, E. V., Dinkova-Kostova, A. T., Lutgens, E., de Winther, M. P. J., & Van den Bossche, J. (2018). A Defective Pentose Phosphate Pathway Reduces Inflammatory Macrophage Responses during Hypercholesterolemia. *Cell Reports*, *25*(8), 2044-2052.e5. https://doi.org/10.1016/j.celrep.2018.10.092

Bailey, J. D., Diotallevi, M., Nicol, T., McNeill, E., Shaw, A., Chuaiphichai, S., Hale, A., Starr, A., Nandi, M., Stylianou, E., McShane, H., Davis, S., Fischer, R., Kessler, B. M., McCullagh, J., Channon, K. M., & Crabtree, M. J. (2019). Nitric Oxide Modulates Metabolic Remodeling in Inflammatory Macrophages through TCA Cycle Regulation and Itaconate Accumulation. *Cell Reports*, *28*(1), 218-230.e7. https://doi.org/10.1016/j.celrep.2019.06.018

Beceiro, S., Radin, J. N., Chatuvedi, R., Piazuelo, M. B., Horvarth, D. J., Cortado, H., Gu, Y., Dixon, B., Gu, C., Lange, I., Koomoa, D.-L., Wilson, K. T., Algood, H. M. S., & Partida-Sánchez, S. (2017). TRPM2 ion channels regulate macrophage polarization and gastric inflammation during Helicobacter pylori infection. *Mucosal Immunology*, *10*(2), 493–507. https://doi.org/10.1038/mi.2016.60

Beckmann, D., Langnaese, K., Gottfried, A., Hradsky, J., Tedford, K., Tiwari, N., Thomas, U., Fischer, K.-D., & Korthals, M. (2023). Ca2+ Homeostasis by Plasma Membrane Ca2+ ATPase (PMCA) 1 Is Essential for the Development of DP Thymocytes. *International Journal of Molecular Sciences*, *24*(2), 1442. https://doi.org/10.3390/ijms24021442

Berridge, M. J., Bootman, M. D., & Roderick, H. L. (2003). Calcium signalling: dynamics, homeostasis and remodelling. *Nature Reviews Molecular Cell Biology*, *4*(7), 517–529. https://doi.org/10.1038/nrm1155

Bootman, M. D. (2012). Calcium signaling. *Cold Spring Harbor Perspectives in Biology*, *4*(7), 1–3. https://doi.org/10.1101/cshperspect.a011171

Cassado, A. dos A., Dâ€™ImpÃ©rio Lima, M. R., & Bortoluci, K. R. (2015). Revisiting Mouse Peritoneal Macrophages: Heterogeneity, Development, and Function. *Frontiers in Immunology*, *6*. https://doi.org/10.3389/fimmu.2015.00225

Chakraborty, R., Acharya, T. K., Tiwari, N., Majhi, R. K., Kumar, S., Goswami, L., & Goswami, C. (2022). Hydrogel-Mediated Release of TRPV1 Modulators to Fine Tune Osteoclastogenesis. *ACS Omega*, *7*(11), 9537–9550. https://doi.org/10.1021/acsomega.1c06915

Chauhan, A., Sun, Y., Sukumaran, P., Quenum Zangbede, F. O., Jondle, C. N., Sharma, A., Evans, D. L., Chauhan, P., Szlabick, R. E., Aaland, M. O., Birnbaumer, L., Sharma, J., Singh, B. B., & Mishra, B. B. (2018). M1 Macrophage Polarization Is Dependent on TRPC1-Mediated Calcium Entry. *IScience*, *8*, 85–102. https://doi.org/10.1016/j.isci.2018.09.014

Chen, A. X., Gartrell, R. D., Zhao, J., Upadhyayula, P. S., Zhao, W., Yuan, J., Minns, H. E., Dovas, A., Bruce, J. N., Lasorella, A., Iavarone, A., Canoll, P., Sims, P. A., & Rabadan, R. (2021). Single-cell characterization of macrophages in glioblastoma reveals MARCO as a mesenchymal pro-tumor marker. *Genome Medicine*, *13*(1), 88. https://doi.org/10.1186/s13073-021-00906-x

Clapham, D. E. (2007). Calcium Signaling. *Cell*, *131*(6), 1047–1058. https://doi.org/10.1016/j.cell.2007.11.028

Coelho, C. (2022). Itaconate or how I learned to stop avoiding the study of immunometabolism. *PLOS Pathogens*, *18*(3), e1010361. https://doi.org/10.1371/journal.ppat.1010361

Corradi, G. R., Mazzitelli, L. R., Petrovich, G. D., de Tezanos Pinto, F., Rochi, L., & Adamo, H. P. (2021). Plasma Membrane Ca2+ Pump PMCA4z Is More Active Than Splicing Variant PMCA4x. *Frontiers in Cellular Neuroscience*, *15*. https://doi.org/10.3389/fncel.2021.668371

Courjaret, R., & Machaca, K. (2014). Mid-range Ca2+ signalling mediated by functional coupling between store-operated Ca2+ entry and IP3-dependent Ca2+ release. *Nature Communications*, *5*(1), 3916. https://doi.org/10.1038/ncomms4916

Czimmerer, Z., Halasz, L., Daniel, B., Varga, Z., Bene, K., Domokos, A., Hoeksema, M., Shen, Z., Berger, W. K., Cseh, T., Jambrovics, K., Kolostyak, Z., Fenyvesi, F., Varadi, J., Poliska, S., Hajas, G., Szatmari, I., Glass, C. K., Bacsi, A., & Nagy, L. (2022). The epigenetic state of IL-4-polarized macrophages enables inflammatory cistromic expansion and extended synergistic response to TLR ligands. *Immunity*, *55*(11), 2006-2026.e6. https://doi.org/10.1016/j.immuni.2022.10.004

Dang, B., Gao, Q., Zhang, L., Zhang, J., Cai, H., Zhu, Y., Zhong, Q., Liu, J., Niu, Y., Mao, K., Xiao, N., Liu, W.-H., Lin, S., Huang, J., Huang, S. C.-C., Ho, P.-C., & Cheng, S.-C. (2023). The glycolysis/HIF-1α axis defines the inflammatory role of IL-4-primed macrophages. *Cell Reports*, *42*(5), 112471. https://doi.org/10.1016/j.celrep.2023.112471

Das, A., Yang, C.-S., Arifuzzaman, S., Kim, S., Kim, S. Y., Jung, K. H., Lee, Y. S., & Chai, Y. G. (2018). High-Resolution Mapping and Dynamics of the Transcriptome, Transcription Factors, and Transcription Co-Factor Networks in Classically and Alternatively Activated Macrophages. *Frontiers in Immunology*, *9*. https://doi.org/10.3389/fimmu.2018.00022

Dejos, C., Gkika, D., & Cantelmo, A. R. (2020). The Two-Way Relationship Between Calcium and Metabolism in Cancer. *Frontiers in Cell and Developmental Biology*, *8*. https://doi.org/10.3389/fcell.2020.573747

del Arco, A., González-Moreno, L., Pérez-Liébana, I., Juaristi, I., González-Sánchez, P., Contreras, L., Pardo, B., & Satrústegui, J. (2023). Regulation of neuronal energy metabolism by calcium: Role of MCU and Aralar/malate-aspartate shuttle. *Biochimica et Biophysica Acta (BBA) - Molecular Cell Research*, *1870*(5), 119468. https://doi.org/10.1016/j.bbamcr.2023.119468

Dell'Albani, P., Santangelo, R., Torrisi, L., Nicoletti, V. G., de Vellis, J., & Giuffrida Stella, A. M. (2001). JAK/STAT signaling pathway mediates cytokine-induced iNOS expression in primary astroglial cell cultures. *Journal of Neuroscience Research*, *65*(5), 417–424. https://doi.org/10.1002/jnr.1169

Deng, F., Fu, M., Zhao, C., Lei, J., Xu, T., Ji, B., Ding, H., Zhang, Y., Chen, J., Qiu, J., & Gao, Q. (2023). Calcium signals and potential therapy targets in ovarian cancer (Review). *International Journal of Oncology*, *63*(5), 125. https://doi.org/10.3892/ijo.2023.5573

Desvignes, L., Weidinger, C., Shaw, P., Vaeth, M., Ribierre, T., Liu, M., Fergus, T., Kozhaya, L., McVoy, L., Unutmaz, D., Ernst, J. D., & Feske, S. (2015). STIM1 controls T cell–mediated immune regulation and inflammation in chronic infection. *Journal of Clinical Investigation*, *125*(6), 2347–2362. https://doi.org/10.1172/JCI80273

Dick, S. A., Wong, A., Hamidzada, H., Nejat, S., Nechanitzky, R., Vohra, S., Mueller, B., Zaman, R., Kantores, C., Aronoff, L., Momen, A., Nechanitzky, D., Li, W. Y., Ramachandran, P., Crome, S. Q., Becher, B., Cybulsky, M. I., Billia, F., Keshavjee, S., … Epelman, S. (2022). Three tissue resident macrophage subsets coexist across organs with conserved origins and life cycles. *Science Immunology*, *7*(67). https://doi.org/10.1126/sciimmunol.abf7777

Dong, X., Shen, D., Wang, X., Dawson, T., Li, X., Zhang, Q., Cheng, X., Zhang, Y., Weisman, L. S., Delling, M., & Xu, H. (2010). PI(3,5)P2 controls membrane trafficking by direct activation of mucolipin Ca2+ release channels in the endolysosome. *Nature Communications*, *1*(1), 38. https://doi.org/10.1038/ncomms1037

Dong, X., Wang, X., & Xu, H. (2010). TRP channels of intracellular membranes. *Journal of Neurochemistry*, *113*(2), 313–328. https://doi.org/10.1111/j.1471-4159.2010.06626.x

Elliott, M. R., & Ravichandran, K. S. (2010). Clearance of apoptotic cells: implications in health and disease. *Journal of Cell Biology*, *189*(7), 1059–1070. https://doi.org/10.1083/jcb.201004096

Endo, M. (2006). Calcium Ion as a Second Messenger With Special Reference to Excitation-Contraction Coupling. *Journal of Pharmacological Sciences*, *100*(5), 519–524. https://doi.org/10.1254/jphs.CPJ06004X

Feng, M., Chen, J. Y., Weissman-Tsukamoto, R., Volkmer, J.-P., Ho, P. Y., McKenna, K. M., Cheshier, S., Zhang, M., Guo, N., Gip, P., Mitra, S. S., & Weissman, I. L. (2015). Macrophages eat cancer cells using their own calreticulin as a guide: Roles of TLR and Btk. *Proceedings of the National Academy of Sciences*, *112*(7), 2145–2150. https://doi.org/10.1073/pnas.1424907112

Feske, S. (2019). CRAC channels and disease – From human CRAC channelopathies and animal models to novel drugs. *Cell Calcium*, *80*, 112–116. https://doi.org/10.1016/j.ceca.2019.03.004

Frede, S., Stockmann, C., Freitag, P., & Fandrey, J. (2006). Bacterial lipopolysaccharide induces HIF-1 activation in human monocytes via p44/42 MAPK and NF-κB. *Biochemical Journal*, *396*(3), 517–527. https://doi.org/10.1042/BJ20051839

Freemerman, A. J., Johnson, A. R., Sacks, G. N., Milner, J. J., Kirk, E. L., Troester, M. A., Macintyre, A. N., Goraksha-Hicks, P., Rathmell, J. C., & Makowski, L. (2014). Metabolic Reprogramming of Macrophages. *Journal of Biological Chemistry*, *289*(11), 7884–7896. https://doi.org/10.1074/jbc.M113.522037

Garaude, J., Acín-Pérez, R., Martínez-Cano, S., Enamorado, M., Ugolini, M., Nistal-Villán, E., Hervás-Stubbs, S., Pelegrín, P., Sander, L. E., Enríquez, J. A., & Sancho, D. (2016). Mitochondrial respiratory-chain adaptations in macrophages contribute to antibacterial host defense. *Nature Immunology*, *17*(9), 1037–1045. https://doi.org/10.1038/ni.3509

Ghonime, M. G., Shamaa, O. R., Das, S., Eldomany, R. A., Fernandes-Alnemri, T., Alnemri, E. S., Gavrilin, M. A., & Wewers, M. D. (2014). Inflammasome Priming by Lipopolysaccharide Is Dependent upon ERK Signaling and Proteasome Function. *The Journal of Immunology*, *192*(8), 3881–3888. https://doi.org/10.4049/jimmunol.1301974

Ginhoux, F., Mildner, A., Gautier, E. L., Schlitzer, A., Jakubzick, C., Varol, C., Bain, C., & Guermonprez, P. (2021). Editorial: Monocyte Heterogeneity and Function. *Frontiers in Immunology*, *11*. https://doi.org/10.3389/fimmu.2020.626725

Gong, D., Chi, X., Ren, K., Huang, G., Zhou, G., Yan, N., Lei, J., & Zhou, Q. (2018). Structure of the human plasma membrane Ca2+-ATPase 1 in complex with its obligatory subunit neuroplastin. *Nature Communications*, *9*(1). https://doi.org/10.1038/s41467-018-06075-7

Halestrap, A. P., & Wilson, M. C. (2012). The monocarboxylate transporter family—Role and regulation. *IUBMB Life*, *64*(2), 109–119. https://doi.org/10.1002/iub.572

Hayashi, M., Sakata, M., Takeda, T., Yamamoto, T., Okamoto, Y., Sawada, K., Kimura, A., Minekawa, R., Tahara, M., Tasaka, K., & Murata, Y. (2004). Induction of glucose transporter 1 expression through hypoxia-inducible factor 1α under hypoxic conditions in trophoblast-derived cells. *Journal of Endocrinology*, *183*(1), 145–154. https://doi.org/10.1677/joe.1.05599

Herrera-Molina, R., Mlinac-Jerkovic, K., Ilic, K., Stöber, F., Vemula, S. K., Sandoval, M., Milosevic, N. J., Simic, G., Smalla, K.-H., Goldschmidt, J., Bognar, S. K., & Montag, D. (2017). Neuroplastin deletion in glutamatergic neurons impairs selective brain functions and calcium regulation: implication for cognitive deterioration. *Scientific Reports*, *7*(1), 7273. https://doi.org/10.1038/s41598-017-07839-9

Herrera-Molina, R., Sarto-Jackson, I., Montenegro-Venegas, C., Heine, M., Smalla, K.-H., Seidenbecher, C. I., Beesley, P. W., Gundelfinger, E. D., & Montag, D. (2014). Structure of Excitatory Synapses and GABAA Receptor Localization at Inhibitory Synapses Are Regulated by Neuroplastin-65. *Journal of Biological Chemistry*, *289*(13), 8973–8988. https://doi.org/10.1074/jbc.M113.514992

Hirayama, D., Iida, T., & Nakase, H. (2017). The Phagocytic Function of Macrophage-Enforcing Innate Immunity and Tissue Homeostasis. *International Journal of Molecular Sciences*, *19*(1), 92. https://doi.org/10.3390/ijms19010092

Hirve, N., Rajanikanth, V., Hogan, P. G., & Gudlur, A. (2018). Coiled-Coil Formation Conveys a STIM1 Signal from ER Lumen to Cytoplasm. *Cell Reports*, *22*(1), 72–83. https://doi.org/10.1016/j.celrep.2017.12.030

Hogan, P. G., & Rao, A. (2015). Store-operated calcium entry: Mechanisms and modulation. *Biochemical and Biophysical Research Communications*, *460*(1), 40–49. https://doi.org/10.1016/j.bbrc.2015.02.110

Hoogerwerf, J. J., de Vos, A. F., van't Veer, C., Bresser, P., de Boer, A., Tanck, M. W. T., Draing, C., van der Zee, J. S., & van der Poll, T. (2010). Priming of Alveolar Macrophages upon Instillation of Lipopolysaccharide in the Human Lung. *American Journal of Respiratory Cell and Molecular Biology*, *42*(3), 349–356. https://doi.org/10.1165/rcmb.2008-0362OC

Jouneaux, C., Mallat, A., Serradeil-Le Gal, C., Goldsmith, P., Hanoune, J., & Lotersztajn, S. (1994). Coupling of endothelin B receptors to the calcium pump and phospholipase C via Gs and Gq in rat liver. *Journal of Biological Chemistry*, *269*(3), 1845–1851. https://doi.org/10.1016/S0021-9258(17)42104-1

Juarez, E., Nuñez, C., Sada, E., Ellner, J. J., Schwander, S. K., & Torres, M. (2010). Differential expression of Toll-like receptors on human alveolar macrophages and autologous peripheral monocytes. *Respiratory Research*, *11*(1), 2. https://doi.org/10.1186/1465-9921-11-2

Kawano, A., Tsukimoto, M., Mori, D., Noguchi, T., Harada, H., Takenouchi, T., Kitani, H., & Kojima, S. (2012). Regulation of P2X7-dependent inflammatory functions by P2X4 receptor in mouse macrophages. *Biochemical and Biophysical Research Communications*, *420*(1), 102–107. https://doi.org/10.1016/j.bbrc.2012.02.122

Keegan, A. D., Nelms, K., White, M., Wang, L.-M., Pierce, J. H., & Paul, W. E. (1994). An IL-4 receptor region containing an insulin receptor motif is important for IL-4-mediated IRS-1 phosphorylation and cell growth. *Cell*, *76*(5), 811–820. https://doi.org/10.1016/0092-8674(94)90356-5

Kleinert, H., Schwarz, P. M., & Förstermann, U. (2003). Regulation of the Expression of Inducible Nitric Oxide Synthase. *Biological Chemistry*, *384*(10–11). https://doi.org/10.1515/BC.2003.152

Korthals, M., Langnaese, K., Smalla, K.-H., Kähne, T., Herrera-Molina, R., Handschuh, J., Lehmann, A.-C., Mamula, D., Naumann, M., Seidenbecher, C., Zuschratter, W., Tedford, K., Gundelfinger, E. D., Montag, D., Fischer, K.-D., & Thomas, U. (2017). A complex of Neuroplastin and Plasma Membrane Ca2+ ATPase controls T cell activation. *Scientific Reports*, *7*(1), 8358. https://doi.org/10.1038/s41598-017-08519-4

Korthals, M., Tech, L., Langnaese, K., Gottfried, A., Hradsky, J., Thomas, U., Zenclussen, A. C., Brunner-Weinzierl, M. C., Tedford, K., & Fischer, K. (2021). Plasma membrane Ca $^{2+}$ ATPase 1 (PMCA1) but not PMCA4 is critical for B-cell development and Ca $^{2+}$ homeostasis in mice. *European Journal of Immunology*, *51*(3), 594–602. https://doi.org/10.1002/eji.202048654

Krebs, J. (2015). The plethora of PMCA isoforms: Alternative splicing and differential expression. *Biochimica et Biophysica Acta (BBA) - Molecular Cell Research*, *1853*(9), 2018–2024. https://doi.org/10.1016/j.bbamcr.2014.12.020

Krick, N., Ryglewski, S., Pichler, A., Bikbaev, A., Götz, T., Kobler, O., Heine, M., Thomas, U., & Duch, C. (2021). Separation of presynaptic Ca $_{v}$ 2 and Ca $_{v}$ 1 channel function in synaptic vesicle exo- and endocytosis by the membrane anchored Ca $^{2+}$ pump PMCA. *Proceedings of the National Academy of Sciences*, *118*(28). https://doi.org/10.1073/pnas.2106621118

Kröncke, K.-D., Fehsel, K., & Kolb-Bachofen, V. (1997). Nitric Oxide: Cytotoxicity versus Cytoprotection— How, Why, When, and Where? *Nitric Oxide*, *1*(2), 107–120. https://doi.org/10.1006/niox.1997.0118

Lacruz, R. S., & Feske, S. (2015). Diseases caused by mutations in *ORAI1* and *STIM1*. *Annals of the New York Academy of Sciences*, *1356*(1), 45–79. https://doi.org/10.1111/nyas.12938

Lacy, P., & Stow, J. L. (2011). Cytokine release from innate immune cells: association with diverse membrane trafficking pathways. *Blood*, *118*(1), 9–18. https://doi.org/10.1182/blood-2010-08-265892

Langnaese, K., Beesley, P. W., & Gundelfinger, E. D. (1997). Synaptic Membrane Glycoproteins gp65 and gp55 Are New Members of the Immunoglobulin Superfamily. *Journal of Biological Chemistry*, *272*(2), 821–827. https://doi.org/10.1074/jbc.272.2.821

Langnaese, K., Tiwari, N., Fischer, K.-D., Thomas, U., & Korthals, M. (2024). Neuroplastin splice variants Np55 and Np65: Who is doing the job in macrophages? *Molecular Immunology*, *170*, 57–59. https://doi.org/10.1016/j.molimm.2024.03.008

LEE, H. C., DENG, Q. W., & ZHAO, Y. J. (2022). The calcium signaling enzyme CD38 - a paradigm for membrane topology defining distinct protein functions. *Cell Calcium*, *101*, 102514. https://doi.org/10.1016/j.ceca.2021.102514

Liou, J., Kim, M. L., Do Heo, W., Jones, J. T., Myers, J. W., Ferrell, J. E., & Meyer, T. (2005a). STIM Is a Ca2+ Sensor Essential for Ca2+-Store-Depletion-Triggered Ca2+ Influx. *Current Biology*, *15*(13), 1235–1241. https://doi.org/10.1016/j.cub.2005.05.055

Liou, J., Kim, M. L., Do Heo, W., Jones, J. T., Myers, J. W., Ferrell, J. E., & Meyer, T. (2005b). STIM Is a Ca2+ Sensor Essential for Ca2+-Store-Depletion-Triggered Ca2+ Influx. *Current Biology*, *15*(13), 1235–1241. https://doi.org/10.1016/j.cub.2005.05.055

Lopreiato, R., Giacomello, M., & Carafoli, E. (2014). The Plasma Membrane Calcium Pump: New Ways to Look at an Old Enzyme. *Journal of Biological Chemistry*, *289*(15), 10261–10268. https://doi.org/10.1074/jbc.O114.555565

Lundahl, M. LE, Mitermite, M., Ryan, D. G., Case, S., Williams, N. C., Yang, M., Lynch, R. I., Lagan, E., Lebre, F. M., Gorman, A. L., Stojkovic, B., Bracken, A. P., Frezza, C., Sheedy, F. J., Scanlan, E. M., O'Neill, L. A., Gordon, S. V, & Lavelle, E. C. (2022). Macrophage innate training induced by IL-4 and IL-13 activation enhances OXPHOS driven anti-mycobacterial responses. *ELife*, *11*. https://doi.org/10.7554/eLife.74690

Ma, J., McCarl, C., Khalil, S., Lüthy, K., & Feske, S. (2010). T-cell-specific deletion of STIM1 and STIM2 protects mice from EAE by impairing the effector functions of Th1 and Th17 cells. *European Journal of Immunology*, *40*(11), 3028–3042. https://doi.org/10.1002/eji.201040614

Manji, S. S. M., Parker, N. J., Williams, R. T., van Stekelenburg, L., Pearson, R. B., Dziadek, M., & Smith, P. J. (2000). STIM1: a novel phosphoprotein located at the cell surface. *Biochimica et Biophysica Acta (BBA) - Protein Structure and Molecular Enzymology*, *1481*(1), 147–155. https://doi.org/10.1016/S0167-4838(00)00105-9

Mass, E., Nimmerjahn, F., Kierdorf, K., & Schlitzer, A. (2023). Tissue-specific macrophages: how they develop and choreograph tissue biology. In *Nature Reviews Immunology* (Vol. 23, Issue 9, pp. 563–579). Nature Research. https://doi.org/10.1038/s41577-023-00848-y

Masuyama, R., Vriens, J., Voets, T., Karashima, Y., Owsianik, G., Vennekens, R., Lieben, L., Torrekens, S., Moermans, K., Vanden Bosch, A., Bouillon, R., Nilius, B., & Carmeliet, G. (2008). TRPV4-Mediated Calcium Influx Regulates Terminal Differentiation of Osteoclasts. *Cell Metabolism*, *8*(3), 257–265. https://doi.org/10.1016/j.cmet.2008.08.002

Meiser, J., Krämer, L., Sapcariu, S. C., Battello, N., Ghelfi, J., D'Herouel, A. F., Skupin, A., & Hiller, K. (2016). Pro-inflammatory Macrophages Sustain Pyruvate Oxidation through Pyruvate Dehydrogenase for the Synthesis of Itaconate and to Enable Cytokine Expression. *Journal of Biological Chemistry*, *291*(8), 3932–3946. https://doi.org/10.1074/jbc.M115.676817

Morales-Lange, B., Ramírez-Cepeda, F., Schmitt, P., Guzmán, F., Lagos, L., Øverland, M., Wong-Benito, V., Imarai, M., Fuentes, D., Boltaña, S., Alcaíno, J., Soto, C., & Mercado, L. (2021). Interferon Gamma Induces the Increase of Cell-Surface Markers (CD80/86, CD83 and MHC-II) in Splenocytes From Atlantic Salmon. *Frontiers in Immunology*, *12*. https://doi.org/10.3389/fimmu.2021.666356

Nascimento Da Conceicao, V., Sun, Y., Ramachandran, K., Chauhan, A., Raveendran, A., Venkatesan, M., DeKumar, B., Maity, S., Vishnu, N., Kotsakis, G. A., Worley, P. F., Gill, D. L., Mishra, B. B., Madesh, M., & Singh, B. B. (2021a). Resolving macrophage polarization through distinct Ca2+ entry channel that maintains intracellular signaling and mitochondrial bioenergetics. *IScience*, *24*(11), 103339. https://doi.org/10.1016/j.isci.2021.103339

Nascimento Da Conceicao, V., Sun, Y., Ramachandran, K., Chauhan, A., Raveendran, A., Venkatesan, M., DeKumar, B., Maity, S., Vishnu, N., Kotsakis, G. A., Worley, P. F., Gill, D. L., Mishra, B. B., Madesh, M., & Singh, B. B. (2021b). Resolving macrophage polarization through distinct Ca2+ entry channel that maintains intracellular signaling and mitochondrial bioenergetics. *IScience*, *24*(11). https://doi.org/10.1016/j.isci.2021.103339

Nonnenmacher, Y., & Hiller, K. (2018). Biochemistry of proinflammatory macrophage activation. *Cellular and Molecular Life Sciences*, *75*(12), 2093–2109. https://doi.org/10.1007/s00018-018-2784-1

Nunes-Hasler, P., Maschalidi, S., Lippens, C., Castelbou, C., Bouvet, S., Guido, D., Bermont, F., Bassoy, E. Y., Page, N., Merkler, D., Hugues, S., Martinvalet, D., Manoury, B., & Demaurex, N. (2017). STIM1 promotes migration, phagosomal maturation and antigen cross-presentation in dendritic cells. *Nature Communications*, *8*(1). https://doi.org/10.1038/s41467-017-01600-6

Orecchioni, M., Ghosheh, Y., Pramod, A. B., & Ley, K. (2019). Macrophage Polarization: Different Gene Signatures in M1(LPS+) vs. Classically and M2(LPS–) vs. Alternatively Activated Macrophages. *Frontiers in Immunology*, *10*. https://doi.org/10.3389/fimmu.2019.01084

Pestka, S., Kotenko, S. V., Muthukumaran, G., Izotova, L. S., Cook, J. R., & Garotta, G. (1997). The interferon gamma (IFN-γ) receptor: a paradigm for the multichain cytokine receptor. *Cytokine & Growth Factor Reviews*, *8*(3), 189–206. https://doi.org/10.1016/S1359-6101(97)00009-9

Philp, N. J., Ochrietor, J. D., Rudoy, C., Muramatsu, T., & Linser, P. J. (2003). Loss of MCT1, MCT3, and MCT4 Expression in the Retinal Pigment Epithelium and Neural Retina of the 5A11/Basigin-Null Mouse. *Investigative Opthalmology & Visual Science*, *44*(3), 1305. https://doi.org/10.1167/iovs.02-0552

Picard, C., McCarl, C.-A., Papolos, A., Khalil, S., Lüthy, K., Hivroz, C., LeDeist, F., Rieux-Laucat, F., Rechavi, G., Rao, A., Fischer, A., & Feske, S. (2009). *STIM1* Mutation Associated with a Syndrome of Immunodeficiency and Autoimmunity. *New England Journal of Medicine*, *360*(19), 1971–1980. https://doi.org/10.1056/NEJMoa0900082

Platanias, L. C. (2005). Mechanisms of type-I- and type-II-interferon-mediated signalling. *Nature Reviews Immunology*, *5*(5), 375–386. https://doi.org/10.1038/nri1604

Prakriya, M. (2013). *Store-Operated Orai Channels* (pp. 1–32). https://doi.org/10.1016/B978-0-12-407870-3.00001-9

Prakriya, M., Feske, S., Gwack, Y., Srikanth, S., Rao, A., & Hogan, P. G. (2006). Orai1 is an essential pore subunit of the CRAC channel. *Nature*, *443*(7108), 230–233. https://doi.org/10.1038/nature05122

Puleston, D. J., Buck, M. D., Klein Geltink, R. I., Kyle, R. L., Caputa, G., O'Sullivan, D., Cameron, A. M., Castoldi, A., Musa, Y., Kabat, A. M., Zhang, Y., Flachsmann, L. J., Field, C. S., Patterson, A. E., Scherer, S., Alfei, F., Baixauli, F., Austin, S. K., Kelly, B., … Pearce, E. L. (2019). Polyamines and eIF5A Hypusination Modulate Mitochondrial Respiration and Macrophage Activation. *Cell Metabolism*, *30*(2), 352-363.e8. https://doi.org/10.1016/j.cmet.2019.05.003

Pulli, I., Asghar, M. Y., Kemppainen, K., & Törnquist, K. (2018). Sphingolipid-mediated calcium signaling and its pathological effects. *Biochimica et Biophysica Acta (BBA) - Molecular Cell Research*, *1865*(11), 1668–1677. https://doi.org/10.1016/j.bbamcr.2018.04.012

Quintana, A., Pasche, M., Junker, C., Al-Ansary, D., Rieger, H., Kummerow, C., Nuñez, L., Villalobos, C., Meraner, P., Becherer, U., Rettig, J., Niemeyer, B. A., & Hoth, M. (2011). Calcium microdomains at the immunological synapse: how ORAI channels, mitochondria and calcium pumps generate local calcium signals for efficient T-cell activation. *The EMBO Journal*, *30*(19), 3895–3912. https://doi.org/10.1038/emboj.2011.289

Raffaello, A., Mammucari, C., Gherardi, G., & Rizzuto, R. (2016). Calcium at the Center of Cell Signaling: Interplay between Endoplasmic Reticulum, Mitochondria, and Lysosomes. *Trends in Biochemical Sciences*, *41*(12), 1035–1049. https://doi.org/10.1016/j.tibs.2016.09.001

Rath, M., MÃ¼ller, I., Kropf, P., Closs, E. I., & Munder, M. (2014). Metabolism via Arginase or Nitric Oxide Synthase: Two Competing Arginine Pathways in Macrophages. *Frontiers in Immunology*, *5*. https://doi.org/10.3389/fimmu.2014.00532

Redecke, V., Wu, R., Zhou, J., Finkelstein, D., Chaturvedi, V., High, A. A., & Häcker, H. (2013). Hematopoietic progenitor cell lines with myeloid and lymphoid potential. *Nature Methods*, *10*(8), 795–803. https://doi.org/10.1038/nmeth.2510

Ren, H., Xia, X., Dai, X., & Dai, Y. (2022). The role of neuroplastin65 in macrophage against E. coli infection in mice. *Molecular Immunology*, *150*, 78–89. https://doi.org/10.1016/j.molimm.2022.08.003

Ridley, A. J., Schwartz, M. A., Burridge, K., Firtel, R. A., Ginsberg, M. H., Borisy, G., Parsons, J. T., & Horwitz, A. R. (2003). Cell Migration: Integrating Signals from Front to Back. *Science*, *302*(5651), 1704–1709. https://doi.org/10.1126/science.1092053

Risco, A., del Fresno, C., Mambol, A., Alsina-Beauchamp, D., MacKenzie, K. F., Yang, H.-T., Barber, D. F., Morcelle, C., Arthur, J. S. C., Ley, S. C., Ardavin, C., & Cuenda, A. (2012). p38γ and p38δ kinases regulate the Toll-like receptor 4 (TLR4)-induced cytokine production by controlling ERK1/2 protein kinase pathway activation. *Proceedings of the National Academy of Sciences*, *109*(28), 11200–11205. https://doi.org/10.1073/pnas.1207290109

Rosato, A. S., Tang, R., & Grimm, C. (2021). Two-pore and TRPML cation channels: Regulators of phagocytosis, autophagy and lysosomal exocytosis. *Pharmacology & Therapeutics*, *220*, 107713. https://doi.org/10.1016/j.pharmthera.2020.107713

Russell, S. M., Keegan, A. D., Harada, N., Nakamura, Y., Noguchi, M., Leland, P., Friedmann, M. C., Miyajima, A., Puri, R. K., Paul, W. E., & Leonard, W. J. (1993). Interleukin-2 Receptor γ Chain: a Functional Component of the Interleukin-4 Receptor. *Science*, *262*(5141), 1880–1883. https://doi.org/10.1126/science.8266078

Sarti, P., Forte, E., Mastronicola, D., Giuffrè, A., & Arese, M. (2012). Cytochrome c oxidase and nitric oxide in action: Molecular mechanisms and pathophysiological implications. *Biochimica et Biophysica Acta (BBA) - Bioenergetics*, *1817*(4), 610–619. https://doi.org/10.1016/j.bbabio.2011.09.002

Schappe, M. S., Szteyn, K., Stremska, M. E., Mendu, S. K., Downs, T. K., Seegren, P. V., Mahoney, M. A., Dixit, S., Krupa, J. K., Stipes, E. J., Rogers, J. S., Adamson, S. E., Leitinger, N., & Desai, B. N. (2018). Chanzyme TRPM7 Mediates the Ca2+ Influx Essential for Lipopolysaccharide-Induced Toll-Like Receptor 4 Endocytosis and Macrophage Activation. *Immunity*, *48*(1), 59-74.e5. https://doi.org/10.1016/j.immuni.2017.11.026

Schmidt, N., Kollewe, A., Constantin, C. E., Henrich, S., Ritzau-Jost, A., Bildl, W., Saalbach, A., Hallermann, S., Kulik, A., Fakler, B., & Schulte, U. (2017). Neuroplastin and Basigin Are Essential Auxiliary Subunits of Plasma Membrane Ca2+-ATPases and Key Regulators of Ca2+ Clearance. *Neuron*, *96*(4), 827-838.e9. https://doi.org/10.1016/j.neuron.2017.09.038

Schmitt, J. M., Wayman, G. A., Nozaki, N., & Soderling, T. R. (2004). Calcium Activation of ERK Mediated by Calmodulin Kinase I. *Journal of Biological Chemistry*, *279*(23), 24064–24072. https://doi.org/10.1074/jbc.M401501200

Schulz, C., Perdiguero, E. G., Chorro, L., Szabo-Rogers, H., Cagnard, N., Kierdorf, K., Prinz, M., Wu, B., Jacobsen, S. E. W., Pollard, J. W., Frampton, J., Liu, K. J., & Geissmann, F. (2012). A Lineage of Myeloid Cells Independent of Myb and Hematopoietic Stem Cells. *Science*, *336*(6077), 86–90. https://doi.org/10.1126/science.1219179

Sefik, E., Qu, R., Junqueira, C., Kaffe, E., Mirza, H., Zhao, J., Brewer, J. R., Han, A., Steach, H. R., Israelow, B., Blackburn, H. N., Velazquez, S. E., Chen, Y. G., Halene, S., Iwasaki, A., Meffre, E., Nussenzweig, M., Lieberman, J., Wilen, C. B., … Flavell, R. A.

(2022). Inflammasome activation in infected macrophages drives COVID-19 pathology. *Nature*, *606*(7914), 585–593. https://doi.org/10.1038/s41586-022-04802-1

Sharif, O., Bolshakov, V. N., Raines, S., Newham, P., & Perkins, N. D. (2007). Transcriptional profiling of the LPS induced NF-κB response in macrophages. *BMC Immunology*, *8*(1), 1. https://doi.org/10.1186/1471-2172-8-1

Shaw, P. J., Weidinger, C., Vaeth, M., Luethy, K., Kaech, S. M., & Feske, S. (2014). CD4+ and CD8+ T cell–dependent antiviral immunity requires STIM1 and STIM2. *Journal of Clinical Investigation*, *124*(10), 4549–4563. https://doi.org/10.1172/JCI76602

Simpson, D. S., Pang, J., Weir, A., Kong, I. Y., Fritsch, M., Rashidi, M., Cooney, J. P., Davidson, K. C., Speir, M., Djajawi, T. M., Hughes, S., Mackiewicz, L., Dayton, M., Anderton, H., Doerflinger, M., Deng, Y., Huang, A. S., Conos, S. A., Tye, H., … Vince, J. E. (2022). Interferon-γ primes macrophages for pathogen ligand-induced killing via a caspase-8 and mitochondrial cell death pathway. *Immunity*, *55*(3), 423-441.e9. https://doi.org/10.1016/j.immuni.2022.01.003

Smalla, K.-H., Matthies, H., Langnäse, K., Shabir, S., Böckers, T. M., Wyneken, U., Staak, S., Krug, M., Beesley, P. W., & Gundelfinger, E. D. (2000). The synaptic glycoprotein neuroplastin is involved in long-term potentiation at hippocampal CA1 synapses. *Proceedings of the National Academy of Sciences*, *97*(8), 4327–4332. https://doi.org/10.1073/pnas.080389297

Sneyers, F., Kerkhofs, M., Speelman-Rooms, F., Welkenhuyzen, K., La Rovere, R., Shemy, A., Voet, A., Eelen, G., Dewerchin, M., Tait, S. W. G., Ghesquière, B., Bootman, M. D., & Bultynck, G. (2023). Intracellular BAPTA directly inhibits PFKFB3, thereby impeding mTORC1-driven Mcl-1 translation and killing MCL-1-addicted cancer cells. *Cell Death & Disease*, *14*(9), 600. https://doi.org/10.1038/s41419-023-06120-4

Soto-Heredero, G., Gómez de las Heras, M. M., Gabandé-Rodríguez, E., Oller, J., & Mittelbrunn, M. (2020). Glycolysis – a key player in the inflammatory response. *The FEBS Journal*, *287*(16), 3350–3369. https://doi.org/10.1111/febs.15327

Stafford, N., Wilson, C., Oceandy, D., Neyses, L., & Cartwright, E. J. (2017). The Plasma Membrane Calcium ATP <scp>ases</scp> and Their Role as Major New Players in Human Disease. *Physiological Reviews*, *97*(3), 1089–1125. https://doi.org/10.1152/physrev.00028.2016

Stathopulos, P. B., Li, G.-Y., Plevin, M. J., Ames, J. B., & Ikura, M. (2006). Stored Ca2+ Depletion-induced Oligomerization of Stromal Interaction Molecule 1 (STIM1) via the EF-SAM Region. *Journal of Biological Chemistry*, *281*(47), 35855–35862. https://doi.org/10.1074/jbc.M608247200

Tannahill, G. M., Curtis, A. M., Adamik, J., Palsson-McDermott, E. M., McGettrick, A. F., Goel, G., Frezza, C., Bernard, N. J., Kelly, B., Foley, N. H., Zheng, L., Gardet, A., Tong, Z., Jany, S. S., Corr, S. C., Haneklaus, M., Caffrey, B. E., Pierce, K., Walmsley, S., … O'Neill, L. A. J. (2013). Succinate is an inflammatory signal that induces IL-1β through HIF-1α. *Nature*, *496*(7444), 238–242. https://doi.org/10.1038/nature11986

Tedesco, Scattolini, Albiero, Bortolozzi, Avogaro, Cignarella, & Fadini. (2019). Mitochondrial Calcium Uptake Is Instrumental to Alternative Macrophage Polarization and Phagocytic Activity. *International Journal of Molecular Sciences*, *20*(19), 4966. https://doi.org/10.3390/ijms20194966

Ueda, Y., Hirai, S., Osada, S., Suzuki, A., Mizuno, K., & Ohno, S. (1996). Protein Kinase C δ Activates the MEK-ERK Pathway in a Manner Independent of Ras and Dependent on Raf. *Journal of Biological Chemistry*, *271*(38), 23512–23519. https://doi.org/10.1074/jbc.271.38.23512

Vaeth, M., Kahlfuss, S., & Feske, S. (2020). CRAC Channels and Calcium Signaling in T Cell-Mediated Immunity. *Trends in Immunology*, *41*(10), 878–901. https://doi.org/10.1016/j.it.2020.06.012

Vaeth, M., Zee, I., Concepcion, A. R., Maus, M., Shaw, P., Portal-Celhay, C., Zahra, A., Kozhaya, L., Weidinger, C., Philips, J., Unutmaz, D., & Feske, S. (2015). Ca2+ Signaling but Not Store-Operated Ca2+ Entry Is Required for the Function of Macrophages and Dendritic Cells. *The Journal of Immunology*, *195*(3), 1202–1217. https://doi.org/10.4049/jimmunol.1403013

Van den Bossche, J., Baardman, J., Otto, N. A., van der Velden, S., Neele, A. E., van den Berg, S. M., Luque-Martin, R., Chen, H.-J., Boshuizen, M. C. S., Ahmed, M., Hoeksema, M. A., de Vos, A. F., & de Winther, M. P. J. (2016). Mitochondrial Dysfunction Prevents Repolarization of Inflammatory Macrophages. *Cell Reports*, *17*(3), 684–696. https://doi.org/10.1016/j.celrep.2016.09.008

Vandewalle, A., Tourneur, E., Bens, M., Chassin, C., & Werts, C. (2014). Calcineurin/NFAT signaling and innate host defence: a role for NOD1-mediated phagocytic functions. *Cell Communication and Signaling*, *12*(1), 8. https://doi.org/10.1186/1478-811X-12-8

Vemula, S. K., Malci, A., Junge, L., Lehmann, A.-C., Rama, R., Hradsky, J., Matute, R. A., Weber, A., Prigge, M., Naumann, M., Kreutz, M. R., Seidenbecher, C. I., Gundelfinger, E. D., & Herrera-Molina, R. (2020). The Interaction of TRAF6 With Neuroplastin Promotes Spinogenesis During Early Neuronal Development. *Frontiers in Cell and Developmental Biology*, *8*. https://doi.org/10.3389/fcell.2020.579513

Vijayan, V., Pradhan, P., Braud, L., Fuchs, H. R., Gueler, F., Motterlini, R., Foresti, R., & Immenschuh, S. (2019). Human and murine macrophages exhibit differential metabolic responses to lipopolysaccharide - A divergent role for glycolysis. *Redox Biology*, *22*, 101147. https://doi.org/10.1016/j.redox.2019.101147

Wang, F., Zhang, S., Vuckovic, I., Jeon, R., Lerman, A., Folmes, C. D., Dzeja, P. P., & Herrmann, J. (2018). Glycolytic Stimulation Is Not a Requirement for M2 Macrophage Differentiation. *Cell Metabolism*, *28*(3), 463-475.e4. https://doi.org/10.1016/j.cmet.2018.08.012

Wang, L., Tassiulas, I., Park-Min, K. H., Reid, A. C., Gil-Henn, H., Schlessinger, J., Baron, R., Zhang, J. J., & Ivashkiv, L. B. (2008). 'Tuning' of type I interferon-induced Jak-STAT1 signaling by calcium-dependent kinases in macrophages. *Nature Immunology*, *9*(2), 186–193. https://doi.org/10.1038/ni1548

Wculek, S. K., Dunphy, G., Heras-Murillo, I., Mastrangelo, A., & Sancho, D. (2022). Metabolism of tissue macrophages in homeostasis and pathology. *Cellular & Molecular Immunology*, *19*(3), 384–408. https://doi.org/10.1038/s41423-021-00791-9

Wellen, K. E., Hatzivassiliou, G., Sachdeva, U. M., Bui, T. V., Cross, J. R., & Thompson, C. B. (2009). ATP-Citrate Lyase Links Cellular Metabolism to Histone Acetylation. *Science*, *324*(5930), 1076–1080. https://doi.org/10.1126/science.1164097

Wilson, M. C., Kraus, M., Marzban, H., Sarna, J. R., Wang, Y., Hawkes, R., Halestrap, A. P., & Beesley, P. W. (2013). The Neuroplastin Adhesion Molecules Are Accessory Proteins That Chaperone the Monocarboxylate Transporter MCT2 to the Neuronal Cell Surface. *PLoS ONE*, *8*(11), e78654. https://doi.org/10.1371/journal.pone.0078654

Xia, P., Wu, Y., Lian, S., Yan, L., Meng, X., Duan, Q., & Zhu, G. (2021). Research progress on Toll-like receptor signal transduction and its roles in antimicrobial immune responses. *Applied Microbiology and Biotechnology*, *105*(13), 5341–5355. https://doi.org/10.1007/s00253-021-11406-8

Yang, Q., Zhang, H., Wei, T., Lin, A., Sun, Y., Luo, P., & Zhang, J. (2021). Single-Cell RNA Sequencing Reveals the Heterogeneity of Tumor-Associated Macrophage in Non-Small

Cell Lung Cancer and Differences Between Sexes. *Frontiers in Immunology*, *12*. https://doi.org/10.3389/fimmu.2021.756722

Yang, S., Zhao, M., & Jia, S. (2023). Macrophage: Key player in the pathogenesis of autoimmune diseases. *Frontiers in Immunology*, *14*. https://doi.org/10.3389/fimmu.2023.1080310

Yeung, P. S., Yamashita, M., & Prakriya, M. (2020). Molecular basis of allosteric Orai1 channel activation by STIM1. *The Journal of Physiology*, *598*(9), 1707–1723. https://doi.org/10.1113/JP276550

Yunna, C., Mengru, H., Lei, W., & Weidong, C. (2020). Macrophage M1/M2 polarization. *European Journal of Pharmacology*, *877*, 173090. https://doi.org/10.1016/j.ejphar.2020.173090

Zumerle, S., Calì, B., Munari, F., Angioni, R., Di Virgilio, F., Molon, B., & Viola, A. (2019). Intercellular Calcium Signaling Induced by ATP Potentiates Macrophage Phagocytosis. *Cell Reports*, *27*(1), 1-10.e4. https://doi.org/10.1016/j.celrep.2019.03.011

Ehrenerklärung

Ich versichere hiermit, dass ich die vorliegende Arbeit ohne unzulässige Hilfe Dritter und ohne Benutzung anderer als der angegebenen Hilfsmittel angefertigt habe; verwendete fremde und eigene Quellen sind als solche kenntlich gemacht.

Ich habe insbesondere nicht wissentlich:

• Ergebnisse erfunden oder widersprüchlich Ergebnisse verschwiegen,

• statistische Verfahren absichtlich missbraucht, um Daten in ungerechtfertigter Weise zu interpretieren,

• fremde Ergebnisse oder Veröffentlichungen plagiiert,

• fremde Forschungsergebnisse verzerrt wiedergegeben.

Mir ist bekannt, dass Verstöße gegen das Urheberrecht Unterlassungs- und Schadensersatzansprüche des Urhebers sowie eine strafrechtliche Ahndung durch die Strafverfolgungsbehörden begründen kann.

Ich erkläre mich damit einverstanden, dass die Arbeit ggf. mit Mitteln der elektronischen Datenverarbeitung auf Plagiate überprüft werden kann.

Magdeburg, 26 Februar 2025

Nikhil Tiwari